

**ENHANCEMENT OF MULTIPLE INPUT MULTIPLE OUTPUT (MIMO)**

**COMMUNICATION SYSTEM WITH POLARIZATION**

A THESIS

Presented to the Department of Electrical Engineering

California State University, Long Beach

In Partial Fulfillment

of the Requirements for the Degree

Master of Science in Electrical Engineering

Committee Members:

Sean Kwon, Ph.D.

Saleh Al Jufout, Ph.D.

Aftab Ahmed, Ph.D.

College Designee:

Hamid Rahai, Ph.D.

By Seungcheol Oh

B.S., 2019, California State University, Long Beach

August 2022

Copyright 2022

Seungcheol Oh

All Rights Reserved

## ABSTRACT

The 5th generation (5G) new radio (NR) access technology and the beyond-5G future wireless communication require an extremely high data rate, spectrum efficiency, as well as energy-efficient transmission/reception schemes. Polarization domain and antenna selection has attracted substantial attention because they provide energy-efficiency. This thesis proposes *multi-polarization superposition beamforming (MPS-Beamforming)* with cross-polarization discrimination (XPD) and cross-polarization ratio (XPR)-aware transmit power allocation utilizing the 5G NR antenna panel structure. The appropriate orthogonal frequency division multiplexing (OFDM) subcarrier assignment algorithm is also proposed to verify the theoretical schemes via simulations. The detailed theoretical derivation along with comprehensive simulation results illustrate that the proposed novel scheme of MPS-Beamforming is significantly beneficial to the improvement of the performance in terms of the symbol error rate (SER) and signal-to-noise ratio (SNR) gain at the user equipment (UE).

Furthermore, this thesis delineates *polarization-reconfigurable (PR)* multiple input multiple output (MIMO) system (PR-MIMO), where both transmitter and receiver can change the (linear) polarization orientation at each element of their antenna arrays. Joint polarization pre-post coding to maximize bounds on the capacity and the maximum eigenvalue of the channel matrix is first introduced. For this, approximate closed form equations of optimal polarization vectors at one link end are derived, then iterative joint polarization pre-post coding to pursue *joint* optimal polarization vectors at both link ends is used. Next, in alignment with the energy efficient scheme combination of PR-MIMO spatial modulation with hybrid antenna selection (PR-HS/MIMO) and the maximal ratio transmission (MRT) with hybrid selection (PR-HS/MRT) which can achieve a remarkable improvement of channel capacity and SER, are investigated. Two novel schemes of element-wise and global polarization reconfiguration are presented for both PR-HS/MIMO and PR-HS/MRT systems. Comprehensive simulation results indicate that the proposed schemes provide 3 – 5 dB signal-to-noise ratio (SNR) gain in PR-MIMO and concomitant improvements of channel capacity in PR-HS/MIMO and PR-HS/MRT.

## **ACKNOWLEDGEMENTS**

First and foremost, I would like to thank Jesus Christ for saving my soul. You have given me the purpose for my life which I will always trust that you will guide.

I would like to express my earnest gratitude to my thesis advising professor, Dr. Sean (Seok-Chul) Kwon, who deserves my most sincere appreciation. You trusted me and accepted me into the WiSE Lab even when I had no prior experience in research. You have not only taught me the technical ways of performing research, but also taught me the mindset and attitude a researcher must have. You ultimately gave me the direction and sparked a desire in me to pursue a career in research. I will always follow your teachings and advice and will always owe you a great debt of gratitude. Next, I thank Dr. Andreas Molisch at USC for your great advice, comments and professionalism in our collaborative research meetings. Researching with you has greatly honed my ability as a researcher. To the thesis committee, Dr. Aftab Ahmed and Dr. Saleh Al Jufout, I appreciate your time and effort in assisting me to finalize this thesis. I also thank the WiSE Lab members who assisted me with their prior experience in publishing their own thesis.

I express my appreciation to my mother, Song-Ja Ko, for your unconditional love, and your spiritual and financial support for all my life. Also to my father Yeong-Ho Oh, brother Gyeongcheol Oh and sister-in-law Subin Ra Oh, for their boundless love, comfort and joy. There will not be anyone in this world that will be more proud of every small step I take more than my family. You all are my motivation.

To my dearest friends, Jaedo Han, Daniel Jae Jung, Junha Yoon, Dong-Woo Jung, who have been there for me through hardships in my life with nothing but encouragement and support. All of you inspire me to become a better person, achieve higher goals, and even motivated me to finish this thesis because each of you are evolving into a better person every day and have been accomplishing much in your own career path.

Finally, to the CSULB faculty who built the academic foundation for me to write the contents in this thesis. I greatly thank you all.

## TABLE OF CONTENTS

ABSTRACT . . . . .	ii
ACKNOWLEDGEMENTS . . . . .	iii
LIST OF TABLES . . . . .	v
LIST OF FIGURES . . . . .	viii
1. INTRODUCTION . . . . .	1
2. MOTIVATION AND CONTRIBUTION . . . . .	4
3. MPS-BEAMFORMING . . . . .	8
4. PR-MIMO SYSTEM . . . . .	22
5. PR-HS/MIMO AND PR-HS/MRT . . . . .	29
6. EFFECT OF POLARIZATION ON THE CHANNEL . . . . .	37
7. EXPERIMENTAL RESULTS FOR MPS-BEAMFORMING . . . . .	42
8. EXPERIMENTAL RESULTS FOR PR-MIMO, PR-HS/MIMO AND PR-HS/MRT .	55
9. CONCLUSION . . . . .	67
APPENDICES . . . . .	68
A. EXPECTATION AND VARIANCE OF $Y = \cos \Theta$ , $X = \sin \Theta$ AND $h_{ij}^{\text{eff}}$ . . . . .	69
B. ELABORATION OF POLARIZATION DETERMINANT MATRIX . . . . .	72
REFERENCES . . . . .	75

## LIST OF TABLES

1.	MPS-Beamforming Subcarrier Assignment Algorithm . . . . .	20
2.	Selected Tx Antenna Index when $L_t = 4$ . . . . .	62
3.	Selected Tx Antenna Index when $L_t = 6$ . . . . .	63
4.	Selected Tx Antenna Index when $L_t = 8$ . . . . .	63

## LIST OF FIGURES

1.	5G beamforming supported by multiple antenna panels at the gNB side agreed by the standard society. . . . .	5
2.	Polarization ellipse and the rotation of the ellipse. . . . .	15
3.	Adjustment of rotation angle and eccentricity of the Rx polarization ellipse. . . . .	19
4.	PR-MIMO system with polarization reconfigurable antennas. . . . .	22
5.	Polarization-determinant ellipse and polarization-vector unit circle. . . . .	26
6.	System Model of Antenna Selection with Reconfigurable Antennas . . . . .	29
7.	Distribution of the elements in polarization vector: $Y = \cos(\Theta)$ and $X = \sin(\Theta)$ . . . . .	38
8.	Empirical histogram of $ h_{ij}^{\text{eff}} ^2$ in PR-HS; the comparison of chi-square distribution with 4 degrees of freedom. . . . .	40
9.	Impact of $L_t$ on the mean of effective channel gain in PR-HS-MIMO systems. . . . .	41
10.	Symbol error rate for different transmit power allocation in the scenario of $45^\circ$ Rx antenna polarization, $\overline{\text{XPD}}^N = 5.48$ dB, $\overline{\text{XPD}}^P = -6.26$ dB, $\overline{\text{XPR}}^N = 5.90$ dB. . . . .	43
11.	Symbol error rate for different transmit power allocation in the scenario of $45^\circ$ Rx antenna polarization, $\overline{\text{XPD}}^N = 4.56$ dB, $\overline{\text{XPD}}^P = -4.15$ dB, $\overline{\text{XPR}}^N = 4.34$ dB. . . . .	44
12.	Complexity/computation time of the proposed subcarrier assignment (SA) algorithm for varying number of OFDM subcarriers. . . . .	45
13.	Squared eccentricity, $\epsilon^2$ for the varying XPD. . . . .	47
14.	Angle of rotation, $\theta$ for the varying XPD. . . . .	47
15.	Direct relation between squared eccentricity, $\epsilon^2$ and rotation angle of the polarization ellipse, $\theta$ . . . . .	48
16.	Received signal power for $0^\circ$ Rx antenna polarization. . . . .	48
17.	Normalized received signal power for $-22.5^\circ$ Rx antenna polarization. . . . .	49

18.	Symbol error rate for different transmit power allocation in the scenario of $-45^\circ$ Rx antenna polarization. . . . .	50
19.	Symbol error rate for different transmit power allocation in the scenario of $-30^\circ$ Rx antenna polarization. . . . .	50
20.	Symbol error rate for different transmit power allocation in the scenario of $0^\circ$ Rx antenna polarization. . . . .	51
21.	Verification of the theoretically determined XPD/XPR-aware transmit power allocation ratio with the best symbol error rate in a deterministic channel; Rx antenna polarization is $5^\circ$ . . . . .	52
22.	Verification of the theoretically determined XPD/XPR-aware transmit power allocation ratio with the best symbol error rate in statistical channels; Rx antenna polarization is $5^\circ$ . . . . .	52
23.	Verification of the proposed XPD/XPR-aware transmit power allocation scheme showing the best symbol error rate in a deterministic channel; Rx antenna polarization is $0^\circ$ . . . . .	53
24.	Verification of the proposed XPD/XPR-aware transmit power allocation scheme showing the best symbol error rate in statistical channels; Rx antenna polarization is $0^\circ$ . . . . .	54
25.	Channel capacity for varying Tx-polarization; 30 dB SNR. . . . .	56
26.	Channel capacity for varying Rx-polarization with optimal Tx-polarization; 30 dB SNR. . . . .	57
27.	Optimal Tx/Rx-polarization angles for the number of iterations; 30 dB. . . . .	58
28.	cdf's of channel capacity for the scenarios of joint polarization pre-post coding with five iterations, random Tx/Rx-polarization; optimal and the worst Tx/Rx-polarization through brute-force numerical search at 5 dB SNR. . . . .	59
29.	cdf's of channel capacity for the scenarios of joint polarization pre-post coding with five iterations, random Tx/Rx-polarization; optimal and the worst Tx/Rx-polarization through brute-force numerical search at 30 dB SNR. . . . .	60

30.	PR-MIMO channel capacity for the varying SNR in the scenarios of random Tx/Rx-polarization, Tx-polarization precoding, and joint polarization pre-post coding. . .	61
31.	cdf curves of channel capacity at 20 dB for PR-HS/MIMO with element-wise (EW) and global polarization reconfiguration schemes, conventional HS-MIMO (Random Polarization); with a variety of $L_t$ . . . . .	62
32.	cdf curves of channel capacity for PR-HS/MRT with EW and global polarization reconfiguration schemes, conventional HS/MRT (Random Polarization), upper and lower bounds; with a variety of $L_t$ . . . . .	64
33.	SER curves for PR-HS/MRT with EW and global polarization reconfiguration schemes and conventional HS/MRT (random polarization); with a variety of $L_t$ . .	65
34.	Validation of analytical SER curves via Monte-Carlo simulation . . . . .	66

## CHAPTER 1

### INTRODUCTION

An electromagnetic wave that propagates from the transmitter (Tx) to the receiver (Rx) of a wireless communications system is characterized *inter alia* by its polarization, that is orientation of the field vector. Interaction of a wave (multipath component, MPC) with environmental objects may change the orientation, and different MPCs may experience different changes in the orientation. This effect can reduce performance, for example, if the (fixed) polarization of the Rx antenna is mismatched to the polarization of the arriving field. However, it can also be an advantage, since the different polarization offer degrees of freedom that can be exploited for diversity and/or spatial multiplexing. With appropriate utilization of its advantage, polarization domain has significant potential to improve the future wireless communication system in terms of channel capacity, spectrum efficiency, and bit/symbol error rate (BER/SER) [1]–[5]. Furthermore, assets of polarization include, but are not limited to the recent achievements as they are described in various studies [6]–[21]. For this reason, the impact of polarization on the performance of the wireless communication systems has attracted substantial attention [22]–[26] and interesting research is being vigorously conducted on several aspects of utilizing polarization domain.

It has been reported that the polarization domain can be combined with other domains such as time and spatial domains to enhance conventional wireless communication system [1]–[3]. In particular, the improvement of the SER is achieved via combining spatial and polarization diversity along with maximum ratio combining (MRC) in the scenarios of fast power control and no power control on Nakagami- $m$  fading channels [1]. Nonetheless, it has also been reported that the advantage of multi-polarization antenna elements significantly depends on the condition of wireless channels [1]–[3]. The reason is that, as aforementioned, different conditions of wireless channels cause different degrees of channel depolarization. That is, the electromagnetic plane waves transmitted with a fixed polarization, for example,  $-45^\circ$  polarization at the next generation Node B (gNB) or the base station, have both the copolarization ( $-45^\circ$ ) and the cross-polarization ( $+45^\circ$ ) components at the end of the user equipment (UE), or receiver; the ratio of those two components

varies depending on the channel environment even for the static UE. This symptom is called channel depolarization, and it is reported by various empirical and theoretical research [24]–[27]. Therefore, the polarization misalignment between the transmitter (Tx) and the receiver (Rx) degrades the system performance in several aspects including the received signal power. As evidence, there is literature that report degrading system performance with multi-polarization. In [2], it is presented that space-time block coding (STBC) with uni-polarization outperforms STBC with dual-polarization in both uncorrelated/correlated Rayleigh and Ricean fading channels.

Whether the effect is constructive or deconstructive, it is demonstrated in the previously reported literature, that the characteristics of the polarization substantially affect the wireless system performance in terms of the channel capacity and SER/BER [2]–[4]. The cases where polarization has improved the system is shown by [3], where it is proved that deploying dual-polarized antennas in the MIMO system exhibits lower spatial diversity gain but higher spatial multiplexing gain than the MIMO system with uni-polarized antennas. In particular, in the Ricean fading channel with the high  $K$ -factor, the dual-polarized MIMO system is highly beneficial for spatial multiplexing, compared to the uni-polarized MIMO system. Resource allocation schemes also need to take the impact of polarization into account, for example, polarization assignment and polarization-aware transmission power allocation contributes to the improvement of channel capacity of the OFDM system [21].

The current state-of-the-art and future key technologies significantly take into account utilizing the polarization domain [6]–[10],[13],[14]. It is shown that deploying dual-polarized massive MIMO systems improve the performance of the conventional non-orthogonal multiple access (NOMA) scheme. Comprehensive analyses and simulations for the outage probability and outage sum-rate of the dual-polarized massive MIMO-NOMA networks are provided in [9]. Spatial modulation (SM) can also take the benefit of polarization diversity via adopting fixed dual-polarization antenna elements as in [14] or flexible polarization-agile/reconfigurable antenna elements as in [10]. Modulation schemes can be also advanced with the improved BER/SER focusing on different polarization state of the wireless channel, for which the polarization shift keying is introduced and described in a sophisticated manner in [6],[7]. The significant

improvement of channel capacity in the reconfigurable multi-polarization MIMO (MP-MIMO) system with practical polarization-agile/reconfigurable antenna elements and polarization pre/post-coding is theoretically derived and validated in simulations [4],[8].

In alignment with employing polarization to current state-of-the-art of fifth-generation (5G) NR system, this thesis delineates two novel schemes that take advantage of polarization domain to conventional wireless communication system to significantly improve their system performance in terms of channel capacity and SER. First such scheme is multi-polarization superposition (MPS) beamforming. This scheme utilizes the antenna panel structure agreed by 5G new radio (NR) standard. This particular antenna panel structure has 8-by-8 antenna elements, resulting in total of 64 antenna elements, where each element has  $-45^\circ$  and  $45^\circ$  polarization. Therefore, a column of antenna subarray can support two beams from  $-45^\circ$  polarized subarrays and  $+45^\circ$  polarized subarrays. The scheme to be explained in this thesis is concerned with superposition of dual-polarization of those transmit beams. This scheme is well introduced with the simulation results in [13]. This thesis further elaborates on [13] and substantially delineates additional contributions such as more theoretical derivation and analysis to reach the closed form, new subcarrier assignment algorithm, and abundant simulation results with both deterministic and statistical channels.

The second scheme is polarization reconfigurable (PR)-MIMO combined with hybrid antenna selection (HS) system. This scheme deals with combining antenna selection and polarization. One of the major changes from 4G long-term evolution (LTE) to 5G NR is the increase in the carrier frequency. As a result, the wavelength of its carrier waves is in the millimeter range for 5G; thus, it is possible to pack massive amount of antenna elements in a single cell. Massive MIMO system, therefore, can be implemented as more antenna elements can be employed in a single antenna panel. However, more antenna elements come with higher hardware complexity as more radio frequency (RF) chains are needed. Hence, to mitigate the hardware complexity, the need for the antenna selection is required for an energy efficient system. Antenna selection technique, also called hybrid selection (HS) system, is explained thoroughly in [28]–[30]. This thesis explains two schemes which combine this HS system with polarization reconfigurable (PR) antennas.

## CHAPTER 2

### MOTIVATION AND CONTRIBUTION

#### **Multi-Polarization Superposition (MPS) Beamforming**

The 5G wireless communication system was first commercialized in 2020, and it is expected to be stabilized during the next decade. 5G NR access technology is a baseline of almost all the renowned communication theories and technologies. On top of that, the future wireless communication systems such as beyond-5G and 6th generation (6G) will demand far higher channel capacity and spectrum efficiency than 5G. Further, research in wireless communication pursues energy efficiency for, so called, green communications. Consequently, this is the time for leading researchers and scholars to consider novel energy-efficient wireless communication schemes in addition to the current state-of-the-art technology in 5G NR.

One of the key features that 5G NR supports is the full utilization of multiple-input multiple-output (MIMO) hybrid beamforming. Multiple antenna panels will be supported by the gNB as illustrated in Fig. 1. Each antenna panel has multiple collocated dual-polarization antenna elements where 8-by-8 dual-polarization antenna array has been regarded as one of the strongest candidates in 5G NR. Based on the agreements achieved so far by the 5G standard society, 5G beamforming is supported by antenna subarray that consists of several spatially separated antenna elements in one column of the antenna panel with the same polarization, whether it is  $+45^\circ$  or  $-45^\circ$  polarization. Although the gNB in 5G NR will support dual-beamforming with both  $+45^\circ$  and  $-45^\circ$  polarization generated by the aforementioned antenna subarray, the current 5G NR design does not consider the impact of dual-beamforming on the polarization of the superimposed received signal at the end of UE. Based on this motivation, this thesis provides novel schemes along with the comprehensive analysis and simulation results for the impact of multi-polarization superposition beamforming (MPS-Beamforming) on the symbol error rate (SER) and the energy efficiency in terms of the signal-to-noise ratio (SNR) to meet a SER at the UE based on the orthogonal frequency division multiplexing (OFDM) system.

The contribution of this thesis on MPS-Beamforming is listed as follows:

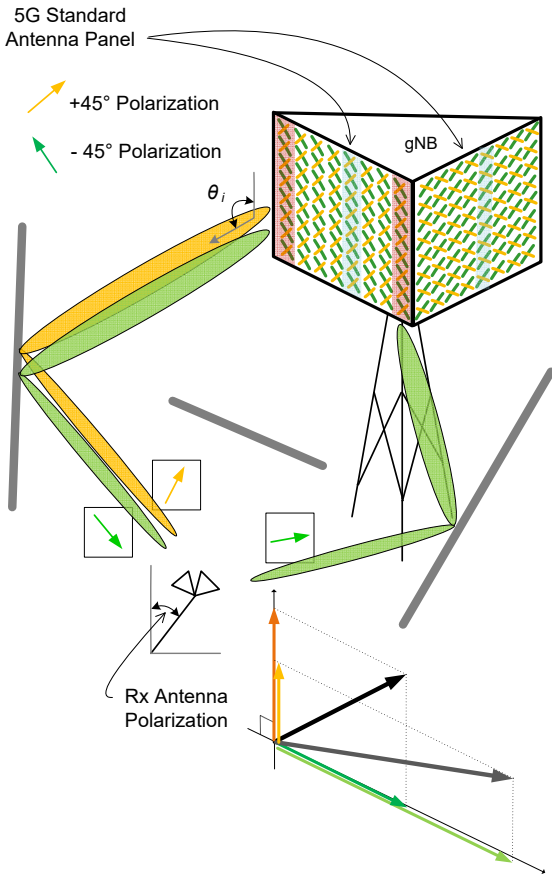


**FIGURE 1. 5G beamforming supported by multiple antenna panels at the gNB side agreed by the standard society.**

- providing novel scheme of MPS-Beamforming based on cross-polarization discrimination (XPD) and cross-polarization ratio (XPR)-aware transmit power allocation aligned with 5G antenna structure;
- illustrating the theoretical derivation of the XPD/XPR-aware transmit power allocation ratio in MPS-beamforming to yield the highest SER performance for the given channel;
- theoretical analysis for the impact of combining transmit beams with different polarization and transmit power ratio on the polarization ellipse and its rotation;
- proposing a new subcarrier assignment algorithm to take into account MPS-Beamforming scheme in the OFDM system;
- comprehensive simulation results and analyses illustrating the remarkable benefit of adopting the novel MPS-Beamforming scheme with XPD/XPR-aware transmit power allocation and subcarrier assignment; and the impact of XPD on the rotation angle of the polarization ellipse

for the received signal.

## PR-HS/MIMO and PR-HS/MRT

Multiple-input multiple-output (MIMO) has been an essential part of communication systems for many years. The two main methods for exploiting MIMO system are spatial multiplexing and diversity. In the former case, independent data streams are transmitted and received through spatial parallelized MIMO channels. The parallelization is created via precoding and postcoding based on singular value decomposition (SVD) of the channel matrix. This thesis explains and analyzes a MIMO system that exploits spatial multiplexing with polarization reconfigurable (PR) antenna elements and the functionality of polarization precoding/postcoding, which is denominated as *polarization reconfigurable MIMO (PR-MIMO)* is explained. It will be shown that the adjustment of the polarization vectors at Tx and Rx antenna elements can improve the capacity of a spatial multiplexing system.

On the other hand, the MIMO system can focus on Tx and Rx diversity for the improvement of the link quality in terms of signal-to-noise ratio (SNR). For example,  $N_t$  Tx antennas employ maximal-ratio transmission (MRT) to simultaneously transmit weighted replica of the single bit stream. The ideal weights are obtained by SVD of the channel impulse matrix. In a similar manner,  $N_r$  Rx antennas utilize maximal-ratio combining (MRC) where the weighted received signals are linearly combined to increase the effective SNR. As a result, a diversity degree of  $N_t \cdot N_r$  can be obtained. Such system that reduces the hardware complexity of MIMO system with antenna selection is a hybrid selection (HS) system [31].

The benefits of HS system and spatial multiplexing are demonstrated in [29],[30],[32],[33]. Further, 5G and beyond-5G gNB, consider setting a large number of antenna elements but with the limited number of antenna ports in each antenna panel as described in [13],[34]–[36]. That is,  $L_t$  out of  $N_t$  Tx antenna elements are selected and supported by  $L_t$  complete RF chains at the Tx. The HS scheme can reduce hardware complexity and is adopted in current communication systems as foreseen in [30]. Overall, the HS reduces the hardware complexity by lowering the number of RF chain from  $N_t$  to  $L_t$ .

HS system can be enhanced through utilization of polarization since polarization diversity is

not taken into account in the majority of previous research works on antenna selection. Although there are previous reports that consider polarization diversity with antenna selection, they consider fixed antenna polarization such as dual-polarized antennas in [37] or tri-polarized antennas in [38]. Meanwhile, this paper is the first one which exploits polarization reconfigurable (PR) HS and MIMO spatial multiplexing (PR-HS/MIMO) and PR HS maximal ratio transmission (PR-HS/MRT) which significantly outperforms that of the conventional scheme of the HS-MIMO and HS-MRT system.

The primary contributions of this thesis on PR-MIMO, PR-HS/MIMO and PR-HS/MRT can be summarized as follows:

- introducing and characterizing the hybrid antenna selection at the Tx with polarization reconfigurable antennas on both link ends;
- providing a closed-form approximation of the optimal Tx/Rx-polarization vectors in the PR-MIMO system at one link end to achieve channel capacity beyond that of a conventional MIMO communication system (with the same number of ports) as well as proposing iterative joint polarization pre-post coding for joint optimal polarization vectors;
- proposing two novel schemes of PR-HS/MIMO and PR-HS/MRT with polarization reconfigurable antenna elements, and providing analysis of the system performance in terms of channel capacity and the distribution of channel gain;
- performing a statistical analysis of the effect of polarization reconfigurable antennas on the distribution of channel gain;
- validating the significant improvement of the system performance in terms of channel capacity and SER caused by the proposed PR-MIMO, PR-HS/MIMO and PR-HS/MRT schemes.

# CHAPTER 3

## MPS-BEAMFORMING

### System Model

The 5G NR system is taken into account where the gNB deploys multiple antenna panels to support Tx beamforming as described in Fig. 1. Based on the current research trend of the assumptions and 5G NR standards, the antenna panel has multiple antenna elements; each cross represents collocated dual-polarization antenna elements with fixed polarization,  $\pm 45^\circ$ . [13],[34]–[36]. Both the line-of-sight (LoS) and non-line-of-sight (NLoS) components are considered as effective ones on the received signal resulted in MPS-Beamforming. [34]–[36].

The gNB in Fig. 1 utilizes uniform linear phase antenna subarrays, that is, antenna elements in a column with single polarization among  $\pm 45^\circ$ . Further, the gNB can transmit a single data stream utilizing dual Tx beams, which have  $+45^\circ$  and  $-45^\circ$  polarization. On the other hand, the receiving antenna polarization at the UE can change owing to the movement of the user. Without the loss of generality, the polarization vector of the received signal supported by  $-45^\circ$  polarization beamforming at the gNB is set to be aligned with a vector  $\overline{a}_x$ , and  $\overline{a}_y$  is for the received signal's polarization caused by  $+45^\circ$  polarization beamforming at the gNB. The polarization of the received signals generated by  $\pm 45^\circ$  polarization beamforming can be regarded as orthogonal, in particular for the LoS path [26]. For NLoS path, two transmit beams with orthogonal polarization have changed polarization after being reflected; however, the changed polarization maintains the orthogonality from the perspective of theoretical channel modeling [26].

The received signals at the UE, supported by  $-45^\circ$  and  $+45^\circ$  polarization transmit beamforming,  $r^{-45^\circ}(t, \tau_1)$  and  $r^{+45^\circ}(t, \tau_2)$ , respectively, can be expressed as [39]

$$\begin{aligned} r^{-45^\circ}(t, \tau_1) &= \overline{a}_x E_x(t, \tau_1) A(\theta_1) \\ &= \overline{a}_x E^{-45^\circ} A(\theta_1) \cos(2\pi f_c(t - \tau_1) + \phi_1) \end{aligned} \quad (1)$$

$$\begin{aligned} r^{+45^\circ}(t, \tau_2) &= \overline{a}_y E_y(t, \tau_2) A(\theta_2) \\ &= \overline{a}_y E^{+45^\circ} A(\theta_2) \cos(2\pi f_c(t - \tau_2) + \phi_2), \end{aligned} \quad (2)$$

where for  $i \in \{1, 2\}$ ,

$$A(\theta_i) = \frac{\sin(N\psi_i/2)}{\sin(\psi_i/2)}, \quad \psi_i = \frac{2\pi}{\lambda}d \cos \theta_i + \zeta_i. \quad (3)$$

In (1) – (3),  $E_x(t, \tau_1)$  and  $E_y(t, \tau_2)$  represent polarization components of  $r^{-45^\circ}(t, \tau_1)$  in (1) and  $r^{+45^\circ}(t, \tau_2)$  in (2), respectively [39]. Further,  $\tau_i$ ,  $\phi_i$ , and  $\theta_i$  for  $i \in \{1, 2\}$  are the path delay, random phase component, and the angle between the line of the linear phase array and the direction of radio propagation, respectively. Further,  $f_c$  is a carrier frequency;  $\zeta_i$  is the phase shift between progressive elements in the phase antenna array; and  $A(\theta_i)$  is called antenna array pattern or array factor [39]. In (3),  $\lambda$  and  $d$  are the wavelength and the distance between the consecutive elements in the phase antenna array. Lastly,  $E^{-45^\circ}$  and  $E^{+45^\circ}$  are the amplitudes of the received signals excluding the antenna array factors in the directions of  $\bar{a}_x$  and  $\bar{a}_y$ . Hence,

$$E_x(t, \tau_1) = E^{-45^\circ} \cos(2\pi f_c(t - \tau_1) + \phi_1), \quad (4)$$

$$E_y(t, \tau_2) = E^{+45^\circ} \cos(2\pi f_c(t - \tau_2) + \phi_2). \quad (5)$$

The representation of baseband signals are utilized for both theoretical analysis and simulation in this paper, while in (1) – (3) focus on the expression of polarization for radio propagation. Aligned with 4G LTE and 5G NR standards, the OFDM system is the fundamental scenario in this paper, and the baseband signals are regarded as the result of LoS along with non-line-of-sight (NLoS) components. After RF demodulation and discrete Fourier transformation (DFT) at the Rx, the received signals on the  $n$ -th OFDM subcarrier at the antennas of the Rx with  $-45^\circ$  and  $45^\circ$  polarization,  $Y_n^{-45^\circ}$  and  $Y_n^{45^\circ}$ , respectively, can be obtained. In the case that no cross-polarized signal exists,  $Y_n^{-45^\circ}$  and  $Y_n^{45^\circ}$ , are respectively,

$$Y_n^{-45^\circ} = \sqrt{E_s} H_n^{(-45^\circ, -45^\circ)} s(n) + w_n^{-45^\circ}, \quad (6)$$

$$Y_n^{45^\circ} = \sqrt{E_s} H_n^{(45^\circ, 45^\circ)} s(n) + w_n^{45^\circ}, \quad (7)$$

where  $E_s$  is the energy of the transmitted information symbol  $s(n)$ , and  $n$  is the OFDM subcarrier

index.  $w_n^{-45^\circ}$  and  $w_n^{45^\circ}$  are, respectively, the noise at the Rx antennas with  $-45^\circ$  and  $45^\circ$  polarization. Finally,  $H_n^{(-45^\circ, -45^\circ)}$  and  $H_n^{(45^\circ, 45^\circ)}$  are frequency-domain channel coefficients between the Tx and Rx antennas with  $-45^\circ$  and  $45^\circ$  polarization, respectively. The cross-polarized received signal components will be taken into account in detail in the next section.

### **Energy-Efficient Multi-Polarization Superposition Beamforming (MPS-Beamforming)**

The system model imply that the polarization of the superimposed transmit beams is primarily dependent on  $E^{-45^\circ}$  and  $E^{+45^\circ}$  in (1) – (2). In this section, novel scheme of determining transmit power allocation ratio to match the polarization of the superimposed received signal to the Rx antenna polarization in a statistical sense is explained. It is also verified in Chapter 7 that the proposed scheme in this section shows the best performance in terms of SER or SNR gain.

### **Novel Scheme of XPD/XPR-Aware Transmit Power Allocation for MPS-Beamforming**

Superimposing two transmit beams with orthogonal polarization, i.e.,  $\pm 45^\circ$ , is expected to cause different polarization from  $\pm 45^\circ$  at the Rx of the UE. Furthermore, tuning the transmit power allocation ratio between two Tx beams with  $\pm 45^\circ$  polarization must reconfigure the polarization of the received signal, due to the cross-polarization component of the received signal. Based on this motivation, this section begins with the mathematical representation of the received signal caused by superimposing two transmit beams with  $\pm 45^\circ$  polarization and the transmit power allocation ratio between those transmit beams. The OFDM system is the fundamental scenario in both the theoretical analysis and simulation in this paper to be aligned with the present 4G LTE and 5G NR standards.

Based on the aforementioned rationale, the  $-45^\circ$  and  $45^\circ$  polarization components of the received signal on the  $n$ -th OFDM subcarrier,  $Y_n^{-45^\circ}$  and  $Y_n^{45^\circ}$  are expressed as

$$Y_n^{-45^\circ} = \sqrt{\alpha E_s} H_n^{(-45^\circ, -45^\circ)} s(n) + \sqrt{\beta E_s} H_n^{(-45^\circ, 45^\circ)} s(n) + w_n^{-45^\circ}, \quad (8)$$

$$Y_n^{45^\circ} = \sqrt{\alpha E_s} H_n^{(45^\circ, -45^\circ)} s(n) + \sqrt{\beta E_s} H_n^{(45^\circ, 45^\circ)} s(n) + w_n^{45^\circ}, \quad (9)$$

where the transmit power allocation ratio,  $\alpha$  and  $\beta$  satisfy  $\beta = 1 - \alpha$ . In the scenario without the proposed MPS-beamforming,  $\alpha = 1$  or  $0$ ; whereas in the scenario of MPS-Beamforming,  $0 \leq \alpha \leq 1$ ; consequently,  $0 \leq \beta = 1 - \alpha \leq 1$ . The XPD of the received signal is the power ratio

between the copolarization component to cross-polarization component of the received signal, and the statistical XPD of the received signal resulted by MPS-beamforming,  $\overline{\text{XPD}}^{\text{MPS}}$  is defined as

$$\overline{\text{XPD}}^{\text{MPS}} \triangleq \frac{\mathbb{E}[|\sqrt{\alpha E_s} H_n^{(-45^\circ, -45^\circ)} + \sqrt{\beta E_s} H_n^{(-45^\circ, 45^\circ)}|^2]}{\mathbb{E}[|\sqrt{\alpha E_s} H_n^{(45^\circ, -45^\circ)} + \sqrt{\beta E_s} H_n^{(45^\circ, 45^\circ)}|^2]}, \quad (10)$$

where the operation  $\mathbb{E}[\cdot]$  is the expectation or equivalently, mean over whole subcarriers.

For further analysis of (10), the statistical Rx cross-polarization discrimination (XPD) without MPS-Beamforming over all subcarriers for the Tx antenna polarization,  $-45^\circ$  and  $45^\circ$  is defined as

$$\overline{\text{XPD}}^N = \overline{\text{XPD}}^{(-45^\circ)} \triangleq \frac{\mathbb{E}[|H_n^{(-45^\circ, -45^\circ)}|^2]}{\mathbb{E}[|H_n^{(45^\circ, -45^\circ)}|^2]} \quad (11)$$

$$= \frac{\sum_{n=1}^N |H_n^{(-45^\circ, -45^\circ)}|^2}{\sum_{n=1}^N |H_n^{(45^\circ, -45^\circ)}|^2}, \quad (12)$$

$$\overline{\text{XPD}}^P = \overline{\text{XPD}}^{(45^\circ)} \triangleq \frac{\mathbb{E}[|H_n^{(-45^\circ, 45^\circ)}|^2]}{\mathbb{E}[|H_n^{(45^\circ, 45^\circ)}|^2]} \quad (13)$$

$$= \frac{\sum_{n=1}^N |H_n^{(-45^\circ, 45^\circ)}|^2}{\sum_{n=1}^N |H_n^{(45^\circ, 45^\circ)}|^2}, \quad (14)$$

where the superscript N or P denotes  $-45^\circ$  or  $+45^\circ$  polarization at the Tx antenna; not at the Rx antenna. As described in (11) and (13), the system defines the statistical Rx XPD as the ratio of mean channel gain at the  $-45^\circ$  polarized Rx antenna to the mean channel gain at the  $45^\circ$  polarized Rx antenna for a given Tx antenna whether it has  $-45^\circ$  or  $+45^\circ$  polarization. Since the total number of subcarriers in the overall OFDM system is the same regardless of the Rx antenna polarization, (12) and (14) can be reached from (11) and (13), respectively.

The received signal power ratio at the Rx antenna with  $-45^\circ$  polarization for the signals from Tx antennas with  $-45^\circ$  and  $45^\circ$  polarization is defined as Rx cross-polarization ratio (XPR). In a

similar manner with the statistical Rx XPD, statistical Rx XPR can be defined as

$$\overline{\text{XPR}}^N = \overline{\text{XPR}}^{(-45^\circ)} \triangleq \frac{E[|H_n^{(-45^\circ, -45^\circ)}|^2]}{E[|H_n^{(-45^\circ, 45^\circ)}|^2]} \quad (15)$$

$$= \frac{\sum_{n=1}^N |H_n^{(-45^\circ, -45^\circ)}|^2}{\sum_{n=1}^N |H_n^{(-45^\circ, 45^\circ)}|^2}, \quad (16)$$

$$\overline{\text{XPR}}^P = \overline{\text{XPR}}^{(45^\circ)} \triangleq \frac{E[|H_n^{(45^\circ, -45^\circ)}|^2]}{E[|H_n^{(45^\circ, 45^\circ)}|^2]} \quad (17)$$

$$= \frac{\sum_{n=1}^N |H_n^{(45^\circ, -45^\circ)}|^2}{\sum_{n=1}^N |H_n^{(45^\circ, 45^\circ)}|^2}. \quad (18)$$

In (15) and (17), the statistical Rx XPR can be interpreted as the ratio between the mean channel gain from the  $-45^\circ$  polarized Tx antenna to the given Rx antenna; and the mean channel gain from the  $45^\circ$  polarized Tx antenna to the same Rx antenna. The equations (12), (14), (16) and (18) are directly used to reach (19) from the definition of  $\overline{\text{XPD}}^{\text{MPS}}$  in (10).

Utilizing (11) – (18),  $\overline{\text{XPD}}^{\text{MPS}}$  in (10) is derived as

$$\begin{aligned} \overline{\text{XPD}}^{\text{MPS}} &\triangleq \frac{E[|\sqrt{\alpha E_s} H_n^{(-45^\circ, -45^\circ)} + \sqrt{\beta E_s} H_n^{(-45^\circ, 45^\circ)}|^2]}{E[|\sqrt{\alpha E_s} H_n^{(45^\circ, -45^\circ)} + \sqrt{\beta E_s} H_n^{(45^\circ, 45^\circ)}|^2]} \\ &= \frac{\alpha + \beta / \overline{\text{XPR}}^N}{\alpha / \overline{\text{XPD}}^N + \beta / (\overline{\text{XPD}}^P \overline{\text{XPR}}^N)} \end{aligned} \quad (19)$$

$$= \frac{\alpha(1 - 1 / \overline{\text{XPR}}^N) + 1 / \overline{\text{XPR}}^N}{\alpha(1 / \overline{\text{XPD}}^N - 1 / (\overline{\text{XPD}}^P \overline{\text{XPR}}^N)) + 1 / (\overline{\text{XPD}}^P \overline{\text{XPR}}^N)}, \quad (20)$$

where once again,  $n$  is the subcarrier index. Substituting  $1 - \alpha$  for  $\beta$ , (20) can be derived from (19). It is noteworthy that  $\overline{\text{XPD}}^{\text{MPS}}$  is the function of  $\alpha$ , monotonically increasing or decreasing as shown in (20).

Finally, the Tx allocates the transmission power to the Tx antennas with  $-45^\circ$  and  $45^\circ$  polarization in the conventional scenario of the fixed total transmission power constraint. In other

words, the Tx determines transmit power allocation ratio,  $\alpha$  and consequently,  $\beta = 1 - \alpha$ ; and the objective is to align  $\overline{\text{XPD}}^{\text{MPS}}$  with the Rx antenna polarization,  $\overline{\text{XPD}}^{\text{Rx-Ant}}$ , i.e.,

$$\overline{\text{XPD}}^{\text{MPS}} = \overline{\text{XPD}}^{\text{Rx-Ant}}. \quad (21)$$

The Rx antenna polarization  $\overline{\text{XPD}}^{\text{Rx-Ant}}$  change by the rotation of antenna origination at the UE is caused by the movement of the UE. Nonetheless, it is worth noting that the polarization state information (PSI) estimation such as XPD and XPR at the Rx can still be accomplished based on the rotated antenna origination. In this scenario,  $\overline{\text{XPD}}^{\text{Rx-Ant}} = \infty$  or  $\overline{\text{XPD}}^{\text{Rx-Ant}} = 0$  corresponding to the Rx antenna polarization angle  $-45^\circ$  or  $45^\circ$ , respectively. In other words, the Rx need not maintain  $-45^\circ$  and  $45^\circ$  Rx antenna polarization angles in a physical sense; whereas, even the rotated antenna origination can be regarded as the basis of PSI estimation such as XPD and XPR. The change of the Rx antenna polarization angle from the basis of PSI estimation can be also measured by the gyroscope embedded in the current commercial UEs such as smartphones. The estimated PSI is reported to gNB through the feedback channel allocated for sharing the PSI in the similar manner with the present conventional CSI feedback.

Based on (20) and (21), the theoretical XPD/XPR-aware transmission power allocation ratio,  $\alpha_{\text{XPD/XPR}}$  and  $\beta_{\text{XPD/XPR}}$  can be derived to have the closed form expression as following.

$$\hat{\alpha}_{\text{XPD/XPR}} = \frac{\overline{\text{XPD}}^{\text{Rx-Ant}} - \overline{\text{XPD}}^{\text{P}}}{\overline{\text{XPD}}^{\text{P}} (\overline{\text{XPR}}^{\text{N}} - 1) + \overline{\text{XPD}}^{\text{Rx-Ant}} (1 - \overline{\text{XPR}}^{\text{P}})}, \quad (22)$$

$$\alpha_{\text{XPD/XPR}} = \min \left\{ 1, \max \{0, \hat{\alpha}_{\text{XPD/XPR}}\} \right\}, \quad (23)$$

$$\beta_{\text{XPD/XPR}} = 1 - \alpha_{\text{XPD/XPR}}. \quad (24)$$

In the scenario that the theoretical XPD/XPR-aware transmit power ratio  $\hat{\alpha}_{\text{XPD/XPR}}$  is not in the range of  $[0, 1]$ , the closest value to boundary values, zero or unity, is selected as (23), for the reason that  $\overline{\text{XPD}}^{\text{MPS}}$  is the function of  $\alpha$ , and monotonically increases or decreases with respect to  $\alpha$  as shown in (20). The following Lemma describes the relation between  $\overline{\text{XPD}}^{\text{N}}$ ,  $\overline{\text{XPD}}^{\text{P}}$ ,  $\overline{\text{XPR}}^{\text{N}}$  and

$\overline{\text{XPR}}^P$ , and is utilized to derive (22).

$$\frac{\overline{\text{XPD}}^N}{\overline{\text{XPD}}^P} = \frac{\overline{\text{XPR}}^N}{\overline{\text{XPR}}^P} \quad (25)$$

$$\frac{\overline{\text{XPD}}^N}{\overline{\text{XPD}}^P} = \frac{\mathbb{E}[|H_n^{(-45^\circ, -45^\circ)}|^2] / \mathbb{E}[|H_n^{(45^\circ, -45^\circ)}|^2]}{\mathbb{E}[|H_n^{(-45^\circ, 45^\circ)}|^2] / \mathbb{E}[|H_n^{(45^\circ, 45^\circ)}|^2]} \quad (26)$$

$$= \frac{\mathbb{E}[|H_n^{(-45^\circ, -45^\circ)}|^2] / \mathbb{E}[|H_n^{(-45^\circ, 45^\circ)}|^2]}{\mathbb{E}[|H_n^{(45^\circ, -45^\circ)}|^2] / \mathbb{E}[|H_n^{(45^\circ, 45^\circ)}|^2]} \quad (27)$$

$$= \frac{\overline{\text{XPR}}^N}{\overline{\text{XPR}}^P} \quad (28)$$

The numerator and denominator in (26) are from the definition of the statistical Tx XPD,  $\overline{\text{XPD}}^N$  and  $\overline{\text{XPD}}^P$  in (11) and (13), respectively; four expectation components in (26) are rearranged as described in (27). Finally, the numerator and denominator of (27) are aligned with the definitions of  $\overline{\text{XPR}}^N$  and  $\overline{\text{XPR}}^P$  in (15) and (17), respectively. The ratio of statistical Rx XPD,  $(\overline{\text{XPD}}^N / \overline{\text{XPD}}^P)$  is the same as the ratio of statistical Rx XPR,  $(\overline{\text{XPR}}^N / \overline{\text{XPR}}^P)$  as presented in (28).

### Rotation and Eccentricity of the Polarization Ellipse in MPS-Beamforming

The mathematical derivation in this section describes that the polarization of MPS-Beamforming can be the elliptical polarization as portrayed in Fig. 2 even for the line-of-sight (LoS) scenario.

At the side of the UE, the superposition of the two signals,  $r^{-45^\circ}(t, \tau_1)$  and  $r^{+45^\circ}(t, \tau_2)$  in (1) and (2), respectively, impinges on the Rx antenna. That is,

$$\begin{aligned} r(t, \tau_1, \tau_2) &= r^{-45^\circ}(t, \tau_1) + r^{+45^\circ}(t, \tau_2) \\ &= \overline{a_x} E^{-45^\circ} A(\theta_1) \cos(\varphi) + \overline{a_y} E^{+45^\circ} A(\theta_2) \cos(\varphi + \Delta) \end{aligned} \quad (29)$$

where

$$\varphi = 2\pi f_c(t - \tau_1) + \phi_1, \quad (30)$$

$$\Delta = -2\pi f_c(\tau_2 - \tau_1) + (\phi_2 - \phi_1). \quad (31)$$

The phase difference between two received signals supported by  $\pm 45^\circ$  polarization beamforming is  $\Delta$ ; even in the scenario of the line-of-sight (LoS) link between the Tx and Rx, the phase difference may not be zero due to the mismatching between  $\pm 45^\circ$  polarization Tx antenna elements.

It is noteworthy that gNB can rotate the polarization ellipse, i.e., the major and minor axes of the polarization ellipse at the UE side via utilizing the proposed scheme, MPS-Beamforming. Furthermore, MPS-Beamforming can also change the eccentricity of the polarization ellipse; as the polarization ellipse becomes narrow and long, i.e., eccentricity comes to be very high, more received signal power can be concentrated on the direction of polarization ellipse's major axis.

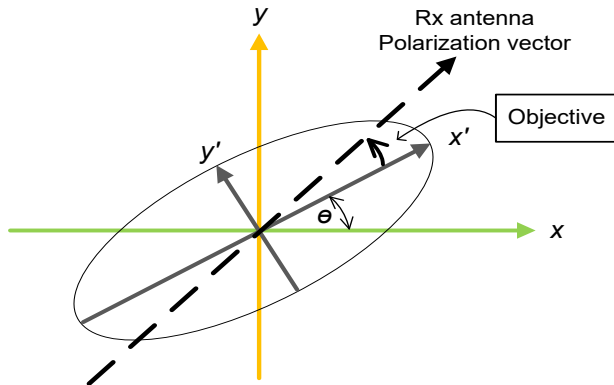


**FIGURE 2. Polarization ellipse and the rotation of the ellipse.**

Based on (1) – (2) and (29) with the auxiliary variables,  $\varphi$  and  $\Delta$  in (30) – (31), utilizing the trigonometric identity for  $\cos(\varphi + \Delta)$  in (29), the polarization of  $r(t, \tau_1, \tau_2)$ , the superimposed signal at the UE, satisfies that

$$\frac{E_y(t, \tau_2)}{E^{+45^\circ}} = \cos \varphi \cos \Delta - \sin \varphi \sin \Delta, \quad (32)$$

$$\frac{E_x(t, \tau_1)}{E^{-45^\circ}} = \cos \varphi. \quad (33)$$

Further, (32) and (33) can be modified as

$$\left( \frac{E_x(t, \tau_1)}{E^{-45^\circ} \sin \Delta} - \frac{\cos \varphi \cos \Delta}{\sin \Delta} \right)^2 = \sin^2 \varphi \quad (34)$$

$$\cos \varphi = \frac{E_x(t, \tau_1)}{E^{-45^\circ}}, \quad \sin^2 \varphi = 1 - \left( \frac{E_x(t, \tau_1)}{E^{-45^\circ}} \right)^2. \quad (35)$$

plug in (35) to (34); then,

$$\left( \frac{E_x(t, \tau_1)}{E^{-45^\circ} \sin \Delta} \right)^2 + \left( \frac{E_y(t, \tau_2)}{E^{+45^\circ} \sin \Delta} \right)^2 - 2 \frac{E_x(t, \tau_1) E_y(t, \tau_2)}{E^{-45^\circ} E^{+45^\circ}} \frac{\cos \Delta}{\sin^2 \Delta} = 1, \quad (36)$$

which is in concord with the expression of the rotated ellipse. Finally, rotating the coordinates verifies that the polarization of the superimposed signal at the UE is elliptic as

$$\left( \frac{E'_x(t, \tau_1)}{a} \right)^2 + \left( \frac{E'_y(t, \tau_2)}{b} \right)^2 = 1, \quad (37)$$

where

$$\begin{bmatrix} E'_x(t, \tau_1) \\ E'_y(t, \tau_2) \end{bmatrix} = \begin{bmatrix} \cos \theta & \sin \theta \\ -\sin \theta & \cos \theta \end{bmatrix} \begin{bmatrix} E_x(t, \tau_1) \\ E_y(t, \tau_2) \end{bmatrix}. \quad (38)$$

In the comparison of (36) with (37) after plugging in (38) into (37), the rotation angle of the

polarization ellipse,  $\theta$  and the squared eccentricity of the polarization ellipse,  $\epsilon^2$  are described as

$$\theta = \frac{1}{2} \tan^{-1} \left( \frac{2 \cos \Delta}{\frac{E^{-45^\circ}}{E^{+45^\circ}} - \frac{E^{+45^\circ}}{E^{-45^\circ}}} \right) \quad (39)$$

$$= \frac{1}{2} \tan^{-1} \left( \frac{2 \cos \Delta}{\sqrt{\text{XPD}} - 1/\sqrt{\text{XPD}}} \right), \quad (40)$$

$$\epsilon^2 \triangleq 1 - \frac{b^2}{a^2} \quad (41)$$

$$= 1 - \frac{\frac{E^{+45^\circ}}{E^{-45^\circ}} (1 + \sec 2\theta) + \frac{E^{-45^\circ}}{E^{+45^\circ}} (1 - \sec 2\theta)}{\frac{E^{+45^\circ}}{E^{-45^\circ}} (1 - \sec 2\theta) + \frac{E^{-45^\circ}}{E^{+45^\circ}} (1 + \sec 2\theta)} \quad (42)$$

$$= 1 - \frac{1 + \sec 2\theta + \text{XPD}(1 - \sec 2\theta)}{1 - \sec 2\theta + \text{XPD}(1 + \sec 2\theta)} \\ = \frac{2(\text{XPD} - 1) \sec 2\theta}{1 - \sec 2\theta + \text{XPD}(1 + \sec 2\theta)}. \quad (43)$$

The instantaneous Rx XPD is defined as

$$\text{XPD} = \left( \frac{E^{-45^\circ}}{E^{+45^\circ}} \right)^2, \quad (44)$$

and plug in the instantaneous Rx XPD to (39) and (42) so that (40) and (43) can be reached. The XPD is the power ratio of two orthogonal polarization components, which are  $E^{-45^\circ}$  and  $E^{+45^\circ}$  in this section. The fundamental definition of the eccentricity in the ellipse is expressed with the squared format in (41). It is worth mentioning that both the rotation angle and the squared eccentricity of the polarization ellipse,  $\theta$  and  $\epsilon^2$ , respectively, are the functions of  $(E^{-45^\circ}/E^{+45^\circ})$ ; therefore, the instantaneous Rx XPD. The eccentricity, denoted by  $\epsilon$ , is the metric to estimate the deviation of the conic section from the circle. The squared eccentricity,  $\epsilon^2$  is utilized in this paper for the simplicity of the expression rather than using the eccentricity,  $\epsilon$ ; it varies from zero to unity. As  $\epsilon^2$  approaches zero, the ellipse converges to a circle; while as  $\epsilon^2$  approaches unity, the ellipse converges to a linear line.

Furthermore, the direct relation between the squared eccentricity,  $\epsilon^2$  and the rotation angle of

the polarization ellipse,  $\theta$  is derived as following via utilizing (40) and (43).

$$\begin{aligned}\epsilon^2 &= 1 - \frac{\sqrt{\cos^2 \Delta + \tan^2 2\theta} - \cos \Delta \sec 2\theta}{\sqrt{\cos^2 \Delta + \tan^2 2\theta} + \cos \Delta \sec 2\theta} \\ &= \frac{2 \cos \Delta \sec 2\theta}{\sqrt{\cos^2 \Delta + \tan^2 2\theta} + \cos \Delta \sec 2\theta}.\end{aligned}\quad (45)$$

The relation between  $\epsilon^2$  and  $\theta$  in (45) for a variety of  $\Delta$  defined in (31) is illustrated in Section 7.

### Fine Adjustment of the XPD in MPS-Beamforming

The theoretical XPD/XPR-aware transmit power ratio,  $\alpha_{XPD/XPR}$ , is determined by the statistical XPD and XPR over the OFDM subcarriers as described in (22) – (24). Further, the MPS-Beamforming OFDM system fulfills subcarrier assignment to be described in Section 3. For the assigned subcarriers, the channel impulse response per subcarrier can be changed before fulfilling subcarrier re-assignment in the practical system. This section describes the manner of fine tuning for the XPD in MPS-Beamforming to cope with practical situations including the aforementioned scenarios.

The gNB can adjust its transmit XPD,  $\alpha/\beta$ , or equivalently, its transmit polarization angle, i.e.,  $\tan^{-1}(\sqrt{\alpha/\beta})$  via assigning transmit power ratio,  $\alpha$  and  $\beta$ , to  $-45^\circ$  and  $+45^\circ$  polarization beamforming, such that the gNB controls the rotation angle and eccentricity of the Rx polarization ellipse caused by the MPS-Beamforming at the UE side. The mechanism of adjusting the receive polarization ellipsis is illustrated in Fig. 3 considering a scenario without the loss of generality. Assuming the Rx antenna polarization angle,  $\tan^{-1}(\sqrt{\overline{XPD}^{Rx-Ant}})$ , is  $75^\circ$ , the best scenario of polarization matching is that the mean receive polarization angle in MPS-Beamforming,  $\tan^{-1}(\sqrt{\overline{XPD}^{MPS}})$ , is  $68^\circ$  in Fig. 3.  $\overline{XPD}^{Rx-Ant}$  and  $\overline{XPD}^{MPS}$  can have different values in general, relying on the wireless channel environment and the rotation of the Rx antenna caused by UE's movement.

The UE Rx reports PSI in terms of the mean receive XPD and XPR estimated at the UE along with the current mean receive polarization angle to the gNB by the feedback channel. The estimation of the mean Rx XPD and XPR can be performed based on dual-polarized antenna elements at the Rx with the support of reference signals. In turn, the gNB changes its transmit polarization angle or

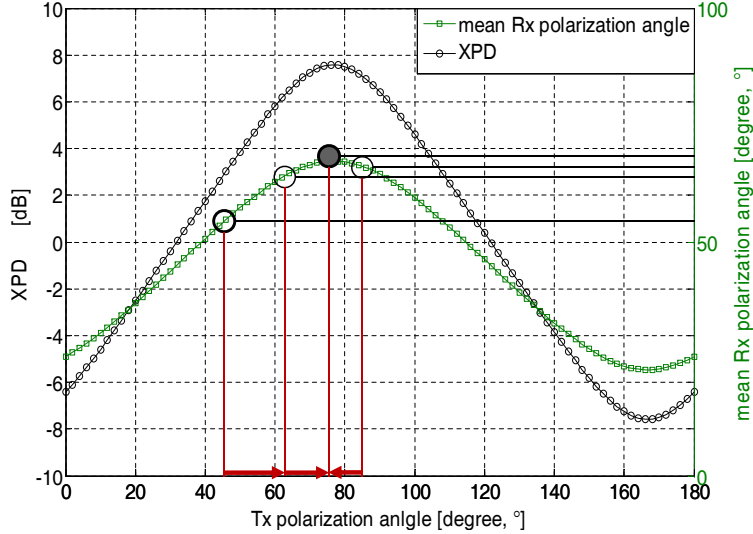


**FIGURE 3. Adjustment of rotation angle and eccentricity of the Rx polarization ellipse.**

transmit power ratio until the condition,  $\tan^{-1} \left( \sqrt{\overline{XPD}^{\text{MPS}}} \right) = \tan^{-1} \left( \sqrt{\overline{XPD}^{\text{Rx-Ant}}} \right)$ , equivalent to (21), or until  $\overline{XPD}^{\text{MPS}}$  approaches  $\overline{XPD}^{\text{Rx-Ant}}$  as closely as possible. The UE and gNB perform iterations of PSI feedback followed by the associated fine tuning of the transmit polarization angle or equivalently, transmit power ratio. The bin of increasing/decreasing transmit polarization angle in Fig. 3 can be dynamic depending on the difference between the reported current and previous mean receive polarization angles via the feedback channel. The sophisticated algorithm for the adjustment of the bin of increasing/decreasing the transmit polarization angle is outside of the scope and contribution of this paper; it is left for future work.

### Subcarrier Assignment for MPS-Beamforming

The novel scheme of the XPD/XPR-aware transmit power allocation with the ratio,  $\alpha_{\text{XPD/XPR}}$  and  $\beta_{\text{XPD/XPR}}$  in the MPS-Beamforming, is verified via comprehensive simulations in Result Section. One of the fundamental assumptions in this paper is the OFDM system, which is in agreement with the current commercial 5G and beyond-5G wireless communication system. The commercial OFDM system and the associated standards select and utilize the proportion of the whole subcarriers. In other words, the gNB assigns the proportion of whole subcarriers to each transmission for each UE or a group of UEs.

In the practical environment of the multipath fading or frequency selective fading channel,

**TABLE 1. MPS-Beamforming Subcarrier Assignment Algorithm**

Step	Execution
1	Among $N_{\text{total}}$ total number of subcarriers, screen out $\eta$ -percentile subcarriers that have the low channel gain. In the simulation of this paper $N_{\text{total}} = 2048$ , and $\eta = 35$ ; they can be adapted to the channel condition.
2	For the selected $(100 - \eta)$ -percentile subcarriers, estimate $\overline{\text{XPD}}^N$ , $\overline{\text{XPD}}^P$ , $\overline{\text{XPR}}^N$ and $\overline{\text{XPR}}^P$ . Estimate the XPD/XPR aware transmit power allocation ratio, $\alpha_{\text{XPD/XPR}}$ and $\beta_{\text{XPD/XPR}}$ based on (22)-(24).
3	Estimate $\overline{\text{XPD}}^{\text{MPS}}$ in (10) and (20), based on Step-2.
4	Select $N$ number of subcarriers that have the per-subcarrier XPD in MPS-Beamforming, $\text{XPD}_n^{\text{MPS}}$ in (46) closest to the estimated $\overline{\text{XPD}}^{\text{MPS}}$ in Step-3. $N$ is set to be 48 in the simulation of this paper, which is in agreement with the fundamental OFDM physical resource block (PRB) size in the current standards.

each subcarrier has different characteristics in terms of the channel gain and thus, Rx XPD and XPR. The subcarrier-dependent characteristics of the XPD/XPR should be coped with in the proposed MPS-Beamforming and transmit power allocation. Table 1 provides novel heuristic algorithm of XPD/XPR-aware OFDM subcarrier assignment to efficiently support the proposed MPS-Beamforming. It is noteworthy that the heuristic methodology has been regarded as an applaudable approach and frequently utilized in OFDM subcarrier and other resource allocation [40]. A single user is considered in this paper; meanwhile, multi-user (MU) OFDM will be considered for further elaborated subcarrier assignment scheme in future works.

As an additional metric based on which the gNB assigns subcarriers to the particular transmission, the per-subcarrier XPD,  $\text{XPD}_n^{\text{MPS}}$  for the subcarrier index,  $n$  is defined as.

$$\begin{aligned} \text{XPD}_n^{\text{MPS}} &= \frac{|\sqrt{\alpha E_s} H_n^{(-45^\circ, -45^\circ)} + \sqrt{\beta E_s} H_n^{(-45^\circ, 45^\circ)}|^2}{|\sqrt{\alpha E_s} H_n^{(45^\circ, -45^\circ)} + \sqrt{\beta E_s} H_n^{(45^\circ, 45^\circ)}|^2} \\ &= \frac{|\sqrt{\alpha} H_n^{(-45^\circ, -45^\circ)} + \sqrt{\beta} H_n^{(-45^\circ, 45^\circ)}|^2}{|\sqrt{\alpha} H_n^{(45^\circ, -45^\circ)} + \sqrt{\beta} H_n^{(45^\circ, 45^\circ)}|^2}. \end{aligned} \quad (46)$$

The subcarrier assignment algorithm in Table 1 is applied in the simulation for the results, and contributes to the improvement of the system performance in terms of SER; equivalently, in terms of energy efficiency or SNR gain for the target SER. The proposed MPS-Beamforming with the

novel XPD/XPR-aware transmit power allocation ratio and XPD/XPR-aware subcarrier assignment algorithm yields the best performance in terms of the SER among any combination of two Tx beams with  $\pm 45^\circ$  polarization including the scenario of single Tx beam transmission with either  $-45^\circ$  or  $45^\circ$  polarization corresponding to  $\alpha_{XPD/XPR} = 1$  or  $\alpha_{XPD/XPR} = 0$ , respectively.

# CHAPTER 4

## PR-MIMO SYSTEM

### System Model

The fundamental block diagram of the PR-MIMO system is shown in Fig. 4, where the Tx and the Rx have  $N_t$  and  $N_r$  antenna elements, respectively. Each antenna element is polarization reconfigurable with the polarization vector  $\vec{p}_{\text{Tx},j}$  and  $\vec{p}_{\text{Rx},i}$  in which  $j \in \{1, \dots, N_t\}; i \in \{1, \dots, N_r\}$ . The polarization vector is adjusted according to the channel state information (CSI); perfect CSI at all antenna elements is assumed to be available at the Rx (CSIR) as well as the Tx (CSIT). It is noteworthy that the CSI is available for both orthogonal polarization directions; it can be obtained through training schemes similar to those employed in antenna selection systems (see, e.g., [28]). The impact of imperfect CSI is outside the scope of this thesis and will be analyzed in future work.

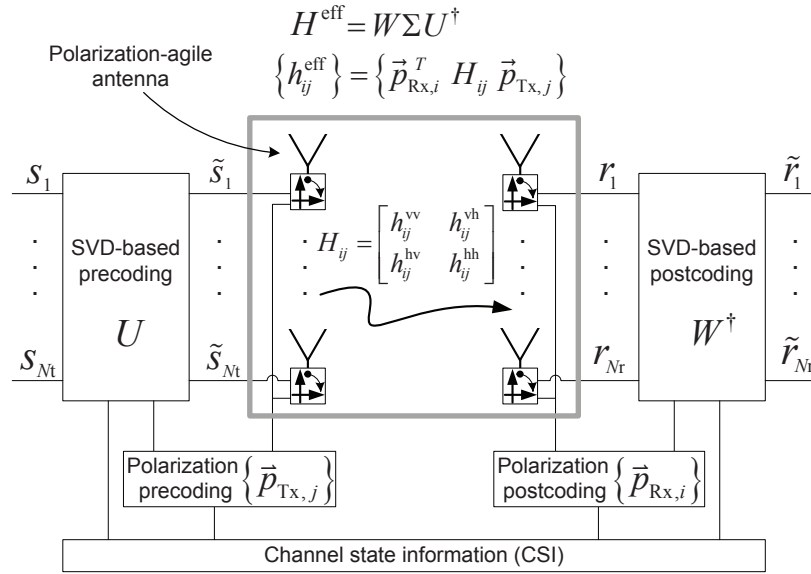


**FIGURE 4. PR-MIMO system with polarization reconfigurable antennas.**

In addition to the polarization precoding/postcoding, the PR-MIMO system contains precoding/postcoding that allows optimum exploitation of the spatial degree of freedom; it is well-known from conventional (non-polarization reconfigurable) spatial multiplexing systems with perfect CSI [41] that linear precoding/postcoding based on the (SVD) of the effective channel impulse matrix maximizes sum-rate. It is intuitive that exploiting polarization reconfigurable

antenna elements with polarization precoding/postcoding - on top of the standard SVD-based spatial precoding/postcoding - can achieve higher capacity than single-polarization or fixed-polarization antenna elements (with the same number of data streams or RF up/down-conversion chains). Mathematical derivations for this intuition are presented below.

The effective channel impulse response matrix in Fig. 4 can be expressed as

$$H^{\text{eff}} = \begin{bmatrix} \vec{p}_{\text{Rx},1}^T H_{11} \vec{p}_{\text{Tx},1} & \dots & \vec{p}_{\text{Rx},1}^T H_{1N_t} \vec{p}_{\text{Tx},N_t} \\ \vdots & \ddots & \vdots \\ \vec{p}_{\text{Rx},N_r}^T H_{N_r 1} \vec{p}_{\text{Tx},1} & \dots & \vec{p}_{\text{Rx},N_r}^T H_{N_r N_t} \vec{p}_{\text{Tx},N_t} \end{bmatrix}, \quad (47)$$

where the operation  $(\cdot)^T$  is the transpose of a given vector or matrix, and the dimension of  $H^{\text{eff}}$  is  $N_r \times N_t$ . Further,  $H_{ij}$  is denominated as “*polarization-basis matrix*” which is

$$H_{ij} = \begin{bmatrix} h_{ij}^{\text{vv}} & h_{ij}^{\text{vh}} \\ h_{ij}^{\text{hv}} & h_{ij}^{\text{hh}} \end{bmatrix}, \quad (48)$$

where  $h_{ij}^{xy}$  with  $x \in \{\text{v}, \text{h}\}; y \in \{\text{v}, \text{h}\}$  is the XY-channel impulse response from the Y-polarization Tx antenna to the X-polarization Rx antenna. For instance,  $h_{ij}^{\text{hv}}$  is the HV-channel impulse response from the vertically polarized (V-Pol) Tx antenna to the horizontally polarized (H-Pol) Rx antenna. It is assumed here a flat-fading channel, such that the  $h_{ij}^{xy}$  are complex scalars. Lastly,  $\vec{p}_{\text{Tx},j}$  and  $\vec{p}_{\text{Rx},i}$  are, respectively, the Tx-polarization vector at the  $j$ th Tx antenna and the Rx-polarization vector at the  $i$ th Rx antenna, and they are expressed as

$$\vec{p}_{\text{Tx},j} = \begin{bmatrix} p_{\text{Tx},j}^{\text{v}} \\ p_{\text{Tx},j}^{\text{h}} \end{bmatrix} = \begin{bmatrix} \cos \theta_j \\ \sin \theta_j \end{bmatrix}, \quad (49)$$

$$\vec{p}_{\text{Rx},i} = \begin{bmatrix} p_{\text{Rx},i}^{\text{v}} \\ p_{\text{Rx},i}^{\text{h}} \end{bmatrix} = \begin{bmatrix} \cos \theta_i \\ \sin \theta_i \end{bmatrix}. \quad (50)$$

Here, angles  $\theta_j$  and  $\theta_i$  are called Tx- and Rx-polarization angles, respectively. It is worth mentioning that Tx- and Rx-polarization vectors are unit vectors so that the overall signal power is

preserved after polarization precoding and postcoding.

### Polarization Precoding and Postcoding with Optimal Tx- and Rx-polarization

The Tx and the Rx can utilize SVD-based precoding and postcoding under the assumption of full CSIT and CSIR. The combination of SVD-based precoding and postcoding achieves the MIMO channel capacity for a given channel matrix via constructing parallel channels [41]. On the other hand, the MIMO communication system with polarization reconfigurable antennas in Fig. 4 can tune of the effective channel impulse response matrix  $H^{\text{eff}}$  itself in (47) by either polarization precoding at the Tx or polarization postcoding at the Rx; or joint polarization pre-post coding at both ends. We first focus on polarization precoding in this section.

The effective channel impulse response matrix can be decomposed by SVD as

$$H^{\text{eff}} = W\Sigma U^\dagger, \quad (51)$$

where  $\Sigma$  is a diagonal matrix containing singular values, and  $W$  and  $U^\dagger$  are unitary matrices composed of the left and right singular vectors, respectively [41]. In this paper,  $(\cdot)^\dagger$  is the Hermitian transpose operation. The channel capacity with SVD-based precoding and postcoding is

$$C = \sum_{k=1}^{R_{H^{\text{eff}}}} \log_2 \left( 1 + \frac{P_k}{\sigma_n^2} \sigma_k^2 \right), \quad (52)$$

where  $R_{H^{\text{eff}}}$  is the rank of the matrix  $H^{\text{eff}}$ , and  $P_k$  is the power allocated to the  $k$ th eigenmode. Further,  $\sigma_k$  is the  $k$ th singular value of the effective channel impulse response matrix  $H^{\text{eff}}$ , and  $\sigma_n^2$  is the noise power. Capacity maximization is achieved by a power allocation  $P_k$  that satisfies waterfilling conditions

$$P_k = \max \left( 0, \epsilon - \frac{\sigma_n^2}{\sigma_k^2} \right) \text{ s.t. } P = \sum_{k=1}^{R_{H^{\text{eff}}}} P_k, \quad (53)$$

i.e., the threshold  $\epsilon$  is determined by the constraint of the total transmitted power  $P$ . It is assumed that the total power is independent of the number of antennas.

Following [42], the Jensen's inequality is used to obtain

$$C \leq R_{H^{\text{eff}}} \log_2 \left( 1 + \frac{1}{R_{H^{\text{eff}}}} \sum_{k=1}^{R_{H^{\text{eff}}}} \frac{P_k}{\sigma_n^2} \sigma_k^2 \right) \quad (54)$$

$$= R_{H^{\text{eff}}} \log_2 \left( \frac{1}{R_{H^{\text{eff}}}} \frac{\epsilon}{\sigma_n^2} \sum_{k=1}^{R_{H^{\text{eff}}}} \sigma_k^2 \right), \quad (55)$$

where high SNR is assumed; all  $P_k$  is greater than zero, i.e.,  $P_k = \epsilon - \sigma_n^2 / \sigma_k^2 > 0$  in (53). Further,  $\sigma_k$  is the singular value of  $H^{\text{eff}}$ ; therefore [43],

$$\sum_{k=1}^{R_{H^{\text{eff}}}} \sigma_k^2 = \text{Tr} \left( H^{\text{eff}} (H^{\text{eff}})^{\dagger} \right) = \sum_{n,m} |h_{nm}^{\text{eff}}|^2. \quad (56)$$

This is the sum of squared envelopes of all channel impulse response elements in  $H^{\text{eff}}$ . This quantity is not only important for the upper bound of channel capacity, but will also play an important role in the polarization pre-post coding and antenna selection in PR-HS-MIMO systems.

It is worth emphasizing that each element of  $H^{\text{eff}}$  is affected by the Tx- and Rx-polarization as implied in (47). Hence, the polarization vectors at polarization reconfigurable antenna elements impact constructively or destructively the MIMO channel capacity itself, even though SVD-based precoding/postcoding reaches the MIMO channel capacity for the given full CSIR/CSIT. The  $j$ th Tx polarization-agile antenna affects the  $j$ th column in (47); thus, the sum of squared singular values in (56) can be written as

$$\begin{aligned} \sum_{k=1}^{R_{H^{\text{eff}}}} \sigma_k^2 &= \sum_{j=1}^{N_t} \sum_{i=1}^{N_r} \vec{p}_{\text{Tx},j}^T \left( H_{ij}^{\dagger} \vec{p}_{\text{Rx},i} \vec{p}_{\text{Rx},i}^T H_{ij} \right) \vec{p}_{\text{Tx},j} \\ &= \sum_{j=1}^{N_t} \vec{p}_{\text{Tx},j}^T H_{\text{Tx},j}^{\text{PD}} \vec{p}_{\text{Tx},j}, \end{aligned} \quad (57)$$

where the “Tx-polarization-determinant matrix” for the  $j$ th Tx polarization-agile antenna,  $H_{\text{Tx},j}^{\text{PD}}$ , is

defined as

$$H_{\text{Tx},j}^{\text{PD}} \triangleq \sum_{i=1}^{N_r} H_{ij}^\dagger \vec{p}_{\text{Rx},i} \vec{p}_{\text{Rx},i}^T H_{ij} . \quad (58)$$

The Tx-polarization vector at each Tx polarization-agile antenna is independent of those at other Tx-polarization antennas; therefore, the optimal Tx-polarization vector at the  $j$ th Tx polarization-agile antenna,  $\vec{p}_{\text{Tx},j}$ , is the one which maximizes  $\vec{p}_{\text{Tx},j}^T H_{\text{Tx},j}^{\text{PD}} \vec{p}_{\text{Tx},j}$  in (57).

From the viewpoint of the linear-algebraic approach,  $\vec{p}_{\text{Tx},j}^T H_{\text{Tx},j}^{\text{PD}} \vec{p}_{\text{Tx},j}$  is positive semi-definite; thus, the equation,  $\vec{p}_{\text{Tx},j}^T H_{\text{Tx},j}^{\text{PD}} \vec{p}_{\text{Tx},j} = c_j$  corresponds to the ellipse as portrayed in Fig. 5, where  $x$  and  $y$  coordinates correspond to the elements of  $\vec{p}_{\text{Tx},j}$ , i.e.,  $p_{\text{Tx},j}^v$  and  $p_{\text{Tx},j}^h$ , respectively [43]. Geometrically, the principal axes of the ellipse are along eigenvectors of the matrix  $H_{\text{Tx},j}^{\text{PD}}$ ,  $\vec{e}_1$  and  $\vec{e}_2$ , and the distances from the origin to the ellipse along the principal axes are  $c_j/\sqrt{\lambda_1^{\text{PD}}}$  and  $c_j/\sqrt{\lambda_2^{\text{PD}}}$ , where  $\lambda_1^{\text{PD}}$  and  $\lambda_2^{\text{PD}}$  are the eigenvalues of  $H_{\text{Tx},j}^{\text{PD}}$ .

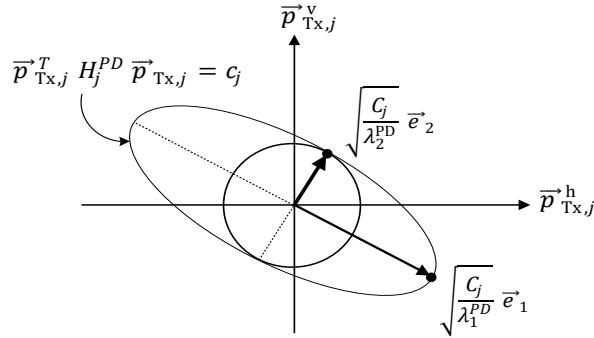


**FIGURE 5. Polarization-determinant ellipse and polarization-vector unit circle.**

The objective at this stage is to estimate the optimal Tx-polarization vector at each Tx polarization-agile antenna element,  $\vec{p}_{\text{Tx},j} \in j = \{1, \dots, N_t\}$ , which maximizes the column-sum of element-wise squared envelopes in  $H^{\text{eff}}$ , i.e.,  $\vec{p}_{\text{Tx},j}^T H_{\text{Tx},j}^{\text{PD}} \vec{p}_{\text{Tx},j}$ . On the other hand, the Tx-polarization vector  $\vec{p}_{\text{Tx},j}$  is on the unit circle as presented in (49); therefore, the ellipse must have, at least, one intersection or contact point with the unit circle; whereas, at the same time it must make  $\vec{p}_{\text{Tx},j}^T H_{\text{Tx},j}^{\text{PD}} \vec{p}_{\text{Tx},j} = c_j$  as large as it can. Hence, the optimal Tx-polarization vector  $\vec{p}_{\text{Tx},j}^{\text{opt}}$  and

corresponding optimal Tx-polarization angle  $\theta_j^{\text{opt}}$  described in (49) are as

$$\vec{p}_{\text{Tx},j}^{\text{opt}} = \arg \max_{\vec{p}_{\text{Tx},j}} \vec{p}_{\text{Tx},j}^T H_{\text{Tx},j}^{\text{PD}} \vec{p}_{\text{Tx},j} = \vec{e}_2, \quad (59)$$

$$\theta_j^{\text{opt}} = \arctan(\vec{e}_2). \quad (60)$$

Notice that  $\vec{e}_2$  is the eigenvector corresponding to  $\lambda_2$ , which is the maximum eigenvalue of the Tx-polarization-determinant matrix,  $H_{\text{Tx},j}^{\text{PD}}$ . In this manner, each Tx polarization-agile antenna element can perform polarization precoding with the optimal Tx-polarization vector.

In a completely analogous manner, the optimal RX-polarization vector can be derived; now, the row-sum (instead of the column-sum) of element-wise squared envelopes in  $H^{\text{eff}}$  have to be employed. The optimum polarization vector can be shown to be

$$\vec{p}_{\text{Rx},i}^{\text{opt}} = \arg \max_{\vec{p}_{\text{Rx},i}} \vec{p}_{\text{Rx},i}^T H_{\text{Rx},i}^{\text{PD}} \vec{p}_{\text{Rx},i} = \vec{e}_2, \quad (61)$$

$$\theta_i^{\text{opt}} = \arctan(\vec{e}_2), \quad (62)$$

where the “Rx-polarization-determinant matrix” for the  $i$ th Rx polarization-agile antenna,  $H_{\text{Rx},i}^{\text{PD}}$ , is defined as

$$H_{\text{Rx},i}^{\text{PD}} \triangleq \sum_{j=1}^{N_t} H_{ij} \vec{p}_{\text{Tx},j} \vec{p}_{\text{Tx},j}^T H_{ij}^\dagger. \quad (63)$$

### **Joint Polarization Pre-Post Coding for Polarization Matching**

The Tx-polarization-determinant matrix at the  $j$ th Tx polarization-agile antenna,  $H_{\text{Tx},j}^{\text{PD}}$ , depends on the Rx-polarization vectors  $\vec{p}_{\text{Rx},i}$  as shown in (58), and vice versa in (63). Further, Tx- and Rx-polarization mismatching will deteriorate the system performance in terms of the channel capacity in this paper. For those reasons, joint polarization pre-post coding is required to maximize PR-MIMO channel capacity.

Joint optimization of the pre-post coding is difficult to obtain in closed form (and also difficult to implement); therefore, an iterative approach is proposed, where one iteration is a sequential loop of polarization precoding; then polarization postcoding. In the  $q$ th iteration stage,  $\vec{p}_{\text{Tx},j}^{\text{opt},(q)}$  is

updated to  $\vec{p}_{\text{Tx},j}^{\text{opt},(q+1)}$  based on  $\vec{p}_{\text{Rx},i}^{\text{opt},(q)}$  according to (58) – (60). Then, in turn,  $\vec{p}_{\text{Rx},i}^{\text{opt},(q)}$  is updated to  $\vec{p}_{\text{Rx},i}^{\text{opt},(q+1)}$  based on the updated  $\vec{p}_{\text{Tx},j}^{\text{opt},(q)}$  following (61) – (63). If initial values of Rx and Tx polarization vectors are

$$\vec{p}_{\text{Tx},j}^{(0)} = \begin{bmatrix} p_{\text{Tx},j}^{\text{v}} \\ p_{\text{Tx},j}^{\text{h}} \end{bmatrix} = \begin{bmatrix} 1 \\ 0 \end{bmatrix}, \quad (64)$$

$$\vec{p}_{\text{Rx},i}^{(0)} = \begin{bmatrix} p_{\text{Rx},i}^{\text{v}} \\ p_{\text{Rx},i}^{\text{h}} \end{bmatrix} = \begin{bmatrix} 1 \\ 0 \end{bmatrix}, \quad (65)$$

the joint optimization iteration is expressed as

$$\vec{p}_{\text{Tx},j}^{\text{opt},(q+1)} = \arg \max_{\vec{p}_{\text{Tx},j}} \vec{p}_{\text{Tx},j}^T H_{\text{Tx},j}^{\text{PD},(q+1)} \vec{p}_{\text{Tx},j} \quad (66)$$

$$H_{\text{Tx},j}^{\text{PD},(q+1)} = \sum_{i=1}^{N_r} H_{ij}^{\dagger} \vec{p}_{\text{Rx},i}^{(q)} \vec{p}_{\text{Rx},i}^{T(q)} H_{ij}. \quad (67)$$

$$\vec{p}_{\text{Rx},i}^{\text{opt},(q+1)} = \arg \max_{\vec{p}_{\text{Rx},i}} \vec{p}_{\text{Rx},i}^T H_{\text{Rx},i}^{\text{PD},(q+1)} \vec{p}_{\text{Rx},i} \quad (68)$$

$$H_{\text{Rx},i}^{\text{PD},(q+1)} = \sum_{j=1}^{N_t} H_{ij}^{\dagger} \vec{p}_{\text{Tx},j}^{(q)} \vec{p}_{\text{Tx},j}^{T(q)} H_{ij}, \quad (69)$$

$$h_{\text{opt},ij}^{\text{eff}} = (\vec{p}_{\text{Rx},i}^{\text{opt},(q+1)})^T H_{ij} \vec{p}_{\text{Tx},j}^{\text{opt},(q+1)}, \quad (70)$$

where  $q$  is the iteration index. Note that while each step increases the capacity, the procedure is not guaranteed to reach the *global* optimum. However, as will be shown by Chapter 8, the capacity resulted from the iterative joint pre-post coding is in a close agreement with the one achieved by brute-force numerical search over all pre-post coding vectors.

# CHAPTER 5

## PR-HS/MIMO AND PR-HS/MRT

### PR-HS/MIMO System Model

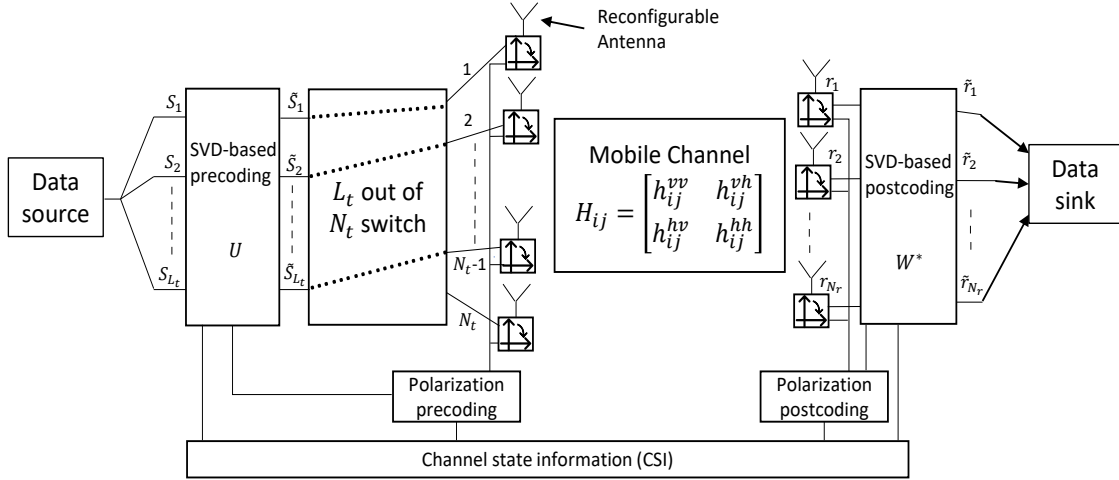


**FIGURE 6. System Model of Antenna Selection with Reconfigurable Antennas**

This section delineates the PR-HS/MIMO and PR-HS/MRT communication system that performs spatial multiplexing with the selected antenna elements as depicted in Fig. 6. For PR-HS/MIMO system, the Tx selects  $L_t$  out of  $N_t$  polarization reconfigurable Tx antenna elements, and performs spatial multiplexing based on SVD-based precoding and postcoding. For PR-HS/MRT system, the Tx selects  $L_t$  out of  $N_t$  polarization reconfigurable Tx antenna elements to perform MRT, while Rx does MRC. Each antenna element is polarization reconfigurable and adjusted to an optimal polarization angle based on the joint polarization pre-post coding proposed and described in the previous section. In the same fashion as the PR-MIMO system, this section assumes perfect CSI. That is, both the Tx and Rx have perfect knowledge of the polarization-basis matrix in (47) – (48).

The partial channel impulse response matrix that represents the channels between selected polarization reconfigurable Tx antenna elements and Rx antenna elements is defined as  $\tilde{H}_k^{\text{eff}}$ , where the index  $k \in \{1, 2, \dots, \binom{N_t}{L_t}\}$  stands for the  $k$ -th subset of  $L_t$  number of antenna selection. Further, the column index matrix  $C_{\text{Index}}$  indicates the list of all possible combination of selected Tx antenna

elements. That is,

$$C_{\text{Index}} = \begin{bmatrix} \alpha_{11} & \dots & \alpha_{1L_t} \\ & \vdots & \\ \alpha_{(N_t)1} & \dots & \alpha_{(N_t)L_t} \end{bmatrix}, \quad (71)$$

where each row represents a subset of polarization reconfigurable Tx antenna indices corresponding to the selected antenna elements.

Each  $\tilde{H}_k^{\text{eff}}$  consists of  $L_t$  selected columns of  $H^{\text{eff}}$ , associated with the selected polarization reconfigurable Tx antenna elements, and is described as

$$\tilde{H}_k^{\text{eff}} = \begin{bmatrix} \vec{p}_{\text{Rx},1}^T H_{1\alpha_{k1}} \vec{p}_{\text{Tx},\alpha_{k1}} & \dots & \vec{p}_{\text{Rx},1}^T H_{1\alpha_{kL_t}} \vec{p}_{\text{Tx},\alpha_{kL_t}} \\ \vdots & \ddots & \vdots \\ \vec{p}_{\text{Rx},N_r}^T H_{N_r\alpha_{k1}} \vec{p}_{\text{Tx},\alpha_{k1}} & \dots & \vec{p}_{\text{Rx},N_r}^T H_{N_r\alpha_{kL_t}} \vec{p}_{\text{Tx},\alpha_{kL_t}} \end{bmatrix}, \quad (72)$$

where  $k \in \{1, 2, \dots, \binom{N_t}{L_t}\}$  corresponds to the  $k$ -th row of the column index matrix  $C_{\text{Index}}$ . From (52) – (56), the achievable PR-HS/MIMO channel capacity for  $\tilde{H}_k^{\text{eff}}$  in (72),  $C_{\text{PR-HS/MIMO},k}$  is

$$C_{\text{PR-HS/MIMO},k} = \sum_{i=1}^{R_{\tilde{H}_k^{\text{eff}}}} \log_2 \left( 1 + \frac{P_i}{\sigma_n^2} \tilde{\sigma}_i^2 \right) \leq R_{\tilde{H}_k^{\text{eff}}} \log_2 \left( \frac{1}{R_{\tilde{H}_k^{\text{eff}}}} \frac{\epsilon}{\sigma_n^2} \sum_{i=1}^{R_{\tilde{H}_k^{\text{eff}}}} \tilde{\sigma}_i^2 \right), \quad (73)$$

where the sum of squared singular values,  $\sum_{i=1}^{R_{\tilde{H}_k^{\text{eff}}}} \tilde{\sigma}_i^2$  in (73) is further elaborated as

$$\begin{aligned} \gamma_{\text{sum},k} &= \sum_{i=1}^{R_{\tilde{H}_k^{\text{eff}}}} \gamma_i = \sum_{i=1}^{R_{\tilde{H}_k^{\text{eff}}}} \tilde{\sigma}_i^2 \\ &= \text{Tr} \left( \tilde{H}_k^{\text{eff}} \tilde{H}_k^{\text{eff}\dagger} \right) = \sum_{n,m} \left| \tilde{h}_{k,nm}^{\text{eff}} \right|^2. \end{aligned} \quad (74)$$

The objective is selecting the column index  $k$  that maximize PR-HS/MIMO channel capacity,  $C_{\text{PR-HS/MIMO},k}$ .

Whereas with PR-HS-MRT, the achievable effective SNR is obtained based on SVD of  $\tilde{H}_k^{\text{eff}}$  in

(72) as

$$\gamma_{\text{PR-HS/MRT}}^{\text{eff}} = \max_k (\tilde{\sigma}_{k,\max}^2), \quad (75)$$

where  $\tilde{\sigma}_{k,\max}^2$  is a maximum eigenvalue of  $\tilde{H}_k^{\text{eff}} \tilde{H}_k^{\text{eff}\dagger}$  [30]. The objective is selecting the column index  $k$  that maximize  $\tilde{\sigma}_{k,\max}^2$ . Therefore, the achievable PR-HS/MRT channel capacity using (75) is expressed as

$$C_{\text{PR-HS/MRT},k} = \log_2 \left( 1 + \frac{P}{\sigma_n^2} \gamma_{\text{PR-HS/MRT}}^{\text{eff}} \right). \quad (76)$$

Furthermore, in the case of quadrature phase shift keying (QPSK) modulation, the instantaneous SER is expressed as

$$SER_n = 1 - \left[ 1 - Q \left( \sqrt{\frac{P}{\sigma_n^2} \left( \gamma_{\text{PR-HS/MRT}}^{\text{eff}} \right)_n} \right) \right]^2, \quad (77)$$

where  $n = 1, 2, \dots, N$  and  $N$  is total number of channel realizations. Finally, average SER is represented as

$$\overline{SER} = \frac{1}{N} \sum_{n=1}^N SER_n. \quad (78)$$

For further theoretical derivation,

$$\tilde{H}_k^{\text{eff}} \tilde{H}_k^{\text{eff}\dagger} = \begin{bmatrix} \vec{p}_{\text{Rx},1}^T H_{\text{Rx},1}^{\text{PD}} \vec{p}_{\text{Rx},1} & \dots & \vec{p}_{\text{Rx},1}^T H_{\text{Rx},1\text{N_r}}^{\text{Off}} \vec{p}_{\text{Rx},\text{N_r}} \\ \vdots & \ddots & \vdots \\ \vec{p}_{\text{Rx},\text{N_r}}^T H_{\text{Rx},\text{N_r}1}^{\text{Off}}, \vec{p}_{\text{Rx},1} & \dots & \vec{p}_{\text{Rx},\text{N_r}}^T H_{\text{Rx},\text{N_r}}^{\text{PD}}, \vec{p}_{\text{Rx},\text{N_r}} \end{bmatrix},$$

where

$$H_{\text{Rx},ij}^{\text{Off}} = \sum_{j=1}^{L_t} H_{ia_{ij}} \vec{p}_{\text{Tx},a_{ij}} \vec{p}_{\text{Tx},a_{ij}}^T H_{ja_{ij}}^\dagger \quad (79)$$

is the polarization determinant matrix of *off-diagonal* components. The algorithm to maximize the diagonal components of the matrix is described in (61) – (62). As described in Section 4, the

algorithm maximizes the sum of squared singular values of  $\tilde{H}_k^{\text{eff}}$  presented in (74), which significantly improves the channel capacity.

In this chapter, two schemes of PR-HS to efficiently achieve polarization reconfigurable antenna selection is proposed. One of the primary contributions of the thesis is enhancing the PR-HS/MIMO channel capacity,  $C_{\text{PR-HS/MIMO},k}$  and PR-HS/MRT channel capacity,  $C_{\text{PR-HS/MRT}}$  and PR-HS/MRT SER based on the two proposed schemes. In both schemes, it is worth of mentioning that, for PR-HS/MIMO, antenna index set associated with  $k$ , which has the greatest  $C_{\text{PR-HS/MIMO},k}$  in (73) can be determined; or its upper bound via comparing the sum of squared singular values,  $\gamma_{\text{sum},k} = \sum_{i=1}^{R_{\tilde{H}_k^{\text{eff}}}} \gamma_i$  in (74) can be determined, based on the trade-off between accuracy and complexity/computation time. For instance, in the scenario where  $N_t = 8$  as in the simulation, after performing joint polarization pre-post coding for each  $\tilde{H}_k^{\text{eff}}$ , the PR-HS/MIMO channel capacity,  $C_{\text{PR-HS/MIMO},k}$  can be directly considered to determine the set of  $L_t$  Tx antenna elements. Meanwhile, in the scenario of numerous antenna elements, e.g.,  $N_t = 64$ , as in a 5G and beyond-5G gNB antenna panel [13],[34]–[36], considering the sum of squared singular values,  $\gamma_{\text{sum},k}$  for PR-HS at the Tx may be the better option with respect to the complexity.

### **Scheme-1: Element-Wise Polarization Reconfiguration**

Polarization pre-post coding is accomplished with  $\tilde{H}_k^{\text{eff}}$  for each  $k \in \{1, 2, \dots, \binom{N_t}{L_t}\}$ , corresponding to the Tx antenna indices in  $k$ -th row of (71), in element-wise polarization reconfiguration. Based on the estimated optimal polarization vectors for each  $\tilde{H}_k^{\text{eff}}$ , the best  $k$  in terms of the greatest PR-HS/MIMO channel capacity,  $C_{\text{PR-HS/MIMO},k}$ , is selected as  $L_t$  Tx antenna elements. As aforementioned, in the scenario where the complexity crucially affects the overall system performance, the sum of squared singular values,  $\gamma_{\text{sum},k} = \sum_{i=1}^{R_{\tilde{H}_k^{\text{eff}}}} \gamma_i$  in (74) may be considered to determine the  $L_t$  antenna elements. The Scheme-1 is denominated as *element-wise* (*EW*) polarization reconfiguration, since optimal polarization vectors of every  $\tilde{H}_k^{\text{eff}}$  for

$k \in \{1, 2, \dots, \binom{N_t}{L_t}\}$  is estimated. The EW optimal Rx-polarization vectors are defined as

$$\vec{p}_{\text{Rx},i}^{\text{EW}} = \arg \max_{\vec{p}_{\text{Rx},i}} \vec{p}_{\text{Rx},i}^T H_{\text{Rx},i}^{\text{EW}} \vec{p}_{\text{Rx},i}, \quad (80)$$

$$H_{\text{Rx},i}^{\text{EW}} = \sum_{j=1}^{L_t} H_{i\alpha_{ij}} \vec{p}_{\text{Tx},\alpha_{ij}} \vec{p}_{\text{Tx},\alpha_{ij}}^T H_{i\alpha_{ij}}^\dagger, \quad (81)$$

where (81) is *EW Rx-polarization-determinant matrix*. In a similar manner, the optimal polarization vectors at the Tx are described as

$$\vec{p}_{\text{Tx},\alpha_{ij}}^{\text{EW}} = \arg \max_{\vec{p}_{\text{Tx},\alpha_{ij}}} \vec{p}_{\text{Tx},\alpha_{ij}}^T H_{\text{Tx},\alpha_{ij}}^{\text{EW}} \vec{p}_{\text{Tx},\alpha_{ij}}, \quad (82)$$

$$H_{\text{Tx},\alpha_{ij}}^{\text{EW}} = \sum_{i=1}^{N_r} H_{i\alpha_{ij}}^\dagger \vec{p}_{\text{Rx},i} \vec{p}_{\text{Rx},i}^T H_{i\alpha_{ij}} \quad (83)$$

where (83) is *EW Tx-polarization-determinant matrix*. With (80) and (82), each  $\tilde{H}_k^{\text{eff}}$  is tuned with corresponding EW Tx/Rx-polarization vectors. That is,

$$\tilde{H}_{\text{EW},k}^{\text{eff}} = \begin{bmatrix} (\vec{p}_{\text{Rx},1}^{\text{EW}})^T H_{1\alpha_{k1}} \vec{p}_{\text{Tx},\alpha_{k1}}^{\text{EW}} \dots (\vec{p}_{\text{Rx},1}^{\text{EW}})^T H_{1\alpha_{kL_t}} \vec{p}_{\text{Tx},\alpha_{kL_t}}^{\text{EW}} \\ \vdots \quad \ddots \quad \vdots \\ (\vec{p}_{\text{Rx},N_r}^{\text{EW}})^T H_{N_r\alpha_{k1}} \vec{p}_{\text{Tx},\alpha_{k1}}^{\text{EW}} \dots \vec{p}_{\text{Rx},N_r}^{\text{EW}} H_{N_r\alpha_{kL_t}} \vec{p}_{\text{Tx},\alpha_{kL_t}}^{\text{EW}} \end{bmatrix}.$$

Besides the EW polarization reconfiguration scheme, as aforementioned in this section, two metrics are also proposed, PR-HS/MIMO channel capacity  $C_{\text{PR-HS/MIMO},k}^{\text{EW}}$  and the sum of squared singular values  $\gamma_{\text{sum},k}^{\text{EW}}$  to determine the estimated best set of  $L_t$  Tx antenna elements corresponding to  $k$ . The metrics are expressed as

$$C_{\text{PR-HS/MIMO},k}^{\text{EW}} = \sum_{i=1}^{R_{\tilde{H}_{\text{EW},k}^{\text{eff}}}} \log_2 \left( 1 + \frac{P_i}{\sigma_n^2} \tilde{\sigma}_i^2 \right), \quad (84)$$

$$\gamma_{\text{sum},k}^{\text{EW}} = \sum_{i=1}^{R_{\tilde{H}_{\text{EW},k}^{\text{eff}}}} \gamma_i = \sum_{i=1}^{R_{\tilde{H}_{\text{EW},k}^{\text{eff}}}} \tilde{\sigma}_i^2 = \sum_{n,m} \left| \tilde{h}_{k,nm}^{\text{eff}} \right|^2. \quad (85)$$

For PR-HS/MRT, the achievable SNR with (84) is expressed as

$$\gamma_{\text{PR-HS/MRT}}^{\text{EW}} = \max_k (\tilde{\sigma}_{k,\max}^{\text{EW}})^2. \quad (86)$$

### Scheme-2: Global Polarization Reconfiguration

This section provides another PR-HS/MIMO spatial multiplexing scheme PR-HS/MRT scheme with successful performance but less complexity than the EW polarization reconfiguration scheme presented in PR-MIMO section. The scheme of global polarization reconfiguration first, estimates the optimal polarization vectors based on the proposed polarization pre-post coding in Section 4 with the full  $N_r \times N_t$  channel impulse response matrix regardless of  $L_t$ , the number of Tx antenna elements to be selected. To reduce the complexity of PR-HS processing, the global effective channel impulse response matrix  $H^{\text{eff}}$  rather than any partial channel impulse response matrix  $\tilde{H}_k^{\text{eff}}$ , is taken into account such that  $L_t$  Tx antenna elements are selected to maximize the metric, PR-HS/MIMO channel capacity or the sum of squared singular values. Hence, the optimal Tx- and Rx-polarization vectors are aligned with (59) – (62). For this reason, Scheme-2 is denominated as *Global* polarization reconfiguration; for the consistency, the optimal Tx- and Rx- polarization vectors of Scheme-2 are, respectively, expressed as

$$\vec{p}_{\text{Tx},j}^{\text{G}} = \vec{p}_{\text{Tx},j}^{\text{opt}}, \quad \vec{p}_{\text{Rx},i}^{\text{G}} = \vec{p}_{\text{Rx},i}^{\text{opt}}. \quad (87)$$

The partial channel impulse response matrix associated with the selected  $L_t$  polarization reconfigurable Tx antenna elements,  $\tilde{H}_{\text{G},k}^{\text{eff}}$  can be described as

$$\tilde{H}_{\text{G},k}^{\text{eff}} = \begin{bmatrix} (\vec{p}_{\text{Rx},1}^{\text{G}})^T H_{1\alpha_{k1}} \vec{p}_{\text{Tx},\alpha_{k1}}^{\text{G}} & \cdots & (\vec{p}_{\text{Rx},1}^{\text{G}})^T H_{1\alpha_{kL_t}} \vec{p}_{\text{Tx},\alpha_{kL_t}}^{\text{G}} \\ \vdots & \ddots & \vdots \\ (\vec{p}_{\text{Rx},N_r}^{\text{G}})^T H_{N_r\alpha_{k1}} \vec{p}_{\text{Tx},\alpha_{k1}}^{\text{G}} & \cdots & (\vec{p}_{\text{Rx},N_r}^{\text{G}})^T H_{N_r\alpha_{kL_t}} \vec{p}_{\text{Tx},\alpha_{kL_t}}^{\text{G}} \end{bmatrix}.$$

In the same fashion as EW polarization reconfiguration, Scheme-2 also consider either PR-HS/MIMO channel capacity  $C_{\text{PR-HS/MIMO},k}^{\text{G}}$  or the sum of squared singular values  $\gamma_{\text{sum},k}^{\text{G}}$  to determine the estimated best set of  $L_t$  Tx antenna elements corresponding to the index  $k$ , which are

$$C_{\text{PR-HS/MIMO},k}^G = \sum_{i=1}^{R_{\tilde{H}_{G,k}^{\text{eff}}}} \log_2 \left( 1 + \frac{P_i}{\sigma_n^2} \tilde{\sigma}_i^2 \right), \quad (88)$$

$$\gamma_{\text{sum},k}^G = \sum_{i=1}^{R_{\tilde{H}_{G,k}^{\text{eff}}}} \gamma_i = \sum_{i=1}^{R_{\tilde{H}_{G,k}^{\text{eff}}}} \tilde{\sigma}_i^2 = \sum_{n,m} \left| \tilde{h}_{k,nm}^{\text{eff}} \right|^2. \quad (89)$$

Further, for PR-HS/MRT, the achievable SNR with (88) is described as

$$\gamma_{\text{PR-HS/MRT}}^G = \max_k (\tilde{\sigma}_{k,\max}^G)^2. \quad (90)$$

### Comparison of Two Schemes

The upper bound of PR-HS/MIMO channel capacity for the considered  $L_t$  Tx antenna elements corresponding to  $k$  in (73) includes the associated sum of squared singular values,  $\gamma_{\text{sum},k}^{\text{EW}}$  in (85) or  $\gamma_{\text{sum},k}^G$  in (89) for EW or global polarization reconfiguration schemes, respectively. Furthermore, the joint polarization pre-post coding is also accomplished based on this metric as elaborated in PR-MIMO section. Hence, it is worth of comparing  $\gamma_{\text{sum},k}^{\text{EW}}$  with  $\gamma_{\text{sum},k}^G$  resulted by EW and global polarization reconfiguration schemes for the considered  $k$  in Sections 5 and 5, respectively.

$\gamma_{\text{sum},k}^{\text{EW}}$  is the sum of squared singular values for  $\tilde{H}_{\text{EW},k}^{\text{eff}}$ ; equivalently, the sum of eigenvalues for  $\tilde{H}_{\text{EW},k}^{\text{eff}} \tilde{H}_{\text{EW},k}^{\text{eff} \dagger}$  that is described as

$$\tilde{H}_{\text{EW},k}^{\text{eff}} \tilde{H}_{\text{EW},k}^{\text{eff} \dagger} = \begin{bmatrix} (\vec{p}_{\text{Rx},1}^{\text{EW}})^T H_{\text{Rx},1}^{\text{EW}} \vec{p}_{\text{Rx},1}^{\text{EW}} & \dots & (\vec{p}_{\text{Rx},1}^{\text{EW}})^T H_{\text{Rx},1N_r}^{\text{Off}} \vec{p}_{\text{Rx},N_r}^{\text{EW}} \\ \vdots & \ddots & \vdots \\ (\vec{p}_{\text{Rx},N_r}^{\text{EW}})^T H_{\text{Rx},N_r1}^{\text{Off}} \vec{p}_{\text{Rx},1}^{\text{EW}} & \dots & (\vec{p}_{\text{Rx},N_r}^{\text{EW}})^T H_{\text{Rx},N_r}^{\text{EW}} \vec{p}_{\text{Rx},N_r}^{\text{EW}} \end{bmatrix}$$

On the other hand,  $\gamma_{\text{sum},k}^G$  is the sum of eigenvalues for  $\tilde{H}_{G,k}^{\text{eff}} \tilde{H}_{G,k}^{\text{eff} \dagger}$  that is expressed as

$$\tilde{H}_{G,k}^{\text{eff}} \tilde{H}_{G,k}^{\text{eff} \dagger} = \begin{bmatrix} (\vec{p}_{\text{Rx},1}^G)^T H_{\text{Rx},1}^G \vec{p}_{\text{Rx},1}^G & \dots & (\vec{p}_{\text{Rx},1}^G)^T H_{\text{Rx},1N_r}^{\text{Off}} \vec{p}_{\text{Rx},N_r}^G \\ \vdots & \ddots & \vdots \\ (\vec{p}_{\text{Rx},N_r}^G)^T H_{\text{Rx},N_r1}^{\text{Off}} \vec{p}_{\text{Rx},1}^G & \dots & (\vec{p}_{\text{Rx},N_r}^G)^T H_{\text{Rx},N_r}^G \vec{p}_{\text{Rx},N_r}^G \end{bmatrix},$$

where the *global Rx-polarization-determinant matrix*,  $H_{\text{Rx},i}^G$  is

$$H_{\text{Rx},i}^G = \sum_{j=1}^{L_t} H_{i\alpha_{ij}} \vec{p}_{\text{Tx},\alpha_{ij}} \vec{p}_{\text{Tx},\alpha_{ij}}^T H_{i\alpha_{ij}}^\dagger. \quad (91)$$

The diagonal components of (91) are maximized with EW polarization reconfiguration, since  $\tilde{H}_{\text{EW},k}^{\text{eff}}$  is tuned for each  $k$  according to its optimal polarization vectors, as described in (80) – (83). Hence,  $\gamma_{\text{sum},k}^{\text{EW}}$  is maximized. Meanwhile, polarization vectors in global polarization reconfiguration are optimized for the full channel impulse response matrix,  $H^{\text{eff}}$  regardless of  $k$ ; therefore, diagonal components of (91) are not maximized for  $L_t < N_t$ . That is, those diagonal elements are aligned with (59) – (62), which maximizes diagonal elements of  $H^{\text{eff}}(H^{\text{eff}})^\dagger$ . Nonetheless, global polarization reconfiguration also successfully increases the sum of squared singular values,  $\gamma_{\text{sum},k}^G$  for the considered  $k$  with less complexity than EW polarization reconfiguration even when applied to each  $\tilde{H}_{\text{G},k}^{\text{eff}}$ . Further, as  $L_t$  approaches  $N_t$ ,  $\tilde{H}_{\text{EW},k}^{\text{eff}}$  approaches  $\tilde{H}_{\text{G},k}^{\text{eff}}$ . Although EW polarization reconfiguration outperforms global polarization reconfiguration, the latter offers an advantage in the complexity and the corresponding computation time.

# CHAPTER 6

## EFFECT OF POLARIZATION ON THE CHANNEL

### Random Polarization Vectors

One of the primary contributions of this paper is the statistical analysis of the polarization reconfigurable wireless channels for the scenario of PR-MIMO, PR-HS/MIMO and PR-HS/MRT. This section analyzes the impact of deploying polarization reconfigurable antenna elements on the conventional MIMO system. Random polarization is first considered; then, the impact of the proposed polarization pre-post coding on the MIMO channel is scrutinized. The elements of polarization-basis matrix, described in (48), are modeled as independent and identically distributed (i.i.d.) complex Gaussian random variables with zero mean and unit variance. Each element of  $H^{\text{eff}}$  can be expressed as

$$\begin{aligned}
 h_{ij}^{\text{eff}} &= \vec{p}_{\text{Rx},i}^T \begin{bmatrix} h_{ij}^{\text{vv}} & h_{ij}^{\text{vh}} \\ h_{ij}^{\text{hv}} & h_{ij}^{\text{hh}} \end{bmatrix} \vec{p}_{\text{Tx},j} \\
 &= h_{ij}^{\text{vv}} \cos(\theta_j) \cos(\theta_i) + h_{ij}^{\text{hv}} \sin(\theta_i) \cos(\theta_j) + h_{ij}^{\text{vh}} \cos(\theta_i) \sin(\theta_j) + h_{ij}^{\text{hh}} \sin(\theta_j) \sin(\theta_i). \\
 &= \beta_1 + \beta_2 + \beta_3 + \beta_4 .
 \end{aligned} \tag{92}$$

For convenience, the four terms in (92) are abbreviated as  $\beta_1, \beta_2, \beta_3$  and  $\beta_4$ , respectively, in the order of the expression in (92). Considering the random movement and rotation of the UE along with depolarization of the wireless channel itself [26],[44], the probability density function (pdf) of the polarization angles,  $f_{\Theta}(\theta)$  can be expressed as

$$f_{\Theta}(\theta) = \begin{cases} \frac{1}{2\pi}, & \text{if } \theta \in [-\pi, \pi]. \\ 0, & \text{otherwise.} \end{cases} \tag{93}$$

The random variable,  $\Theta \sim U(-\pi, \pi)$ , can be transformed to  $Y = \cos(\Theta)$  and  $X = \sin(\Theta)$ . The

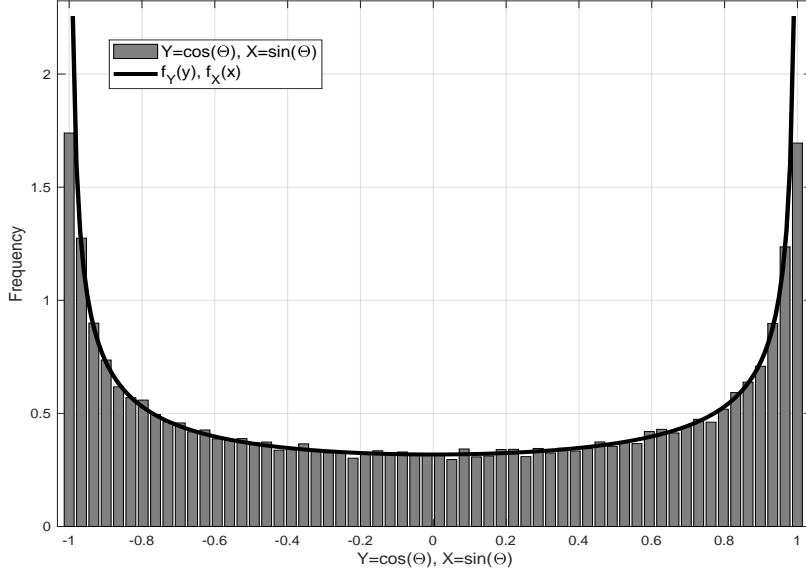


**FIGURE 7. Distribution of the elements in polarization vector:  $Y = \cos(\Theta)$  and  $X = \sin(\Theta)$ .**

cumulative distribution functions (cdf's) of  $\Theta$  and  $Y = \cos(\Theta)$ , i.e.,  $F_\Theta$  and  $F_Y$ , respectively, are as

$$F_\Theta(\theta) = \frac{\theta}{\pi}, \quad F_Y(y) = \frac{\arccos(y)}{\pi}. \quad (94)$$

Based on (94) the pdf of  $Y$ ,  $f_Y$  is derived; in the similar fashion, the pdf of  $X = \sin(\Theta)$ ,  $f_X$  is obtained as

$$f_Y(y) = \frac{1}{\pi} \frac{1}{\sqrt{1-y^2}}, \quad f_X(x) = \frac{1}{\pi} \frac{1}{\sqrt{1-x^2}}. \quad (95)$$

The distributions of  $Y = \cos(\Theta)$  and  $X = \sin(\Theta)$  are portrayed in Fig. 7, where  $\Theta$  is independently generated  $10^6$  times. The curve fitting of the empirical distribution exhibits excellent agreement with the theoretical analysis in (95).

The mean and variance of (95) are 0 and  $1/2$ , respectively; furthermore, the variance of  $h^{\text{eff}}$  is

$$\text{Var}(h_{ij}^{\text{eff}}) = \text{Var}(\beta_1) + \text{Var}(\beta_2) + \text{Var}(\beta_3) + \text{Var}(\beta_4). \quad (96)$$

Owing to the page limit, the extensive description of deriving expectation and variance of (95) as well as (96) is provided in Appendix A. Three terms in each  $\beta_i$  for  $i \in \{1, 2, 3, 4\}$  are independent of

each other. Thus, the variance of the real and imaginary parts in  $\beta_i$  is  $\frac{1}{2} \times \frac{1}{2} \times \frac{1}{2} = \frac{1}{8}$ ; consequently,  $h_{ij}^{\text{eff}}$  has unit variance as described in detail in Appendix A. It is noteworthy that the mean and variance of reconfigurable antennas with random channel polarization are the same as those of conventional channels without polarization reconfigurable antenna elements. Furthermore, the squared envelope of  $h_{ij}^{\text{eff}}$ , with random polarization, follows chi-square distribution with 2 degrees of freedom.

### Optimal Polarization Vectors

It is worth emphasizing that the combination of polarization reconfiguration and hybrid antenna selection, i.e., PR-HS can provide significant improvement in effective channel gain, i.e., the squared envelop of  $h_{ij}^{\text{eff}}$ . The proposed polarization pre-post coding scheme is based on the closed-form derivation for the optimal polarization vectors at one end; whereas, the optimal polarization vectors at both ends of the Tx and Rx are achieved by the iterative methodology. For this reason, the complete analysis to reach the closed-form description is unfeasible. However, the comprehensive simulation results in Figs. 8 – 9 show that the proposed PR-HS scheme substantially improves the system performance in terms of SNR, channel capacity and the associated distribution of channel gain. Empirical distributions of channel gain, i.e.,  $|h_{ij}^{\text{eff}}|^2$  are depicted in Fig. 8, where the PR-MIMO system applies hybrid antenna selection, i.e., PR-HS-MIMO with  $N_t = 8$  and  $L_t \in \{1, 2, \dots, 8\}$ . As  $L_t$  decreases from  $L_t = 8$  to  $L_t = 1$ , i.e., the number of residual antennas,  $N_t - L_t$  increases, the distribution of  $|h_{ij}^{\text{eff}}|^2$  and the corresponding average exhibit the significant improvement in channel gain.

As  $L_t$  increases to reach  $N_t = 8$ , the empirical histogram converge to chi-square distribution with 4 degrees of freedom. It is noteworthy that the channel gain, i.e., the squared envelope of the channel coefficient in conventional MIMO systems, has chi-square distribution with 2 degrees of freedom; whereas, PR-MIMO systems without hybrid antenna selection have 4 degrees of freedom. The reason is that PR-MIMO systems exploit the polarization domain where 2 degrees of freedom can be supported by orthogonal polarization, e.g., vertical and horizontal polarization.

Without loss of generality, an element in  $H^{\text{eff}}$  has the following description of its squared

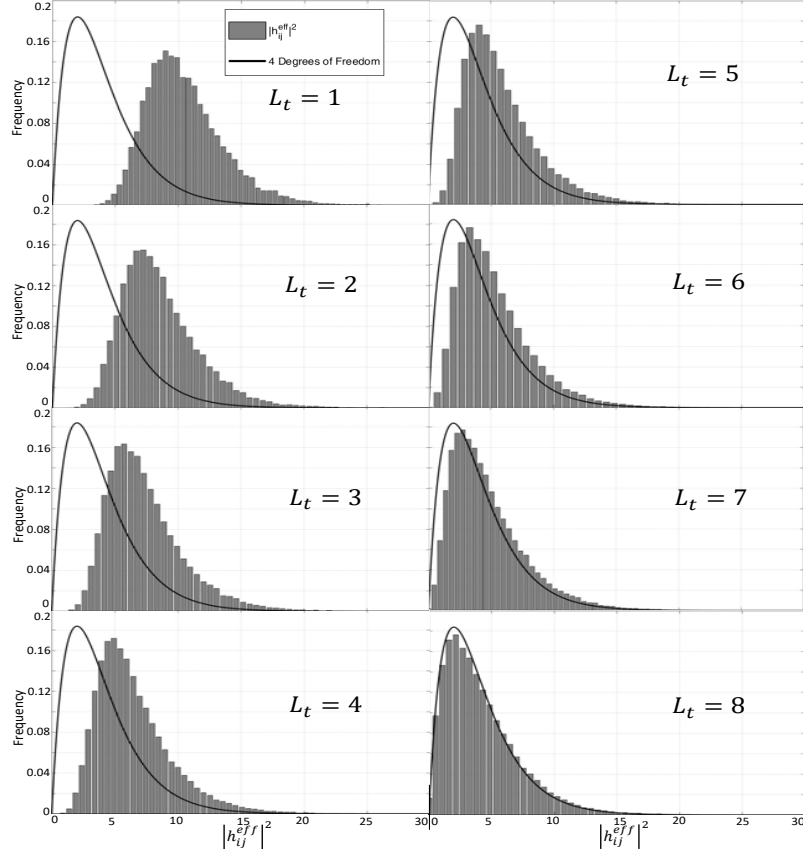


**FIGURE 8. Empirical histogram of  $|h_{ij}^{\text{eff}}|^2$  in PR-HS; the comparison of chi-square distribution with 4 degrees of freedom.**

envelope.

$$|h_{11}^{\text{eff}}|^2 = \vec{p}_{\text{Rx},1}^T (H_{11} \vec{p}_{\text{Tx},1} \vec{p}_{\text{Tx},1}^T H_{11}^\dagger) \vec{p}_{\text{Rx},1} . \quad (97)$$

From the analysis of (97), we can have an intuition for the mathematical interpretation of the aforementioned simulation results. Appendix A provides further analysis on (97).

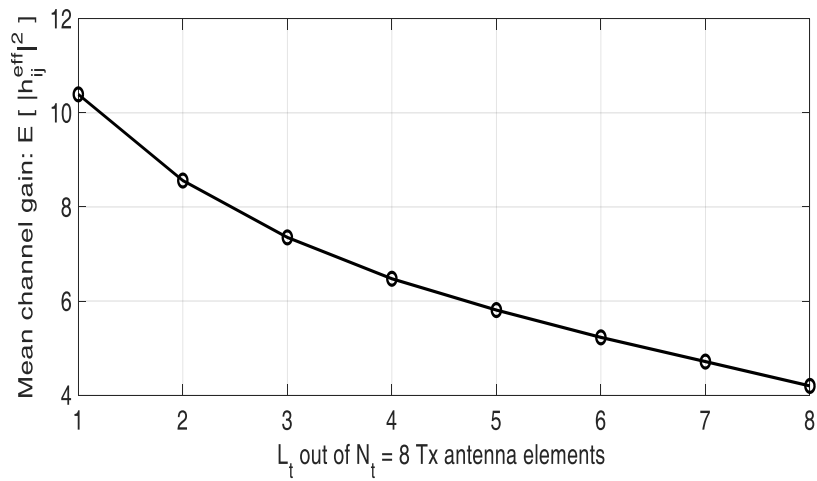


**FIGURE 9. Impact of  $L_t$  on the mean of effective channel gain in PR-HS-MIMO systems.**

## CHAPTER 7

### EXPERIMENTAL RESULTS FOR MPS-BEAMFORMING

This section provides comprehensive simulation results and the associated analyses for the novel scheme of MPS-Beamforming with the XPD/XPR-aware transmit power allocation scheme and the subcarrier assignment algorithm. Theoretical analyses in Section 3 are verified and strongly supported by the simulation results, via showing that adopting proposed schemes yields the best performance with the significant improvement in SER among possible transmit power allocation ratios. The abundant comparisons of the proposed scheme with the conventional schemes is accomplished via setting up the transmit power allocation ratio,  $\alpha$ . The conventional scheme of single beam transmission with either  $-45^\circ$  or  $45^\circ$  is included in the simulation results via realizing the scenario with  $\alpha = 1$  or  $\alpha = 0$ , respectively. Furthermore, MPS-Beamforming with random transmit power allocation ratio is also considered to verify that the theoretically obtained XPD/XPR-aware transmit power allocation ratio shows the best performance in terms of SER. This paper is the first to propose superposition of two transmit beams with orthogonal polarization; therefore, the further comparison with other scheme of superimposing multi-polarization Tx beams is unfeasible.

Both the statistical and deterministic polarized wireless channels are utilized for the simulations based on [5],[26], where the polarized channel model has been verified with the remarkable agreement with the previously reported empirical data from several channel sounding campaigns. The considered scenario is the urban or metropolitan area with the street canyon where the received signal's angles of arrival at the Rx follows verified distribution with the directivity, and beamforming and its gain are regarded as included in the channel realizations and the associated simulations based on [5],[26]. Each SER curve in the statistical polarized wireless channels is the result of Monte Carlo simulation over 100 individual wireless channel realizations which have the same PSI in terms of XPD and XPR. In turn, for one individual channel realization, the simulation accomplishes  $10^4$  iterations of estimating SER. This is the first paper to propose the novel MPS-Beamforming scheme; therefore, the simulations focus the primary consideration on the

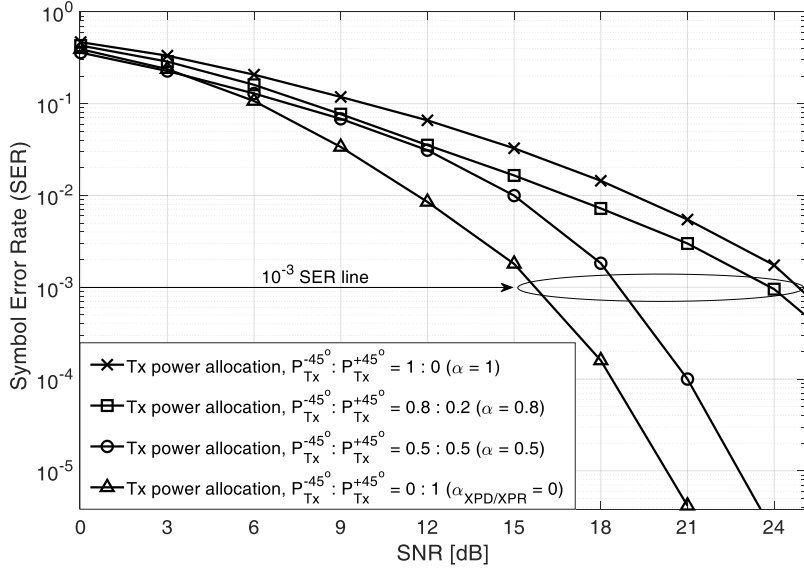


**FIGURE 10. Symbol error rate for different transmit power allocation in the scenario of 45° Rx antenna polarization,  $\overline{XPD}^N = 5.48$  dB,  $\overline{XPD}^P = -6.26$  dB,  $\overline{XPR}^N = 5.90$  dB.**

lowest modulation order, i.e., quadrature phase shift keying (QPSK) with the modulation order 2, in the current 5G NR standards.

The significant improvement of the SER performance in the OFDM system adopting MPS-Beamforming with XPD/XPR-aware transmit power allocation and subcarrier allocation, is illustrated in Figs. 10 and 11. The Rx antenna polarization is 45° in both figures. Following the 5G NR standard, the Rx antenna polarization angle can also be analyzed based on the axes of the coordinates,  $-45^\circ$  and  $45^\circ$ ; and  $\overline{XPD}^{Rx-Ant} = \tan^2(45^\circ - \text{Rx antenna polarization angle})$  in linear scale. The transmit power allocation ratio is determined based on (22) – (24). The scenario of PSI in Fig. 10 is  $\overline{XPD}^N = 5.48$  dB,  $\overline{XPD}^P = -6.26$  dB,  $\overline{XPR}^N = 5.90$  dB. In contrast, The scenario of PSI in Fig. 11 is  $\overline{XPD}^N = 5.48$  dB,  $\overline{XPD}^N = 4.56$  dB,  $\overline{XPD}^P = -4.15$  dB,  $\overline{XPR}^N = 4.34$  dB. All those PSI parameters are practical and reasonable [25],[26].

The simulation results apparently show that MPS-Beamforming with the XPD/XPR-aware transmit power allocation and subcarrier assignment, remarkably improves the conventional OFDM and beamforming based system performance in terms of SER. For instance, in the scenario of Fig. 10, the novel proposed scheme with XPD/XPR-aware transmit power allocation ratio,  $\alpha = 0$  and  $\beta = 1$  has 9 dB gain of the SNR for  $10^{-3}$  SER comparing with the scenario of  $\alpha = 1$  and  $\beta = 0$ . The different Rx antenna polarization and polarization state of the given channel require different

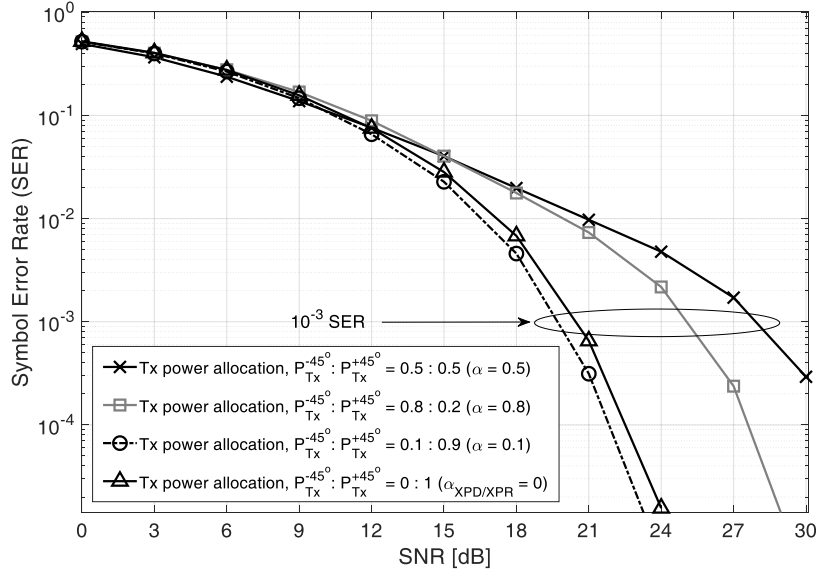


**FIGURE 11. Symbol error rate for different transmit power allocation in the scenario of  $45^\circ$  Rx antenna polarization,  $\overline{XPD}^N = 4.56$  dB,  $\overline{XPD}^P = -4.15$  dB,  $\overline{XPR}^N = 4.34$  dB.**

transmit power allocation ratio as will be illustrated in this section. It is noteworthy that the selection of a  $-45^\circ$  polarization transmit beam achieves substantial SNR gain by 9 dB and 3 dB, respectively, comparing with the selection of a  $45^\circ$  polarization transmit beam or utilizing both  $-45^\circ$  and  $45^\circ$  polarization transmit beams with equal power allocation, in case of the channel state in Fig. 10.

The theoretical XPD/XPR-aware transmit power allocation ratio,  $\alpha_{XPD/XPR}$ , is obtained from the estimation of PSI in the given channel of Fig. 11. However, note that the proposed subcarrier allocation algorithm is not applied to the simulation in Fig. 11.  $N = 48$  different subcarriers that have the highest channel gains are selected for MPS-Beamforming that is, PSI is not considered in subcarrier allocation. Even in this case, the simulation results show that MPS-Beamforming still remarkably improves the system performance in terms of SER. In Fig. 11, the proposed scheme of XPD/XPR-aware transmit power allocation with  $\alpha_{XPD/XPR} = 0$  and  $\beta_{XPD/XPR} = 1$  has 7 dB gain of the SNR for  $10^{-3}$  SER compared to the case of arbitrarily combining two transmit beams adopting  $-45^\circ$  and  $45^\circ$  polarization with  $\alpha = 0.5$  and  $\beta = 0.5$ .

One of the important observations in Fig. 11 is that the theoretically obtained  $\alpha_{XPD/XPR}$  and  $\beta_{XPD/XPR}$  do not exhibit the best SER curve for the reason that the MPS-Beamforming in the OFDM system does not apply the appropriate subcarrier assignment algorithm proposed and described in Table 1. The MPS-Beamforming with  $\alpha = 0.1$  and  $\beta = 0.9$  results in slightly better

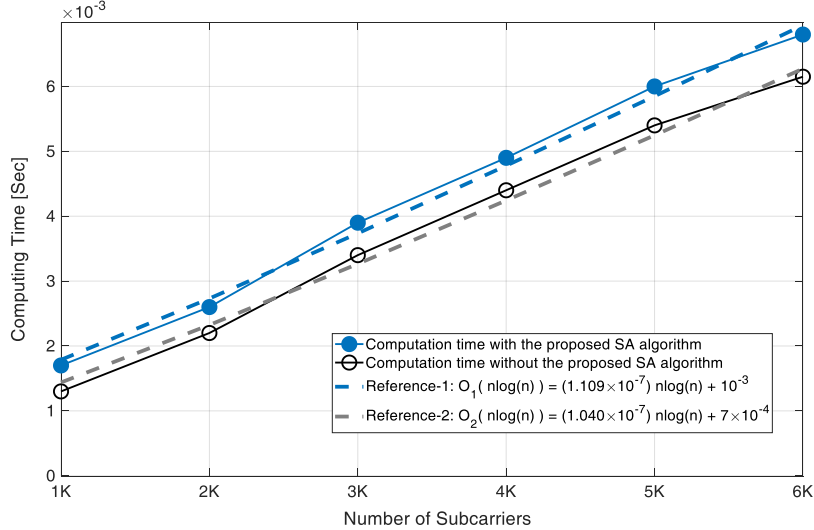


**FIGURE 12. Complexity/computation time of the proposed subcarrier assignment (SA) algorithm for varying number of OFDM subcarriers.**

SNR curve than the MPS-Beamforming with theoretically obtained  $\alpha_{XPD/XPR}$  and  $\beta_{XPD/XPR}$ , i.e., 0.7 dB SNR gain at  $10^{-3}$  SER.

For the remaining simulation results, novel subcarrier assignment algorithm described in Table 1 is applied to result in the best SER performance of MPS-Beamforming in the OFDM system with the theoretically obtained XPD/XPR-aware transmit power allocation ratio. The complexity of the proposed subcarrier assignment algorithm in terms of the computation time is illustrated in Fig. 12. The simulation results are in great agreement with the analysis of the complexity. The expected computation time for  $n$  OFDM subcarriers,  $T(n)$  is shown to be the Big-O function of  $n \ln n$ , i.e., [45]

$$T(n) = O(n \ln n). \quad (98)$$

The computation with the proposed XPD-aware OFDM subcarrier assignment algorithm shows good agreement with Reference-1 in the legend of Fig. 12.

The simulation of the proposed subcarrier assignment algorithm utilizes MATLAB's sort function, which is based on Quicksort with the expectation of the complexity,  $O(n \ln n)$ . Considering the benefit of applying the proposed subcarrier assignment algorithm to be shown in the remaining simulation results, the cost in terms of the increased complexity is acceptable. The trade-off is the significant improvement in SNR, e.g., 4 dB SNR gain in statistical channel

realization as will be presented in the remaining simulation results. The computation time without the proposed subcarrier assignment algorithm also follows Big-O function as described in Reference-2 in the legend of Fig. 12. Further, although the total number of subcarriers increases from 1K (1024) to 6K ( $6 \times 1024$ ), the increase of the additional computation time is marginal.

The analytic results of MPS-Beamforming are provided in Figs. (13) – (17). It is shown that the instantaneous Rx XPD affects the rotation angle of the Rx polarization ellipse at the UE. A variety of phase difference,  $\Delta$  in (29) – (31) along with varying  $XPD = (E^{-45^\circ}/E^{+45^\circ})^2$  are taken into account. Further, several Rx antenna polarization angles at the UE are considered to reflect the movement of the UE on the rotation of the Rx antenna orientation. Although some prior research defines XPD in slightly different manners, the prevalent conventional definition of instantaneous or statistical XPD, which is described in Section 3 is followed.

The squared eccentricity is a function of XPD as described in (41). The curves of the squared eccentricity  $\epsilon^2$  for varying XPD and a variety of phase difference  $\Delta$  are illustrated in Fig.13. Four scenarios with respect to  $\Delta$  are considered to analyze the behavior of squared eccentricity for varying XPD. In the ideal scenario that  $\Delta = 0$ , the squared eccentricity is unity, i.e.,  $\epsilon^2 = 1$ ; it corresponds to linear polarization created by the superposition of two synchronized transmit beams. This scenario is omitted in Fig. 13 since the behavior is straightforward from (41). On the other hand, if the phase difference is greater than  $45^\circ$ , squared eccentricity at  $XPD = 1$  is significantly less than unity. Even for the large phase difference, the squared eccentricity can be greater than 0.9 yielding the narrow ellipse of polarization. As mentioned in Section 3, as  $\epsilon^2$  approaches unity, the polarization ellipse converges to a linear line, which is the desired scenario.

The polarization angle of the superimposed received signal at the UE,  $\theta$ , is a function of XPD as demonstrated in (39). The behavior of  $\theta$  is depicted for varying XPD and a variety of phase difference in Fig. 14. When XPD is unity in linear scale, it yields  $\theta = 45^\circ$  for all the scenarios with respect to the phase difference. In the coordinates described in Figs. 1 and 2,  $E^{-45^\circ}$  is the component for  $x$ -axis; therefore, as XPD increases, the polarization on  $x$ -axis increases, corresponding to the scenario that  $\theta$  converges to zero.

The direct relation between the squared eccentricity,  $\epsilon^2$  and rotation angle of the polarization

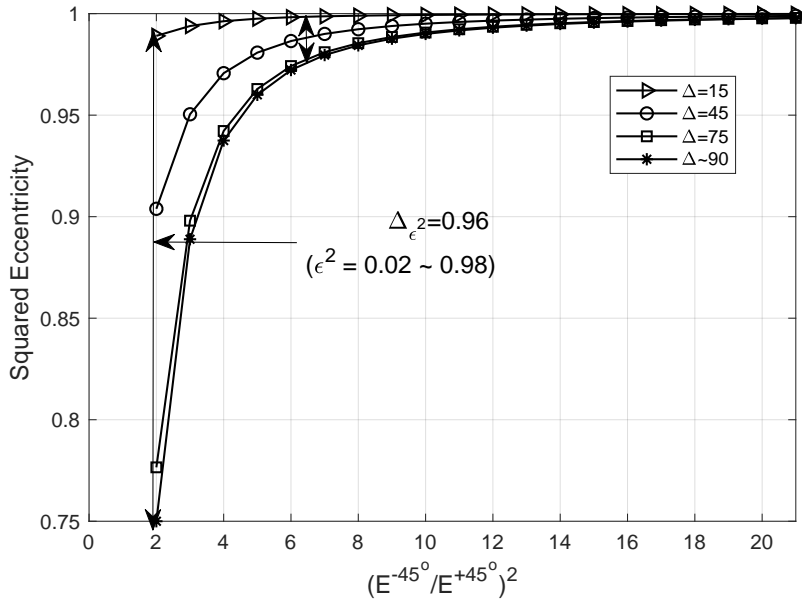


**FIGURE 13.** Squared eccentricity,  $\epsilon^2$  for the varying XPD.

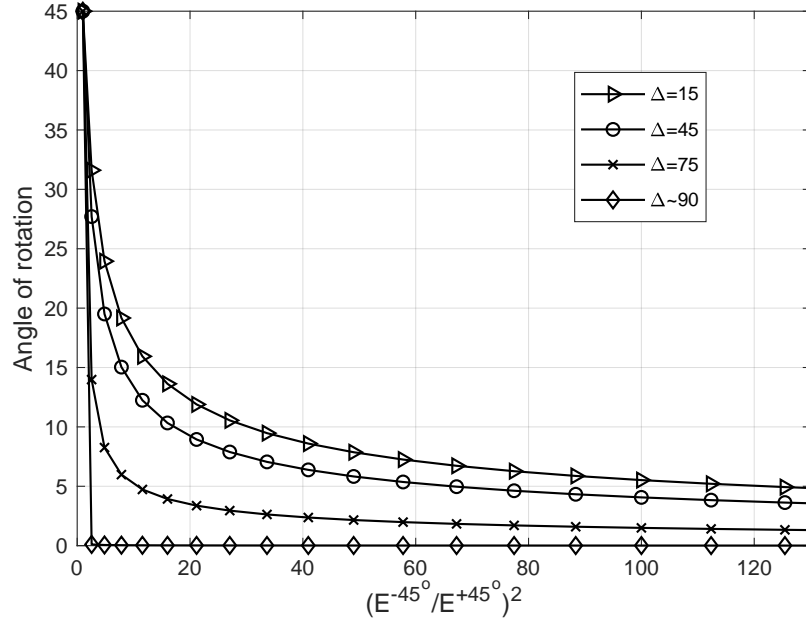


**FIGURE 14.** Angle of rotation,  $\theta$  for the varying XPD.

ellipse,  $\theta$  in (45) is portrayed in Fig. 15. As the polarization ellipse rotates further up to  $45^\circ$ , the squared eccentricity tends to decrease, i.e., the polarization gets farther from the linear polarization, in particular, in the scenario that the phase difference  $\Delta$  is greater than  $45^\circ$  such as  $\Delta = 75^\circ$ . However, for the phase difference less than  $45^\circ$  ( $\Delta \leq 45^\circ$ ), the rotation angle of the polarization ellipse do not affect the squared eccentricity seriously as exhibited in Fig. 15.

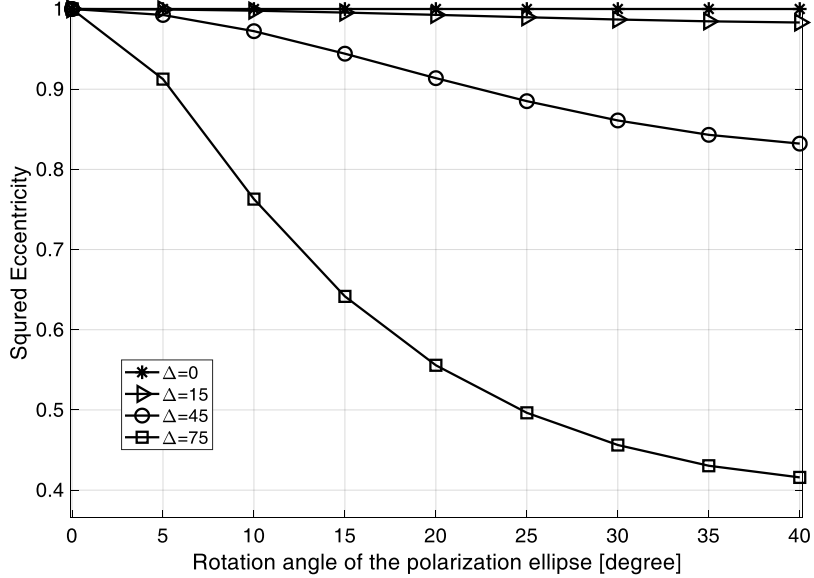


**FIGURE 15.** Direct relation between squared eccentricity,  $\epsilon^2$  and rotation angle of the polarization ellipse,  $\theta$ .

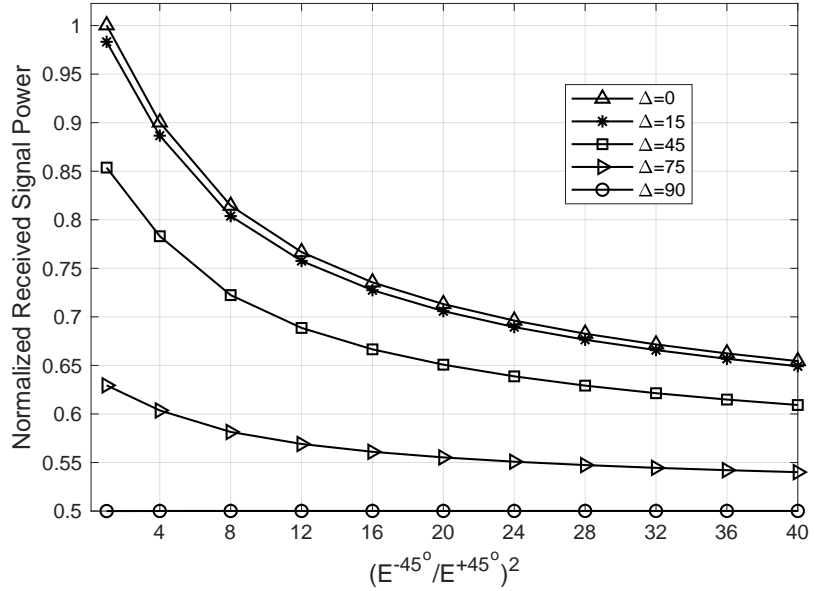


**FIGURE 16.** Received signal power for 0° Rx antenna polarization.

The next set of simulation results provided in Figs. 16 – 17 takes into account the normalized received signal power for the limited total transmit power. XPD is varied from 1 to 40 in linear scale; further, different scenarios with diverse Rx antenna polarization angles of 0° and  $-22.5^\circ$  at the UE are taken into account.

The normalized received signal power at the Rx with 0° Rx antenna polarization is illustrated in Fig. 16. In the scenario that  $\Delta = 0^\circ$ , and XPD = 1;  $\theta = 45^\circ$ . That is, the polarization of the

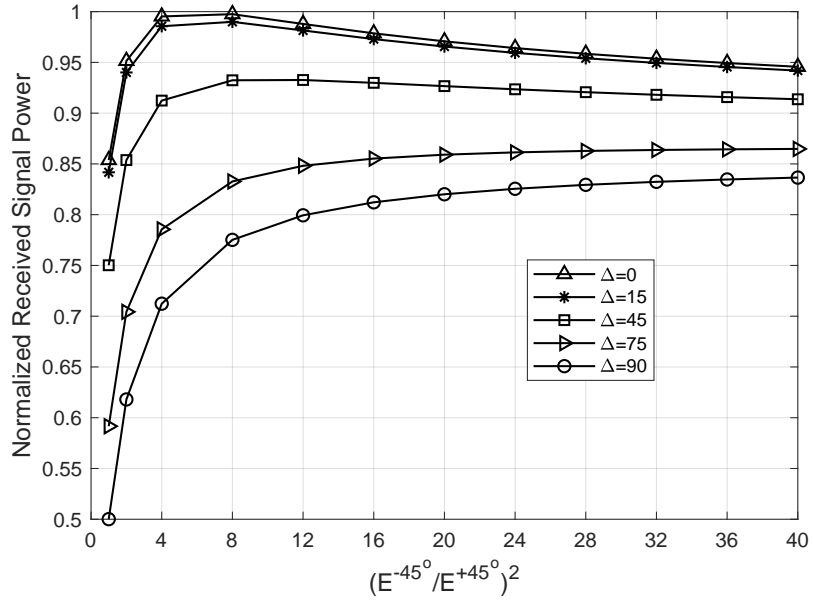


**FIGURE 17. Normalized received signal power for  $-22.5^\circ$  Rx antenna polarization.**

received signal is exactly aligned with the Rx antenna polarization; thus, the received signal power will be maximized. As illustrated in Fig. 16, compared to the scenario of no MPS-Beamforming, i.e.,  $E^{+45^\circ} = 0$  or equivalently,  $\text{XPD} = \infty$ , MPS-Beamforming with  $\text{XPD} = 1$  can save 35% of transmission power in coherent MPS-Beamforming ( $\Delta = 0^\circ$ ). Nonetheless, when  $\Delta < 45^\circ$ , the UE can still expect approximately 85% of the maximum received signal power. They are impressive results describing that the proposed MPS-Beamforming is significantly energy-efficient, for example, power loss is minimized when the polarization ellipse is well aligned to the Rx antenna polarization.

The curves of normalized received signal power for the Rx antenna polarization angle,  $-22.5^\circ$  is depicted in Fig. 17. It is noteworthy that the UE cannot have a peak for the normalized received signal power at the point,  $\text{XPD} = 1$ . Eventually, it will be matched when  $\text{XPD} = \tan^2(45^\circ - (-22.5^\circ)) = 5.83$ , which is in good agreement with Fig. 17, where the curve with  $\Delta = 0^\circ$  has a peak of the normalized received signal power at  $\text{XPD} = 5.8$ .

With the observation that different Rx antenna polarization requires different XPD of the received signal in Figs. 16 – 17, the different XPD/XPR-aware transmit power allocation ratios for different Rx antenna polarization are described and verified in Figs. 18 – 20. The Rx antenna polarization is varying among the three different values,  $-45^\circ$ ,  $-30^\circ$  and  $0^\circ$  in Figs. 18, 19 and 20,

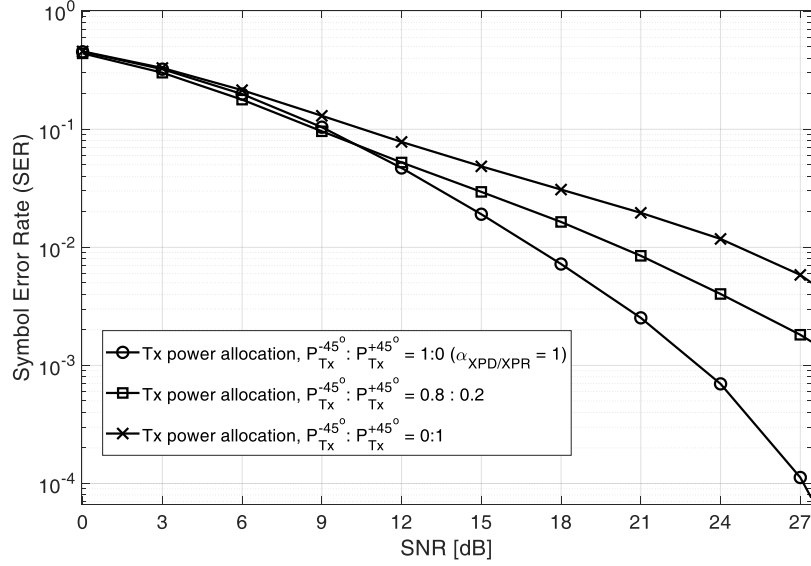


**FIGURE 18. Symbol error rate for different transmit power allocation in the scenario of  $-45^\circ$  Rx antenna polarization.**

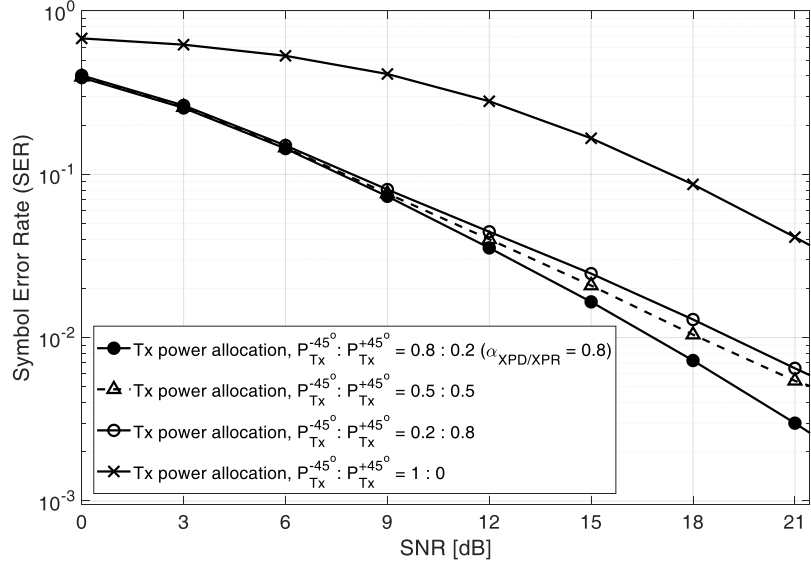


**FIGURE 19. Symbol error rate for different transmit power allocation in the scenario of  $-30^\circ$  Rx antenna polarization.**

respectively. The corresponding XPD/XPR-aware transmission power allocation ratios are, respectively,  $\alpha_{XPD/XPR} = 1$ ,  $\alpha_{XPD/XPR} = 0.8$  and  $\alpha_{XPD/XPR} = 0.5$ ; it is noteworthy that  $\alpha_{XPD/XPR} = 1$  is the case of single transmit beam with  $-45^\circ$  polarization. In the scenario of  $-30^\circ$  or  $0^\circ$  Rx antenna polarization in Fig. 19 or 20, the value of  $\alpha$  which satisfies (21) with (10) – (20), are  $\alpha = 0.8$  or  $\alpha = 0.5$ , respectively as described in the legend of Fig. 19 or 20. In each scenario of Rx antenna polarization, the proposed XPD/XPR-aware transmit power allocation with the theoretically

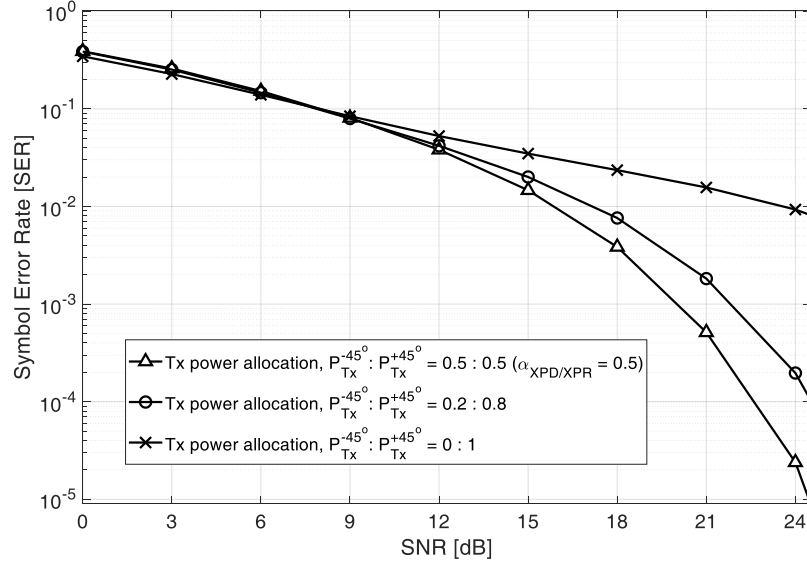


**FIGURE 20. Symbol error rate for different transmit power allocation in the scenario of 0° Rx antenna polarization.**

obtained  $\alpha$  based on (21), outperforms that of any other choice of  $\alpha$ .

Finally, two sets of simulation results in both deterministic and statistical channels are presented in Figs. 21 – 22. The PSI of the channels are,  $\overline{XPD}^N = 4.56$  dB,  $\overline{XPD}^P = -4.15$  dB, and  $\overline{XPR}^N = 4.34$  dB, although the detailed channel impulse response of one channel realization is different from others. For the same PSI of the channel in a statistical sense, Figs. 21 and 22 are in the scenario that the Rx antenna polarization is 5°; whereas, the scenario of Figs. 23 and 24 is 0° Rx antenna polarization.

The theoretically determined XPD/XPR-aware transmit power allocation ratio,  $\alpha_{XPD/XPR}$  is 0.28 in the scenario of Figs. 21 and 22, and it is verified that the MPS-Beamforming with the theoretically determined  $\alpha_{XPD/XPR}$  and the proposed subcarrier assignment algorithm results in the best SER curve in 21 and 22. In statistical channels of Fig. 22, 3 dB and 2.5 db SNR gain for  $10^{-5}$  and  $10^{-4}$  SER can be observed, respectively, in a statistical sense. That is, the proposed MPS-Beamforming with a novel transmit power allocation and subcarrier assignment algorithm outperforms the single transmit beamforming with  $-45^\circ$  polarization with the highest SNR gain among a variety of  $\alpha$ 's. It is worth mentioning that in a given particular channel environment such as the deterministic channel in Fig. 21, the SNR gain can be higher than the statistical SNR gain. For instance, Fig. 21 represents 6 dB and 5 dB SNR gain for  $10^{-5}$  and  $10^{-4}$  SER, respectively.

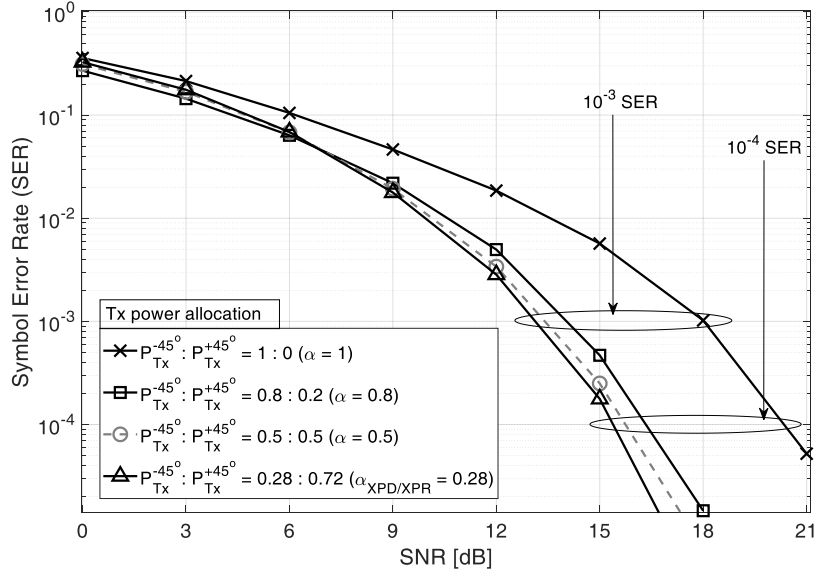


**FIGURE 21.** Verification of the theoretically determined XPD/XPR-aware transmit power allocation ratio with the best symbol error rate in a deterministic channel; Rx antenna polarization is  $5^\circ$ .

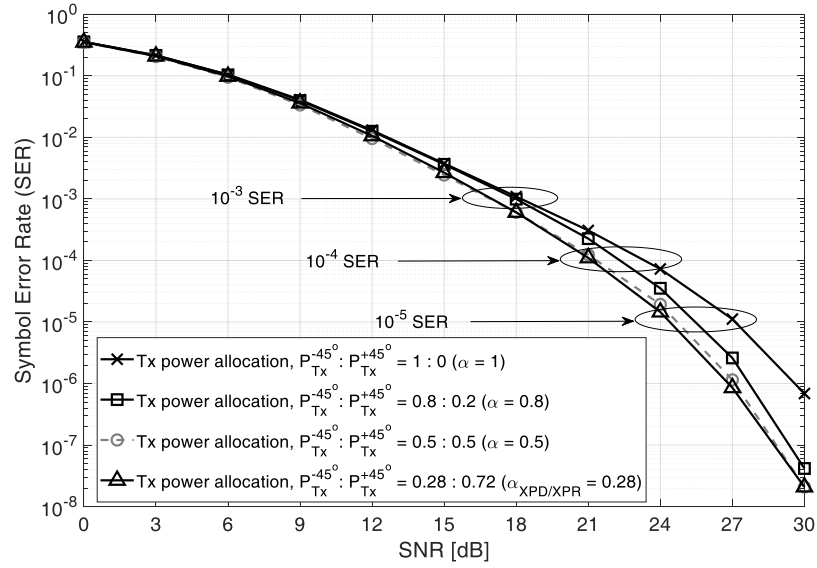


**FIGURE 22.** Verification of the theoretically determined XPD/XPR-aware transmit power allocation ratio with the best symbol error rate in statistical channels; Rx antenna polarization is  $5^\circ$ .

The Rx antenna can be rotated owing to the movement of the UE, and Figs. 23 and 24 are in the scenario of  $0^\circ$  Rx antenna polarization. That is, the Rx antenna that has to receive the signal from the Tx is rotated by  $5^\circ$  from the scenario of Figs. 21 and 22. It is remarkable that the theoretically estimated XPD/XPR-aware transmit power allocation ratio,  $\alpha_{XPD/XPR}$ , is substantially changed even for the slight change of Rx antenna polarization by  $5^\circ$  at the aspect of UEs. The

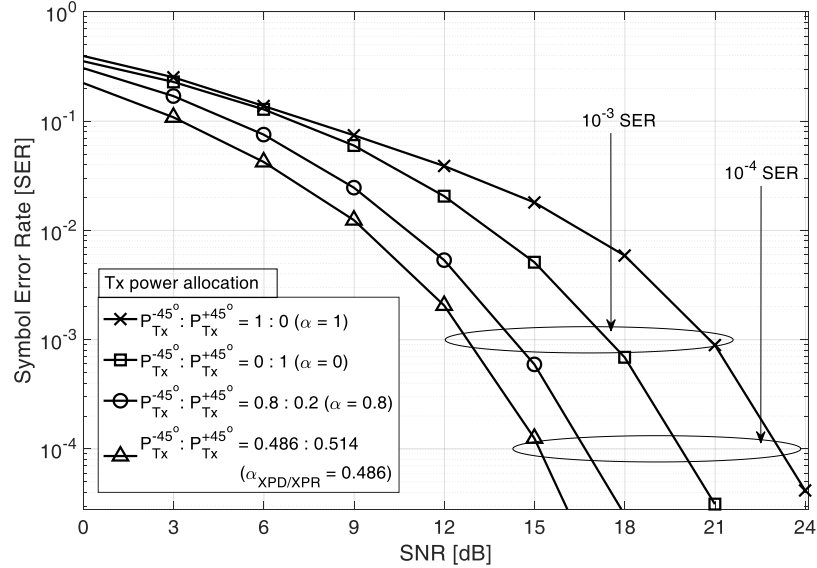


**FIGURE 23.** Verification of the proposed XPD/XPR-aware transmit power allocation scheme showing the best symbol error rate in a deterministic channel; Rx antenna polarization is  $0^\circ$ .

XPD/XPR-aware transmit power allocation ratio for the scenario of Figs. 23 and 24 is

$\alpha_{XPD/XPR} = 0.486$ ; meanwhile, for Figs. 21 and 22,  $\alpha = 0.28$ , which is regarded as significant change. That is, as  $\alpha_{XPD/XPR}$  changes from 0.28 to 0.486, the MPS-Beamforming OFDM system imposes 74 % more transmission power on the transmit beamforming with  $-45^\circ$  polarization.

In the similar fashion with Figs. 21 and 22, the SNR gain of 4 dB and 2 db for  $10^{-5}$  and  $10^{-4}$  SER, respectively, are observed in a statistical sense, as illustrated by the simulation with statistical channels in Fig. 24. The proposed MPS-beamforming with a novel transmit power allocation and subcarrier assignment algorithm outperforms the single transmit beamforming with  $-45^\circ$  polarization exhibiting the highest SNR gain among a variety of  $\alpha$ 's. It is noteworthy that a provided channel environment can show the more significant SNR gain such as around 8 dB for both  $10^{-3}$  and  $10^{-4}$  SER in Fig. 23.

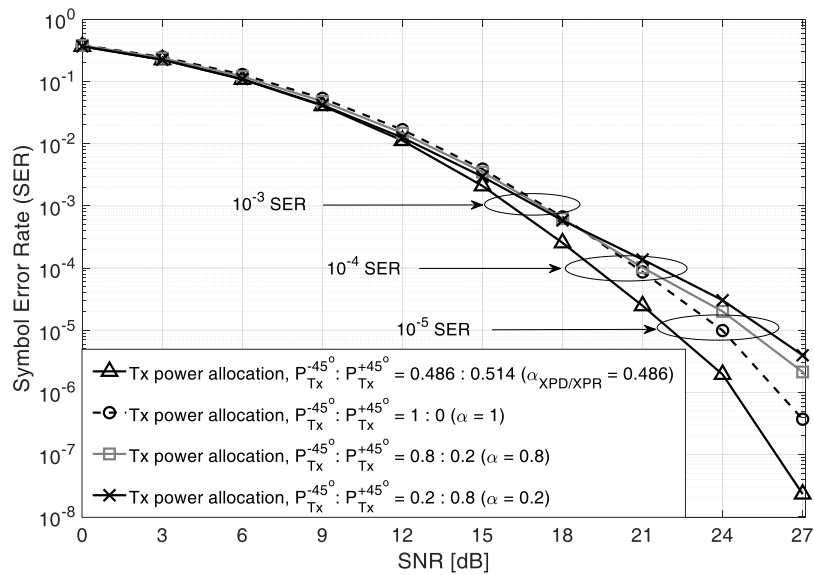


**FIGURE 24.** Verification of the proposed XPD/XPR-aware transmit power allocation scheme showing the best symbol error rate in statistical channels; Rx antenna polarization is 0°.

## CHAPTER 8

### EXPERIMENTAL RESULTS FOR PR-MIMO, PR-HS/MIMO AND PR-HS/MRT

#### Simulations in PR-MIMO

This section provides evaluations of the closed-form equations for optimum polarization vectors and the associated PR-MIMO channel capacity. The results are also compared to brute-force numerical optimization, where the simulation steps through all possible (discretized) values of the Tx/Rx-polarization angle and choose the optimal values that correspond to the maximum capacity for each PR-MIMO channel realization. The step width of the brute-force numerical search are, respectively,  $1^\circ$  in Fig. 25;  $5^\circ$  in Figs. 26 and 27;  $10^\circ$  in Figs. 28 and 29. Unless stated otherwise, independent and identically distributed (i.i.d.) Rayleigh fading channels is considered with a cross-polarization discrimination, XPD = 0 dB.

The investigation the impact of polarization reconfiguration in several deterministic channels is considered first. The PR-MIMO channel capacity in a  $2 \times 2$  system with polarization reconfigurable antenna elements is shown for varying Tx-polarization angles in Fig. 25. In the high SNR regime, i.e., 30 dB in Fig. 25, the channel capacity obtained by the polarization precoding at the Tx exhibits negligible difference from that yielded by the numerical result as indicated in the figure. The differences between theoretically and numerically obtained optimal Tx-polarization angles are considerable. This is due to the fact that the approximation (54) is less accurate at higher SNRs. However, the difference in capacity is still remarkably small. In case of polarization postcoding at the Rx, similar results are attained owing to the symmetry described in Sections 4; therefore, the results are omitted here. It is worth mentioning that optimal Tx- or Rx-polarization vectors are not necessarily orthogonal, which corresponds to  $90^\circ$  difference in Tx- or Rx-polarization angles, as described in Fig. 25. For the low SNR regime such as 5 dB SNR, the theoretically derived optimal Tx-polarization angles themselves have insignificant differences from numerically derived optimal Tx-polarization angles. The simulation results for the low SNR regime are omitted owing to the page limit.

The PR-MIMO channel capacity with the optimal Tx-polarization angles is demonstrated to

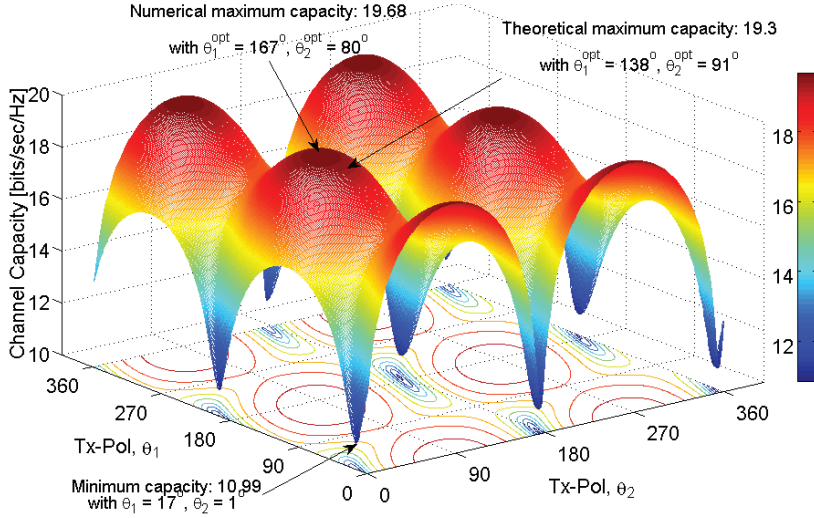


**FIGURE 25. Channel capacity for varying Tx-polarization; 30 dB SNR.**

depend on varying Rx-polarization angles in Fig. 26, where  $2 \times 2$  PR-MIMO system with polarization-agile antenna elements at both ends of the Tx and the Rx is also considered. The channel capacity exhibits substantial variation from 21.47 bits/sec/Hz to 13.60 bits/sec/Hz depending on Rx-polarization angles, although Tx-polarization angles are already set to the optimum obtained by brute-force numerical search as will be shown in Fig. 27, i.e.,  $\theta_{Tx-1} = 80^\circ$ ;  $\theta_{Tx-2} = 50^\circ$ . This result obviously shows that the polarization mismatching between the Tx and the Rx can cause significant deterioration in the capacity of the whole system, even if one end of the Tx and the Rx is already set to the optimal polarization. However, the proposed scheme of joint polarization pre-post coding also shows negligible difference from numerical results in both optimal Tx- and Rx-polarization angles and channel capacity.

Local optimal Tx- and Rx-polarization vectors at each iteration of joint polarization pre-post coding are depicted in Fig. 27 considering the same scenario of channel impulse matrices and SNR as that in Fig. 26. The  $2 \times 2$  PR-MIMO system is again considered in this figure. Here, one iteration is a sequential loop of polarization precoding and then polarization postcoding as described in Section 4. Tx/Rx-polarization vectors quickly converge; moreover, these global optimal polarization vectors show relatively small difference from the numerical optimum.

In contrast to Figs. 25 – 27, from this point on, investigation how much the joint polarization pre-post coding improves the PR-MIMO channel capacity in a statistical sense in Figs. 28 – 30 is

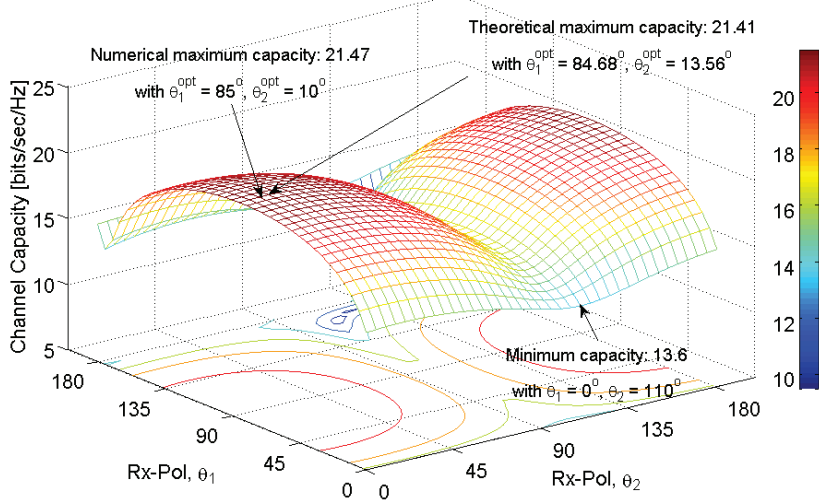


**FIGURE 26. Channel capacity for varying Rx-polarization with optimal Tx-polarization; 30 dB SNR.**

made. The simulation results are based on the  $10^4$  times realizations of i.i.d. Rayleigh fading channels. Figures 28 and 29 depict cumulative density functions (cdf's) of the  $2 \times 2$  PR-MIMO channel capacity at 5 dB SNR and 30 dB SNR, respectively, for the scenarios of joint polarization pre-post coding with Tx/Rx polarization-agile antennas; and random Tx/Rx-polarization. It is noteworthy that the cdf resulting from the fixed Tx/Rx-polarization exhibits exactly the same cdf of random Tx/Rx-polarization at each channel realization owing to the random generation of the i.i.d. Rayleigh fading channels. Furthermore, the cdf's of the optimal and the worst Tx/Rx-polarization obtained by brute-force numerical search at each channel realization, are presented in Figs. 28 and 29. Five iterations for the joint polarization pre-post coding at each PR-MIMO channel realization is performed, which results in the satisfactory convergence of Tx/Rx-polarization vectors on the global optimal ones as demonstrated in Fig. 27.

Our joint polarization pre-post coding significantly improves the PR-MIMO channel capacity at both 5 dB SNR and 30 dB SNR. In Fig. 28, the probability of the PR-MIMO channel capacity less than 4.2 bits/sec/Hz is 0.75 with 5 dB SNR and random Tx/Rx-polarization; whereas, with the proposed joint polarization pre-post coding, the probability of the capacity greater than 4.2 bits/sec/Hz is 0.94. For the improvement of the PR-MIMO channel capacity at 30 dB SNR in Fig. 29, the probability of the capacity greater than 20 bits/sec/Hz is 0.75 in the scenario of utilizing joint polarization pre-post coding, while that probability is just 0.12 with random

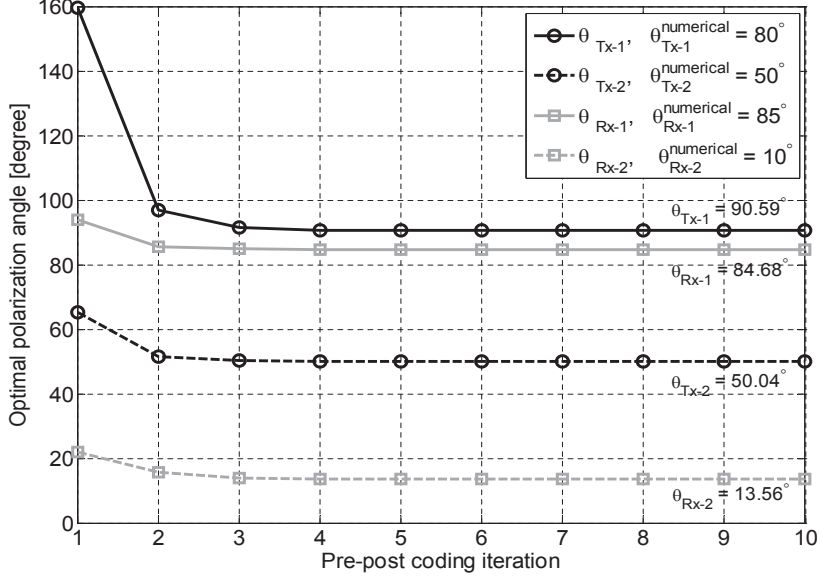


**FIGURE 27. Optimal Tx/Rx-polarization angles for the number of iterations; 30 dB.**

Tx/Rx-polarization. It is noteworthy that the cdf curves of random Tx/Rx-polarization scenarios in both Figs. 28 and 29 can be regarded as the expectation of the cdf curves in a statistical sense when the joint polarization pre-post coding is not utilized; however, the practical channel capacity would exhibit substantial variations between the cdf curves associated with the optimal and the worst Tx/Rx-polarization obtained by brute-force numerical search in both figures.

The joint polarization pre-post coding achieves significant improvement of PR-MIMO channel capacity so that its cdf curve approaches the best cdf curve obtained by brute-force numerical search, in particular, at 5 dB SNR in Fig. 28. The cdf curve corresponding to the proposed scheme also exhibits slight difference from the best cdf curve obtained from brute-force numerical search at 30 dB SNR in Fig. 29, compared to the significant difference between that best-scenario cdf and the cdf of random Tx/Rx-polarization or, more pronouncedly, between the best- and the worst-scenario cdf's obtained by the numerical search.

Finally, channel capacity for varying SNRs and varying number of polarization-agile antennas is compared in Fig. 30. For each setting of the number of polarization-agile antennas, Fig. 30 demonstrates three scenarios: joint polarization pre-post coding at both link ends; Tx-polarization precoding only at the transmitter; and random Tx/Rx-polarization as the baseline control. In the high SNR regime, utilizing our joint polarization pre-post coding improves PR-MIMO channel

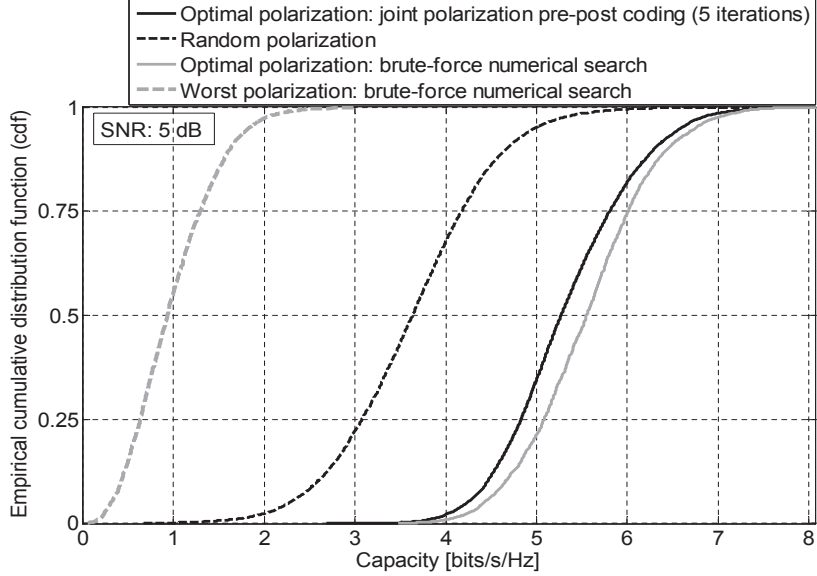


**FIGURE 28. cdf's of channel capacity for the scenarios of joint polarization pre-post coding with five iterations, random Tx/Rx-polarization; optimal and the worst Tx/Rx-polarization through brute-force numerical search at 5 dB SNR.**

capacity with around 5 dB, 4 dB, and 3dB SNR gains in the cases of  $2 \times 2$ ,  $3 \times 3$ , and  $4 \times 4$  PR-MIMO channels, respectively.

Moreover, it is noteworthy that in a relatively low SNR regime below 9 dB,  $2 \times 2$  and  $3 \times 3$  PR-MIMO systems adopting the proposed joint polarization pre-post coding accomplishes almost the same channel capacity as, respectively,  $3 \times 3$  and  $4 \times 4$  MIMO systems with random Tx/Rx-polarization. It is worth noting that the PR-MIMO system with our joint polarization pre-post coding shows better channel capacity even than the PR-MIMO system that has one more antenna element at both link ends of the transmitter and receiver and uses random polarization, in the low SNR regime (below 3 dB).

### Simulations in PR-HS/MIMO

This section presents simulation results focusing on the system performance when applying the proposed PR-HS/MIMO scheme. The results include improved channel capacity; and the comparison of EW and global polarization reconfiguration schemes in terms of channel capacity and selected Tx antenna indices. In the simulation,  $N_t = 8$ ;  $L_t = N_r \in \{1, 2, \dots, 8\}$ ; and we compare the PR-HS/MIMO channel capacity in (84) and (88) rather than the sum of squared singular values in (85) and (89) to select  $L_t$  polarization reconfigurable Tx antenna indices. The reason is that for

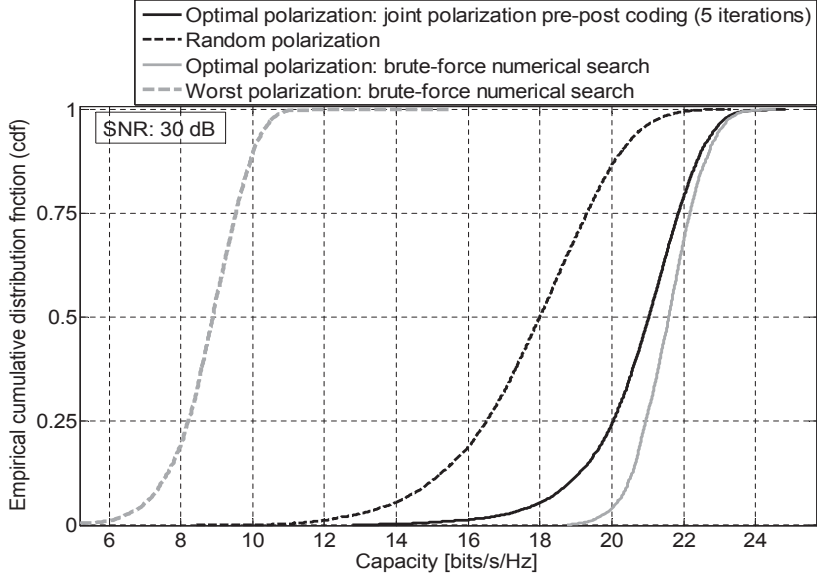


**FIGURE 29. cdf's of channel capacity for the scenarios of joint polarization pre-post coding with five iterations, random Tx/Rx-polarization; optimal and the worst Tx/Rx-polarization through brute-force numerical search at 30 dB SNR.**

$N_t = 8$  total Tx antenna elements, directly comparing channel capacity has insignificant increase of the complexity beyond that of comparing the sum of squared singular values; whereas, the former provides the more appropriate hybrid selection of Tx antenna indices with the concomitant better improvement of channel capacity than the latter.

Simulation results in Fig. 31 show the impact of PR-HS/MIMO schemes on the channel capacity. Regardless of the number of selected Tx antenna elements,  $L_t$ , the proposed PR-HS/MIMO schemes outperform the conventional HS-MIMO scheme without polarization reconfiguration, i.e., the case of Random polarization in the legend of Fig. 31. The benefit of adopting polarization reconfigurable antenna elements becomes enlarged as  $L_t$  increases. Further, it is verified that EW polarization reconfiguration has better performance than global polarization reconfiguration although the difference in performance is not substantial in the scenario that  $N_t = 8$ . Hence, global polarization reconfiguration can also be a good suboptimal scheme considering the lower complexity and computation time than those of EW polarization reconfiguration.

Another observation of the selected Tx antenna indices in PR-HS/MIMO and conventional HS-MIMO, is given in Tables 2 – 4. Even for a set of selected Tx antenna elements based on the conventional HS-MIMO, the channel capacity is improved via joint polarization pre-post coding

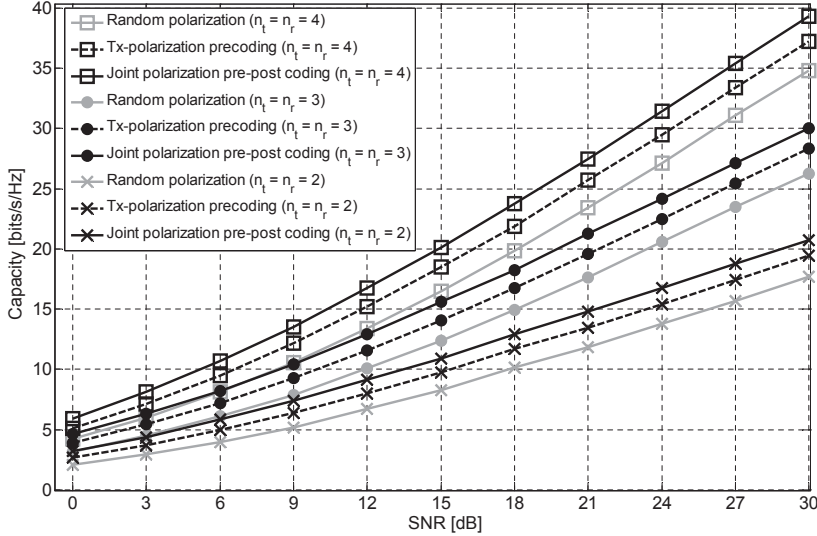


**FIGURE 30. PR-MIMO channel capacity for the varying SNR in the scenarios of random Tx/Rx-polarization, Tx-polarization precoding, and joint polarization pre-post coding.**

after the hybrid antenna selection. However, that hybrid selection of Tx antenna elements is different from the selection based on the proposed PR-HS/MIMO schemes. Selected antenna indices in EW polarization reconfiguration scheme are also different from those in global polarization reconfiguration scheme. Tables 2 – 4 illustrate the selected Tx antenna indices in 10 independent channel realizations for  $L_t = 4$  and 8.

The conventional HS-MIMO scheme does not show full-matching of selected antenna indices with any of two PR-HS/MIMO schemes in the scenarios that  $L_t = 4$  and 8. On the other hand, the two PR-HS/MIMO schemes, i.e., EW and global polarization reconfiguration, have a considerable number of cases in which their selected antenna indices fully match as described in Tables 2 – 4. Their selected antenna indices are partially in great agreement. It is worth emphasizing that estimation of optimal polarization vectors before the hybrid antenna selection stage is inevitable to have full benefit of joint polarization pre-post coding and the corresponding polarization reconfigurable antenna selection in PR-HS/MIMO spatial multiplexing.

### Simulations in PR-HS/MRT

In this section, simulation results focusing on the system performance when applying the proposed PR-HS/MRT scheme are presented. The results include improved effective SNR, channel capacity and SER; the comparison of EW and global polarization reconfiguration schemes in terms of performance and selected Tx antenna indices; and verification of the theoretically derived SER in

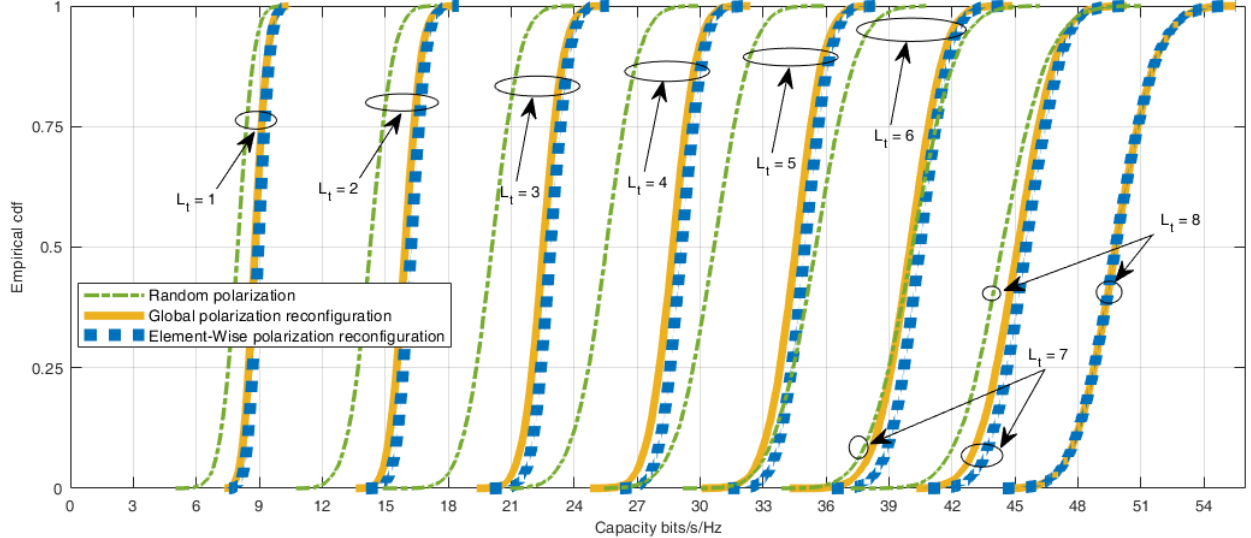


**FIGURE 31.** cdf curves of channel capacity at 20 dB for PR-HS/MIMO with element-wise (EW) and global polarization reconfiguration schemes, conventional HS-MIMO (Random Polarization); with a variety of  $L_t$ .

**TABLE 2. Selected Tx Antenna Index when  $L_t = 4$**

Random	G	EW	Matching Index
1 3 5 6	<b>2 4 5 7</b>	<b>2 4 5 7</b>	4
2 3 7 8	<b>1 2 3 8</b>	<b>1 2 3 8</b>	4
1 5 7 8	<b>1 5 7 8</b>	<b>1 5 7 8</b>	4
2 3 6 7	<b>1 3 5 6</b>	<b>1 3 4 6</b>	3
1 3 4 8	<b>1 5 6 8</b>	<b>1 3 6 8</b>	3
1 3 5 7	<b>2 3 4 7</b>	<b>1 2 3 7</b>	3
1 2 4 8	<b>1 3 7 8</b>	<b>1 3 7 8</b>	4
2 3 5 7	<b>2 4 6 8</b>	<b>2 6 7 8</b>	3
1 2 3 4	<b>2 4 6 7</b>	<b>4 6 7 8</b>	3
3 4 6 8	<b>4 5 7 8</b>	<b>4 5 7 8</b>	4

PR-HS/MRT via Monte-Carlo simulations. Unless otherwise stated, the following system

parameters will be used:  $\frac{P}{\sigma_n^2} = 20$  dB,  $N_t = 8$  and  $N_r = 2$  (MRC).

Simulation results in Fig. 32 show the impact of PR-HS/MRT schemes on the channel capacity. Regardless of the number of selected Tx antenna elements,  $L_t$ , the proposed PR-HS/MRT schemes outperform the conventional HS/MRT without polarization reconfiguration, i.e., the case of Random Polarization in the legend of Fig. 32, by around 1 bit/s/Hz. Further, it is verified that EW polarization reconfiguration (Scheme-1) has better performance than global polarization reconfiguration (Scheme-2). However, the difference in performance decreases as  $L_t$  increases.

**TABLE 3. Selected Tx Antenna Index when  $L_t = 6$**

Random	G	EW	Matching Index
1 4 5 6 7 8	<b>1 4 5 6 7 8</b>	<b>2 4 5 6 7 8</b>	6
1 3 4 5 7 8	<b>1 3 4 5 6 7</b>	<b>2 3 4 5 6 8</b>	4
1 2 3 6 7 8	<b>1 2 3 4 7 8</b>	<b>2 4 5 6 7 8</b>	4
3 4 5 6 7 8	<b>1 2 4 5 7 8</b>	<b>1 2 4 5 7 8</b>	6
3 4 5 6 7 8	<b>2 4 5 6 7 8</b>	<b>1 2 4 5 6 8</b>	5
1 2 3 5 6 8	<b>2 3 5 6 7 8</b>	<b>1 2 3 5 6 8</b>	5
2 3 4 5 7 8	<b>1 2 4 5 7 8</b>	<b>1 2 4 5 7 8</b>	6
1 2 4 5 6 8	<b>1 3 4 6 7 8</b>	<b>1 3 4 6 7 8</b>	6
1 3 4 6 7 8	<b>2 4 5 6 7 8</b>	<b>1 3 4 6 7 8</b>	4
1 2 3 4 6 8	<b>1 3 4 5 6 8</b>	<b>1 3 4 5 6 8</b>	6

**TABLE 4. Selected Tx Antenna Index when  $L_t = 8$**

Random	G	EW	Matching Index
1 2 ... 8	<b>1 2 ... 8</b>	<b>1 2 ... 8</b>	8
1 2 ... 8	<b>1 2 ... 8</b>	<b>1 2 ... 8</b>	8
1 2 ... 8	<b>1 2 ... 8</b>	<b>1 2 ... 8</b>	8
1 2 ... 8	<b>1 2 ... 8</b>	<b>1 2 ... 8</b>	8
1 2 ... 8	<b>1 2 ... 8</b>	<b>1 2 ... 8</b>	8
1 2 ... 8	<b>1 2 ... 8</b>	<b>1 2 ... 8</b>	8
1 2 ... 8	<b>1 2 ... 8</b>	<b>1 2 ... 8</b>	8
1 2 ... 8	<b>1 2 ... 8</b>	<b>1 2 ... 8</b>	8
1 2 ... 8	<b>1 2 ... 8</b>	<b>1 2 ... 8</b>	8

Hence, global polarization reconfiguration can also be a good suboptimal scheme considering the lower complexity and computation time than those of EW polarization reconfiguration, in particular, when  $L_t \geq 4$  in the scenario of Fig. 32.

Effective SER in PR-HS/MRT is also significantly lower than that in conventional HS/MRT, showing approximately 3 dB SNR gain to for  $10^{-3}$  SER in every case of  $L_t$ , as described in Fig. 33. The SER curves are based on the analytical result in (78) considering QPSK modulation as a baseline. Besides, the difference in SER performance between EW and global polarization reconfiguration schemes is inconsiderable for a variety of  $L_t$  in the scenario of Fig. 33. This is not surprising, given the straightforward mapping between SNR and SER for the chosen modulation.

Monte-Carlo simulation results in Fig. 34 validate the analytical SER curves based on (78). SER curves are generated via Monte-Carlo simulation, where  $10^7$  randomly generated symbols are

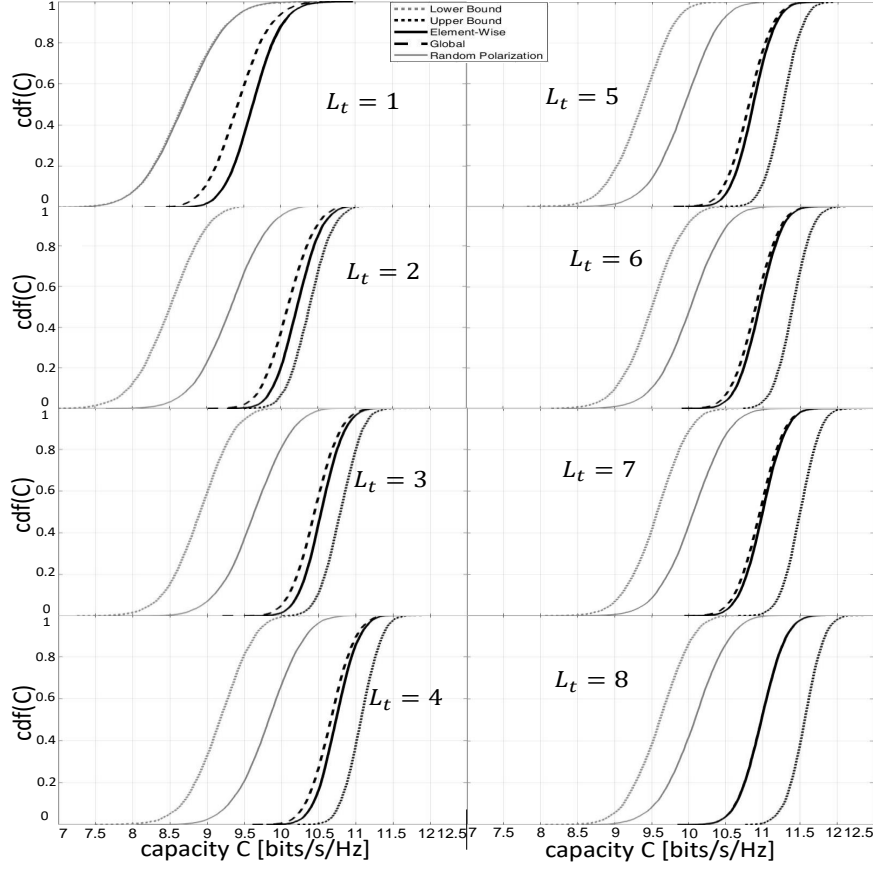


**FIGURE 32.** cdf curves of channel capacity for PR-HS/MRT with EW and global polarization reconfiguration schemes, conventional HS/MRT (Random Polarization), upper and lower bounds; with a variety of  $L_t$ .

transmitted based on PR-HS/MRT at the Tx, and MRC at the Rx. The scenarios of  $L_t = 1, 2, 5$  and  $8$  are considered, and SER curves resulted in Monte-Carlo simulation shows good agreement with the analytical ones with with average SER.

Another observation of the selected Tx antenna indices in PR-HS/MRT and conventional HS/MRT, is given in Tables 2 – 4. Even for a set of selected Tx antenna elements based on the conventional HS/MRT, the channel capacity and SER performance is improved via joint polarization pre-post coding after the selection. However, that selection of Tx antenna elements is different from the selection based on the proposed PR-HS/MRT. Moreover, selected antenna indices in EW polarization reconfigurable scheme is also different from those in global polarization reconfigurable scheme. Tables 2 – 4 illustrate the selected Tx antenna indices in 10 independent channel realizations for  $L_t = 4, 6$  and  $8$ .

The conventional HS/MRT scheme does not show full-matching of selected antenna indices

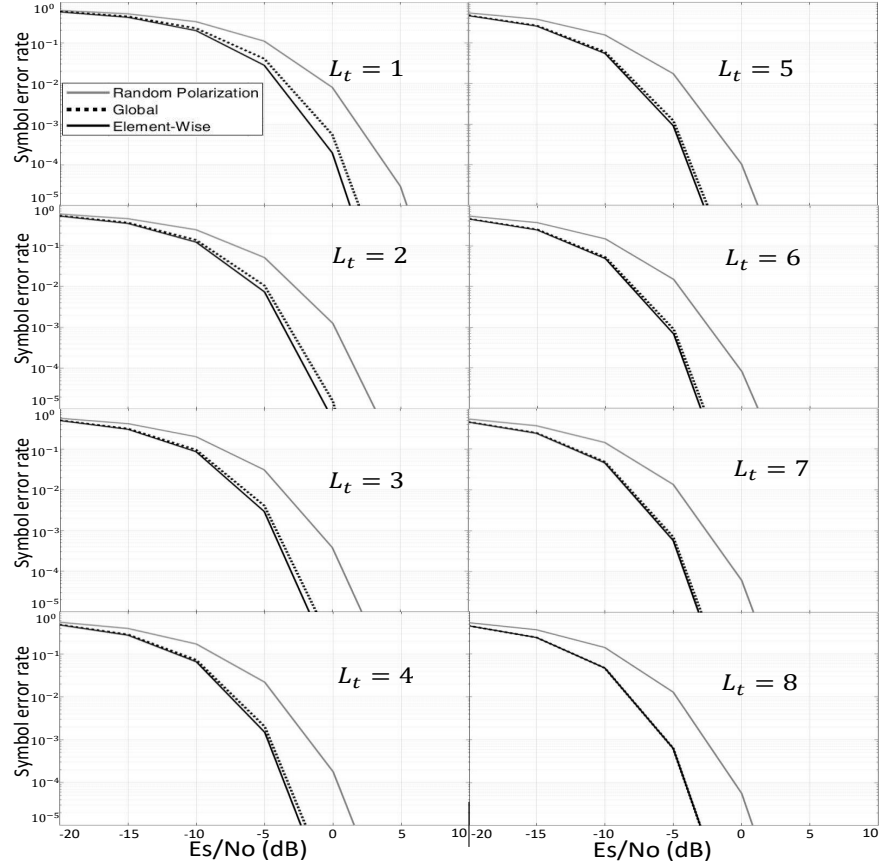


**FIGURE 33. SER curves for PR-HS/MRT with EW and global polarization reconfiguration schemes and conventional HS/MRT (random polarization); with a variety of  $L_t$ .**

with any of two PR-HS/MRT schemes. On the other hand, the two PR-HS/MRT schemes, i.e., EW and global polarization reconfiguration, have a considerable number of cases in which their selected antenna indices fully match. As described in Tables 2 – 4, the greater  $L_t$  is, the more selected antenna indices are matched between proposed two PR-HS/MRT schemes. It is worth emphasizing that estimation of optimal polarization vectors before the hybrid antenna selection stage is inevitable to have full benefit of joint polarization pre-post coding.

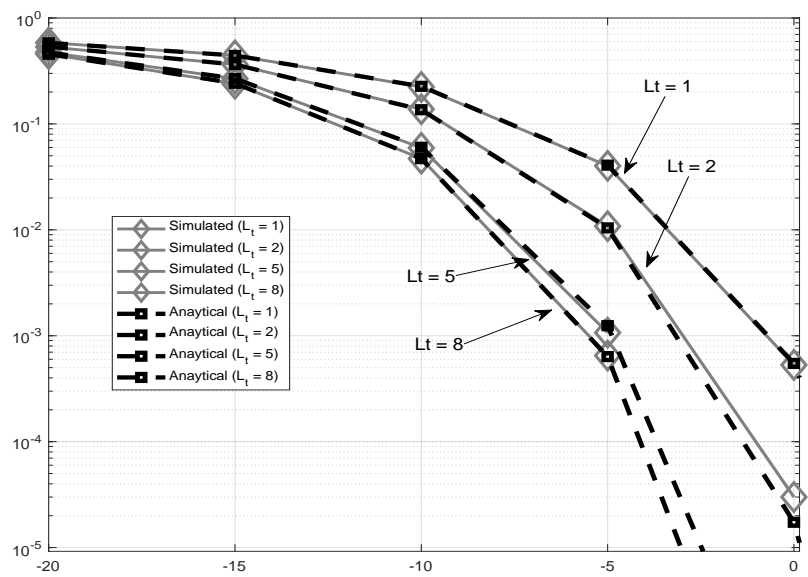


**FIGURE 34. Validation of analytical SER curves via Monte-Carlo simulation**

## CHAPTER 9

### CONCLUSION

This thesis is the first to propose a novel scheme of MPS-Beamforming with XPD/XPR-aware transmit power allocation and the appropriate XPD/XPR-aware OFDM subcarrier assignment. Based on the 5G antenna panel structure agreed by the 5G NR standard society, the proposed scheme can be utilized to have the significant benefit of improving SER or SNR gain to satisfy the required SER; therefore, energy efficiency. The transmit dpower allocation ratio is theoretically obtained based on the given PSI of the wireless channel such as XPD and XPR. This theoretical scheme is verified by abundant simulations with a variety of scenarios in terms of PSI and Rx antenna polarization. The comprehensive simulation results include the remarkable improvement of the system, including 8 dB SNR gain for  $10^{-3}$  and  $10^{-4}$  SER in a given realistic scenario, i.e., in a deterministic channel. Further, the long-term simulations with abundant statistical channels also exhibit the SNR gain of 4 dB for  $10^{-4}$  in a provided realistic scenario of PSI and Rx antenna polarization in a statistical sense. The complexity of the proposed OFDM subcarrier assignment algorithm is acceptable considering the aforementioned benefits. The proposed scheme of MPS-Beamforming has the significant potential to be utilized in the advanced revision of 5G NR, beyond-5G or 6G wireless communication standards and systems in the future.

Furthermore, this thesis proposed several novel schemes to support PR-HS/MIMO spatial multiplexing and PR-HS/MRT whose system is composed of multiple polarization reconfigurable antenna elements at both the Tx and Rx. In the proposed iterative joint polarization pre-post coding, the local optimum usually reached the global optimum of Tx/Rx-polarization vectors within five iterations. The proposed method offers an energy-efficient as well as cost-efficient method to significantly increase channel capacity in PR-HS-MIMO spatial multiplexing. Furthermore, we proposed two PR-HS-MIMO schemes, i.e., EW and global polarization reconfiguration, and both schemes remarkably outperformed the conventional HS-MIMO without polarization reconfigurable antennas. The theoretical analysis along with extensive simulation results demonstrate the outstanding performance of the schemes proposed in this paper.

## **APPENDICES**

## **APPENDIX A**

**EXPECTATION AND VARIANCE OF  $Y = \cos \Theta$ ,  $X = \sin \Theta$  AND  $h_{ij}^{\text{eff}}$**

To find the expectation and variance of  $Y = \cos \Theta$  and  $X = \sin \Theta$ , we start from (95). The expectation is found by solving the integral

$$E[Y] = \frac{1}{\pi} \int_{-1}^1 \frac{dy}{\sqrt{1-y^2}}. \quad (99)$$

To solve, we substitute  $u = 1 - y^2$ ,  $du = -2ydy$  and  $dy = \frac{1}{-2x}du$ . Therefore,

$$\begin{aligned} E[Y] &= \frac{1}{2\pi} \int \frac{1}{\sqrt{u}} du \\ &= \frac{1}{2\pi} \sqrt{u} = \left[ \frac{1}{2\pi} \sqrt{1-y^2} \right]_{-1}^1 \\ &= 0. \end{aligned} \quad (100)$$

We find variance by solving the integral

$$\begin{aligned} Var(Y) &= \int_{-\infty}^{\infty} y^2 f_Y(y) dy - (E[Y])^2 \\ &= \frac{1}{\pi} \int_{-1}^1 y^2 \frac{1}{\sqrt{1-y^2}} dy. \end{aligned} \quad (101)$$

The second term of (101) disappears because expectation is 0. Substitute  $y = \sin u$ ,  $dy = \cos u du$ , and  $u = \arcsin y$ ,

$$\begin{aligned} Var(Y) &= \frac{1}{\pi} \int \frac{\sin^2 u}{\sqrt{1-\sin^2 u}} \cos u du \\ &= \frac{1}{\pi} \int \frac{\sin^2 u}{\cos u} \cos u du \\ &= \frac{1}{2\pi} \int 1 - \cos 2u du \\ &= \frac{1}{2\pi} u - \frac{1}{4\pi} \sin 2u = \frac{1}{2\pi} (u - \sin u \cos u) \\ &= \frac{1}{2\pi} \left( \arcsin(y) - y \sqrt{1-y^2} \right)_{-1}^1 \\ Var(Y) &= \frac{1}{2}. \end{aligned} \quad (102)$$

To find  $Var(h_{ij}^{\text{eff}})$ , we start from (92)

$$\begin{aligned} h_{ij}^{\text{eff}} &= \vec{p}_{\text{Rx},i}^T \begin{bmatrix} h_{ij}^{\text{vv}} & h_{ij}^{\text{vh}} \\ h_{ij}^{\text{hv}} & h_{ij}^{\text{hh}} \end{bmatrix} \vec{p}_{\text{Tx},j} \\ &= h_{ij}^{\text{vv}} \cos(\theta_j) \cos(\theta_i) + h_{ij}^{\text{hv}} \sin(\theta_i) \cos(\theta_j) + h_{ij}^{\text{vh}} \cos(\theta_i) \sin(\theta_j) + h_{ij}^{\text{hh}} \sin(\theta_j) \sin(\theta_i) \\ &= \beta_1 + \beta_2 + \beta_3 + \beta_4. \end{aligned} \quad (103)$$

Therefore, the variance is

$$Var(h_{ij}^{\text{eff}}) = E[(\beta_1 + \beta_2 + \beta_3 + \beta_4)^2] - \left( E[\beta_1 + \beta_2 + \beta_3 + \beta_4] \right)^2. \quad (104)$$

All  $\beta_i$ 's are independent from each other; hence second term is addition of expectations of each  $\beta_i$ 's. Since they are zeros, they are eliminated from the equation.

When first term is foiled, it consists of squares and cross terms of  $\beta_i$ 's. The cross terms cancel out because elements of polarization basis matrix are independent from each other. Therefore, the variance is

$$\begin{aligned} Var(h_{ij}^{\text{eff}}) &= E[\beta_1^2 + \beta_2^2 + \beta_3^2 + \beta_4^2] \\ &= E[\beta_1^2] + E[\beta_2^2] + E[\beta_3^2] + E[\beta_4^2] \\ &= Var(\beta_1) + Var(\beta_2) + Var(\beta_3) + Var(\beta_4). \end{aligned} \quad (105)$$

Variance of product of independent random variable is product of variance of the random variables.

Note that each three terms of  $\beta_i$ 's, where  $i \in \{1, 2, 3, 4\}$  are independent. Therefore, the variance of each  $\beta_i$  is product of variances of three terms. Moreover, because each polarization-basis matrix element consists of real and imaginary part, we analyze the two parts separately. Both real and imaginary parts of all  $\beta_i$ 's, therefore, have variance of 1/8. Then, these variances are added to yield variance of  $h_{ij}^{\text{eff}}$ , (96); that is 1/2 for both real and imaginary parts. Hence, real and imaginary part of  $h_{ij}^{\text{eff}}$  has means of 0 and variances of 1/2, which brings the element back to  $H_0$ .

**APPENDIX B**

**ELABORATION OF POLARIZATION DETERMINANT MATRIX**

From (97),

$$\begin{aligned} |h_{11}^{\text{eff}}|^2 &= \vec{p}_{\text{Rx},1}^T (H_{11} \vec{p}_{\text{Tx},1} \vec{p}_{\text{Tx},j}^T H_{11}^\dagger) \vec{p}_{\text{Rx},1} \\ &= [\cos(\theta_{\text{Rx},1}) \sin(\theta_{\text{Rx},1})] \begin{bmatrix} h_{\text{Rx},11}^{\text{PD}} & h_{\text{Rx},12}^{\text{PD}} \\ h_{\text{Rx},21}^{\text{PD}} & h_{\text{Rx},22}^{\text{PD}} \end{bmatrix} \begin{bmatrix} \cos(\theta_{\text{Rx},1}) \\ \sin(\theta_{\text{Rx},1}) \end{bmatrix}, \end{aligned} \quad (106)$$

where

$$\begin{aligned} h_{\text{Rx},11}^{\text{PD}} &= |h_{11}^{\text{vv}}|^2 \cos^2(\theta_{\text{Tx},1}) + h_{11}^{\text{vh}}(h_{11}^{\text{vv}})^* \sin(\theta_{\text{Tx},1}) \cos(\theta_{\text{Tx},1}) \\ &\quad + h_{11}^{\text{vv}}(h_{11}^{\text{vh}})^* \sin(\theta_{\text{Tx},1}) \cos(\theta_{\text{Tx},1}) + |h_{11}^{\text{vh}}|^2 \sin^2(\theta_{\text{Tx},1}) \end{aligned} \quad (107)$$

$$\begin{aligned} h_{\text{Rx},12}^{\text{PD}} &= h_{11}^{\text{vv}}(h_{11}^{\text{hv}})^* \cos^2(\theta_{\text{Tx},1}) + h_{11}^{\text{vh}}(h_{11}^{\text{hv}})^* \sin(\theta_{\text{Tx},1}) \cos(\theta_{\text{Tx},1}) \\ &\quad + h_{11}^{\text{vv}}(h_{11}^{\text{hh}})^* \sin(\theta_{\text{Tx},1}) \cos(\theta_{\text{Tx},1}) + h_{11}^{\text{vh}}(h_{11}^{\text{hh}})^* \sin^2(\theta_{\text{Tx},1}) \end{aligned} \quad (108)$$

$$\begin{aligned} h_{\text{Rx},21}^{\text{PD}} &= h_{11}^{\text{hv}}(h_{11}^{\text{vv}})^* \cos^2(\theta_{\text{Tx},1}) + h_{11}^{\text{hh}}(h_{11}^{\text{vv}})^* \sin(\theta_{\text{Tx},1}) \cos(\theta_{\text{Tx},1}) \\ &\quad + h_{11}^{\text{hv}}(h_{11}^{\text{vh}})^* \sin(\theta_{\text{Tx},1}) \cos(\theta_{\text{Tx},1}) + h_{11}^{\text{hh}}(h_{11}^{\text{vh}})^* \sin^2(\theta_{\text{Tx},1}) \end{aligned} \quad (109)$$

$$\begin{aligned} h_{\text{Rx},22}^{\text{PD}} &= |h_{11}^{\text{hv}}|^2 \cos^2(\theta_{\text{Tx},1}) + h_{11}^{\text{hh}}(h_{11}^{\text{hv}})^* \sin(\theta_{\text{Tx},1}) \cos(\theta_{\text{Tx},1}) \\ &\quad + h_{11}^{\text{hv}}(h_{11}^{\text{hh}})^* \sin(\theta_{\text{Tx},1}) \cos(\theta_{\text{Tx},1}) + |h_{11}^{\text{hh}}|^2 \sin^2(\theta_{\text{Tx},1}) . \end{aligned} \quad (110)$$

Note that the greatest values that we can acquire are the squared enveloped terms. The elements of polarization determinant matrices can be transformed into a different form with trigonometric properties. They result as

$$\begin{aligned} |h_{11}^{\text{eff}}|^2 &= \frac{1}{4} \left\{ |h_{11}^{\text{vv}}|^2 + |h_{11}^{\text{vh}}|^2 + |h_{11}^{\text{hv}}|^2 + |h_{11}^{\text{hh}}|^2 \right. \\ &\quad + \cos(2\theta_{\text{Tx},1}) [ |h_{11}^{\text{vv}}|^2 - |h_{11}^{\text{vh}}|^2 + |h_{11}^{\text{hv}}|^2 - |h_{11}^{\text{hh}}|^2 ] \\ &\quad + \sin(2\theta_{\text{Tx},1}) [ h_{11}^{\text{vh}}(h_{11}^{\text{vv}})^* + h_{11}^{\text{vv}}(h_{11}^{\text{vh}})^* + h_{11}^{\text{hh}}(h_{11}^{\text{hv}})^* + h_{11}^{\text{hv}}(h_{11}^{\text{hh}})^* ] \Big\} \\ &\quad + \frac{1}{4} \cos(2\theta_{\text{Rx},1}) \left\{ |h_{11}^{\text{vv}}|^2 + |h_{11}^{\text{vh}}|^2 + |h_{11}^{\text{hv}}|^2 + |h_{11}^{\text{hh}}|^2 \right. \\ &\quad + \cos(2\theta_{\text{Tx},1}) [ |h_{11}^{\text{vv}}|^2 - |h_{11}^{\text{vh}}|^2 + |h_{11}^{\text{hv}}|^2 - |h_{11}^{\text{hh}}|^2 ] \\ &\quad + \sin(2\theta_{\text{Tx},1}) [ h_{11}^{\text{vh}}(h_{11}^{\text{vv}})^* + h_{11}^{\text{vv}}(h_{11}^{\text{vh}})^* + h_{11}^{\text{hh}}(h_{11}^{\text{hv}})^* + h_{11}^{\text{hv}}(h_{11}^{\text{hh}})^* ] \Big\} \\ &\quad + \frac{1}{4} \sin(2\theta_{\text{Rx},1}) \left\{ h_{11}^{\text{vh}}(h_{11}^{\text{vv}})^* + h_{11}^{\text{vv}}(h_{11}^{\text{vh}})^* + h_{11}^{\text{hh}}(h_{11}^{\text{hv}})^* + h_{11}^{\text{hv}}(h_{11}^{\text{hh}})^* \right. \\ &\quad + \cos(2\theta_{\text{Tx},1}) [ h_{11}^{\text{vh}}(h_{11}^{\text{vv}})^* - h_{11}^{\text{vv}}(h_{11}^{\text{vh}})^* + h_{11}^{\text{hh}}(h_{11}^{\text{hv}})^* - h_{11}^{\text{hv}}(h_{11}^{\text{hh}})^* ] \\ &\quad \left. + \sin(2\theta_{\text{Tx},1}) [ h_{11}^{\text{hh}}(h_{11}^{\text{vv}})^* + h_{11}^{\text{hv}}(h_{11}^{\text{vh}})^* + h_{11}^{\text{vh}}(h_{11}^{\text{hv}})^* + h_{11}^{\text{hv}}(h_{11}^{\text{hh}})^* ] \right\}. \end{aligned} \quad (111)$$

Depending on the channel condition, squared envelopes of elements of polarization-basis matrix are maximized with optimal values of  $\theta_{\text{Tx},j}$  and  $\theta_{\text{Rx},i}$  in each iteration.

$|h_{11}^{\text{eff}}|^2$  consists of four squared envelope of the elements in polarization-basis matrix, i.e.,  $|h_{11}^{\text{vv}}|^2$ ,  $|h_{11}^{\text{vh}}|^2$ ,  $|h_{11}^{\text{hv}}|^2$  and  $|h_{11}^{\text{hh}}|^2$ . Besides,  $|h_{11}^{\text{eff}}|^2$  includes cross-term products between the elements in polarization-basis matrix. Squared envelope terms outcome higher values than that of the product

of the cross terms; therefore, we focus on utilizing the squared envelope terms rather than the cross terms. Each aforementioned squared envelope terms follow chi-square distribution with 2 degrees of freedom; hence, summing them will result degrees of freedom up to 8. However, the four terms are multiplied by one fourth of  $\cos(2\theta_{Tx,1})$  and one fourth of  $\cos(2\theta_{Rx,1})$ ; therefore, each four squared envelope term will be multiplied by a weight less than unity. The weighted terms are then summed up at the end. Tx and Rx polarization angles are adjusted to yield greater squared envelope terms. Since squared envelope terms have weights less than unity and are superimposed, distribution will not always fit to degrees of freedom of an integer. Such case is represented in Fig. 8.

## **REFERENCES**

## REFERENCES

- [1] J. Jootar, J.-F. Diouris, and J. Zeidler, “Performance of polarization diversity in correlated Nakagami-m fading channels,” vol. 55, no. 1, pp. 128–136, 2006.
- [2] Y. Deng, A. Burr, and G. White, “Performance of MIMO systems with combined polarization multiplexing and transmit diversity,” vol. 2, pp. 869–873, May 2005.
- [3] R. Nabar, H. Bolcskei, V. Erceg, D. Gesbert, and A. Paulraj, “Performance of multiantenna signaling techniques in the presence of polarization diversity,” vol. 50, pp. 2553–2562, Oct. 2002.
- [4] S.-C. Kwon and A. F. Molisch, “Capacity maximization with polarization-agile antennas in the MIMO communication system,” pp. 1–6, Dec. 2015.
- [5] S.-C. Kwon and G. Stüber, “Polarization division multiple access on NLoS wide-band wireless fading channels,” vol. 13, pp. 3726–3737, Jul. 2014.
- [6] X. Wu, T. G. Pratt, and T. E. Fuja, “Hybrid constellations for dual-polarized wireless communications,” vol. 19, no. 8, pp. 5321–5332, 2020.
- [7] J. Zhang, K. J. Kim, A. A. Glazunov, Y. Wang, L. Ding, and J. Zhang, “Generalized polarization-space modulation,” *IEEE Trans. Computers*, vol. 68, pp. 258–273, Jan. 2020.

- [8] S. H. Doan, S. Kwon, and H. Yeh, “Achievable capacity of multipolarization MIMO with the practical polarization-agile antennas,” *IEEE Systems Jour.*, pp. 1–12, Jun. 2020.
- [9] A. Sousa de Sena, D. Benevides da Costa, Z. Ding, and P. H. J. Nardelli, “Massive MIMO-NOMA networks with multi-polarized antennas,” vol. 18, no. 12, pp. 5630–5642, 2019.
- [10] L. A. Gutierrez, S. An, S. Kwon, and H. G. Yeh, “Novel approach of spatial modulation: Polarization-aware OFDM subcarrier allocation,” *Proceedings of IEEE Green Energy and Smart Systems Conference (IGESSC), 2020*, pp. 1–6, 2020.
- [11] K. Satyanarayana, T. Ivanescu, M. El-Hajjar, P. . Kuo, A. Mourad, and L. Hanzo, “Hybrid beamforming design for dual-polarised millimetre wave MIMO systems,” *IET Electronics Letters*, vol. 54, no. 22, pp. 1257–1258, 2018.
- [12] X. Zhang, B. Zhang, and D. Guo, “Performance of poly-polarization multiplexing in narrow-band wireless communication aided by pre-compensation and multi-notch OPPFs,” vol. 6, pp. 478–481, Aug 2017.
- [13] P. Oh and S. Kwon, “Multi-polarization superposition beamforming with XPD-aware transmit power allocation,” pp. 1–6, Dec. 2020.
- [14] G. Zafari, M. Koca, and H. Sari, “Dual-polarized spatial modulation over correlated fading channels,” *IEEE Trans. Computers*, vol. 65, pp. 1336–1352, Mar. 2017.
- [15] P.-Y. Qin, S.-L. Chen, and Y. J. Guo, “A compound reconfigurable microstrip antenna with agile polarizations and steerable beams,” *Proceedings of IEEE International Symposium on Antennas and Propagation (ISAP), 2017*, pp. 1–2, 2017.
- [16] G. Wolosinski, V. Fusco, and O. Malyuskin, “2-bit polarisation agile antenna with high port decoupling,” *Electronics Letters*, vol. 52, no. 4, pp. 255–256, 2016.
- [17] B. Babakhani, S. K. Sharma, and N. R. Labadie, “A frequency agile microstrip patch phased array antenna with polarization reconfiguration,” vol. 64, no. 10, pp. 4316–4327, 2016.

- [18] H. Sun and S. Sun, “A novel reconfigurable feeding network for quad-polarization-agile antenna design,” vol. 64, no. 1, pp. 311–316, 2016.
- [19] L.-P. Cai and K.-K. M. Cheng, “Continuously tunable polarization agile antenna design using a novel varactor-only signal control device,” vol. 16, pp. 1147–1150, 2017.
- [20] Y.-J. Liao, H.-L. Lin, *et al.*, “Polarization reconfigurable eccentric annular ring slot antenna design,” vol. 63, no. 9, pp. 4152–4155, 2015.
- [21] S.-C. Kwon, “Optimal power and polarization for the capacity of polarization division multiple access channels,” pp. 1–5, Dec. 2014.
- [22] M. R. Andrews, P. P. Mitra, and R. deCarvalho, “Tripling the capacity of wireless communications using electromagnetic polarization,” *Nature*, vol. 409, pp. 316–318, Jan. 2001.
- [23] V. Erceg, P. Soma, D. Baum, and S. Catrux, “Multiple-input multiple-output fixed wireless radio channel measurements and modeling using dual-polarized antennas at 2.5 GHz,” vol. 3, pp. 2288 – 2298, Nov. 2004.
- [24] M. Shafi, M. Zhang, A. Moustakas, P. Smith, A. Molisch, F. Tufvesson, and S. Simon, “Polarized MIMO channels in 3-D: Models, measurements, and mutual information,” vol. 24, pp. 514–527, Mar. 2006.
- [25] M. Landmann, K. Sivasondhivat, J.-I. Takada, I. Ida, and R. Thoma, “Polarisation behaviour of discrete multipath and diffuse scattering in urban environments at 4.5 GHz,” *EURASIP J. Wireless Commun. Netw.*, p. 60, Jan. 2007 Article ID 57980.
- [26] S.-C. Kwon and G. L. Stüber, “Geometrical theory of channel depolarization,” vol. 60, pp. 3542–3556, Oct. 2011.
- [27] V. Erceg, H. Sampath, and S. Catrux-Erceg, “Dual-polarization versus single-polarization MIMO channel measurement results and modeling,” vol. 5, pp. 28–33, Jan. 2006.

- [28] A. Molisch and M. Win, “MIMO systems with antenna selection,” *IEEE Microwave Mag.*, vol. 5, pp. 46–56, Mar 2004.
- [29] A. Molisch, M. Win, Y.-S. Choi, and J. Winters, “Capacity of mimo systems with antenna selection,” *IEEE Transactions on Wireless Communications*, vol. 4, no. 4, pp. 1759–1772, 2005.
- [30] A. Molisch, M. Win, and J. Winters, “Reduced-complexity transmit/receive-diversity systems,” *IEEE Transactions on Signal Processing*, vol. 51, no. 11, pp. 2729–2738, 2003.
- [31] M. Win and J. Winters, “Analysis of hybrid selection/maximal-ratio combining in Rayleigh fading,” in *1999 IEEE International Conference on Communications (Cat. No. 99CH36311)*, vol. 1, pp. 6–10 vol.1., 1999.
- [32] M. Win and J. Winters, “Virtual branch analysis of symbol error probability for hybrid selection/maximal-ratio combining in Rayleigh fading,” *IEEE Transactions on Communications*, vol. 49, no. 11, pp. 1926–1934, 2001.
- [33] D. Gore, R. Heath, and A. Paulraj, “Transmit selection in spatial multiplexing systems,” *IEEE Communications Letters*, vol. 6, no. 11, pp. 491–493, 2002.
- [34] W. Roh, J.-Y. Seol, J. Park, B. Lee, J. Lee, Y. Kim, J. Cho, K. Cheun, and F. Aryanfar, “Millimeter-wave beamforming as an enabling technology for 5g cellular communications: theoretical feasibility and prototype results,” vol. 52, no. 2, pp. 106–113, 2014.
- [35] Y.-H. Nam, B. L. Ng, K. Sayana, Y. Li, J. Zhang, Y. Kim, and J. Lee, “Full-dimension MIMO (FD-MIMO) for next generation cellular technology,” vol. 51, no. 6, pp. 172–179, 2013.
- [36] G. Xu, Y. Li, J. Yuan, R. Monroe, S. Rajagopal, S. Ramakrishna, Y. H. Nam, J.-Y. Seol, J. Kim, M. M. U. Gul, A. Aziz, and J. Zhang, “Full dimension MIMO (FD-MIMO): Demonstrating commercial feasibility,” vol. 35, no. 8, pp. 1876–1886, 2017.
- [37] V. R. Anreddy and M. A. Ingram, “Wlc11-6: Antenna selection for compact dual-polarized MIMO systems with linear receivers,” in *IEEE Globecom 2006*, pp. 1–6, 2006.

- [38] A. Habib, “Multiple polarized MIMO with antenna selection,” in *2011 18th IEEE Symposium on Communications and Vehicular Technology in the Benelux (SCVT)*, pp. 1–8, 2011.
- [39] T. A. Milligan, *Modern Antenna Design*. Chichester, UK: John Wiley & Sons, Inc, 2005.
- [40] C. Y. Wong, R. Cheng, K. Lataief, and R. Murch, “Multiuser OFDM with adaptive subcarrier, bit, and power allocation,” vol. 17, no. 10, pp. 1747–1758, 1999.
- [41] A. F. Molisch, *Wireless Communications*. Wiley and IEEE, 2 ed., 2010.
- [42] D. Tse and P. Viswanath, *Fundamentals of Wireless Communication*. Cambridge, 1 ed., 2005.
- [43] G. Strang, *Linear Algebra and Its Applications*. Thomson Learning, Inc., 4 ed., 2005.
- [44] S.-C. Kwon, “Geometrical theory, modeling and applications of channel polarization,” *Ph.D. Thesis, Georgia Institute of Technology*, pp. 1–128, 2014.
- [45] R. L. R. Thomas H. Cormen, Charles E. Leiserson and C. Stein, *Introduction to Algorithms*. Cambridge, Massachusetts, US and London, UK: The MIT Press, 2009.